The Hong Kong Polytechnic University

DEPARTMENT OF LAND SURVEYING AND GEO-INFORMATICS

Positioning Performance Improvements with European Multiple-Frequency Satellite Navigation System - Galileo

Shengyue JI

A THESIS

SUBMITTED IN PARTIAL FULFILMENT OF THE REQUIREMENTS

FOR THE DEGREE OF DOCTOR OF PHILOSOPHY

DECEMBER 2007

CERTIFICATE OF ORIGINALITY

I hereby declare that this thesis is my own work and that, to the best of my knowledge and belief, if reproduces no material previously published or written, nor material that has been accepted for the award of any other degree or diploma, except where due acknowledgement has been made in the text.

_____ (Signed)

Shengyue JI

_____ (Name of student)

Abstract

The rapid development of the Global Positioning System has demonstrated the advantages of satellite based navigation systems. In near future, there will be a number of Global Navigation Satellite System (GNSS) available, i.e. modernized GPS, Galileo, restored GLONASS, BeiDou and many other regional GNSS augmentation systems. Undoubtedly, the new GNSS systems will significantly improve navigation performance over current GPS, with a better satellite coverage and multiple satellite signal bands. In this dissertation, the positioning performance improvement of new GNSS has been investigated based on both theoretical analysis and numerical study.

First of all, the navigation performance of new GNSS systems has been analyzed, particularly for urban applications. The study has demonstrated that Receiver Autonomous Integrity Monitoring (RAIM) performance can be significantly improved with multiple satellite constellations, although the position accuracy improvement is limited. Based on a three-dimensional urban building model in Hong Kong streets, it is found that positioning availability is still very low in high-rising urban areas, even with three GNSS systems. On the other hand, the discontinuity of navigation solutions is significantly reduced with the combined constellations. Therefore, it is possible to use cheap DR systems to bridge the gaps of GNSS positioning, with high accuracy.

Secondly, the ambiguity resolution performance has been investigated with Galileo multiple frequency band signals. The ambiguity resolution performance of three different algorithms is compared, including CAR, ILS and improved CAR methods (a new method proposed in this study). For short baselines, with four frequency Galileo data, it is highly possible to achieve reliable single epoch ambiguity

resolution, when the carrier phase noise level is reasonably low (i.e. less than 6mm). For long baselines (up to 800 km), the integer ambiguity can be determined within 1 min on average.

Ambiguity validation is crucial for any ambiguity resolution algorithm using searching method. This study has proposed to use both Ellipsoidal Integer Aperture (EIA) estimator and R-ratio test for ambiguity validation. Using real GPS data and simulated Galileo data, it has been demonstrated that the new method performs better than the use of EIA or the R-ratio test alone, with much less ambiguity mis-fixed rate.

Special thanks to:

my advisor – Professor Wu CHEN and my wife – Xiaoming YI

Table of Contents

List of Tables

List of Figures

Chapter 1 Introduction

1.1 Background

In past thirty years, we have witnessed rapid development in satellite positioning, particularly the development of the Global Positioning System (GPS). GPS has found widespread applications in different fields from navigation (Igor and Francois, 2003; Civil Aviation Authority 2004; Federal Radionavigation Plan 2005; Lachapelle and Mezentsev, 2005), surveying (Frei and Beutler, 1990; Chen, 1992; Leick, 2004), to geophysics and geodynamic studies (Chen et al., 2004; Colombo et al., 2004) and atmospheric research (Hirahara, 2000; Joachim, 2003). On the other hand, it is well known that GPS has some drawbacks (Civil Aviation Authority 2004):

- The navigation availability and integrity provided by current GPS alone cannot meet certain navigation requirements due to the few satellites available and inadequate ground tracking stations;
- Signal interference threats due to only one civilian frequency;
- GPS is a military system controlled by a single nation;
- Ionospheric delay estimation error using a single frequency correction model (Klobuchar model);
- In urban areas, GPS signal availability is significantly reduced (Miller et al., 1995; Kozlov and Tkachenko, 1998; Grejner-Brzezinska et al., 2001; Berefelt et al., 2004);
- For precise real-time kinematic (RTK) positioning, the reliability and efficiency of ambiguity resolution is generally low due to only two frequency bands being available.

To overcome these problems and to enhance its military and civil navigation capabilities, a GPS modernization program has begun (McDonald, 2001). Parallel to that, the replenishment of GLONASS has also been scheduled (GLONASS ICD 2002).

In the early 1990s, the European Union (EU) began to conceive its own global satellite navigation system. It includes two steps, to implement a GNSS-1 system to augment the existing GPS and GLONASS (EGNOS) and to develop a new civilian control GNSS-2 system. In 1998, a series of studies were formally commissioned concerning the design of an independent, civil satellite navigation service. In 1999, the European-based Galileo system was announced. The European Commission (EC) assumed political responsibility for Galileo and the European Space Agency (ESA) led the programme's development. A tentative Galileo frequency and signal plan was published in early 2000. In 2002, the development phases of Galileo were finally decided in a meeting of the Transport Council of the EU. Taking into account the compatibility and interoperability with GPS, Galileo frequencies and signals were refined in the same year. In mid-2004, a few more important changes were carried out in the waveforms on E1 and E6 as a consequence of the agreement made between the US and EU (USA and CE 2004). In addition, the orbit selection for the Galileo constellation was finalized. The first experimental satellite Giove-A was launched on 28 December 2005 (Oliver et al., 2006) and the system is expected to be operational in the 2010s.

Different from GPS and GLONASS, Galileo is a completely new civil navigation system with two distinguished features:

- To ensure safety of navigation, an integrity message is provided;
- Navigation signals are transmitted in four frequency bands.

Except the above three systems, China, Japan and India are planning their own navigation systems. All of them are forming the basis of the future new GNSS systems.

Within the next a few years, there will be more than 100 navigation satellites and much more navigation signals available. These will dramatically improve navigation performance over the current GPS system. Studies have demonstrated that with multiple GNSS systems, positioning availability and integrity will be significantly improved (Kyle, 2001; Hewitson and Wang, 2004; O'Keefe, 2001). Utilizing multiple frequency bands from new GNSS will also improve the capability for fast ambiguity resolution (Alves, 2001; Schlotzer and Martin, 2005). On the other hand, there are some questions that need to be stressed, i.e.:

- Will the combination of new GNSS solve the urban navigation problem, as more satellites are available?
- Currently, most studies use three frequency bands from GPS modernization and Galileo for fast ambiguity resolution study. Actually, Galileo provides four frequency bands. Although E6 is a restricted signal for navigation, it is possible to extract carrier phase from E6 signal as well. What is the ambiguity resolution performance with four frequency bands?
- Is it possible to resolve ambiguity within a single epoch reliably? If it is, then we are able to provide centimetre level real-time navigation to greatly extend the applications of satellite navigation.

This study tries to answer some of these questions.

1.2 Objectives

The objectives of this study are:

- Developing new GNSS data simulator and data processing software

In the near future, there will be multiple GNSS systems available, i.e. modernized GPS, GLONASS, Galileo and BeiDou. Therefore, there is a need to develop GNSS data processing software which is able to use measurements from all these systems to achieve better positioning performance with multiple frequency signals from combined satellite constellations. As Galileo is not available, it is necessary to develop a data simulator to simulate the Galileo data. Fortunately, Galileo's signal is also in the L band and therefore the error models developed by GPS studies can be applied to Galileo signals. In this study, software packages will be developed to enable the processing of pseudorange and carrier phase measurements from multiple GNSS systems.

- Evaluating navigation performances with multiple GNSS systems, including GPS, GLONASS and Galileo

With multiple GNSS systems, satellite positioning availability and integrity can be significantly improved (Kyle, 2001; Hewitson and Wang, 2004; O'Keefe, 2001), due to the fact that more satellites will be available. In this study, the observation models will be developed for integrating various GNSS systems and the navigation performances with multiple GNSS systems (accuracy and integrity) will be analyzed. As GPS availability in Hong Kong (urban areas) is very low (Miller et al., 1995; Kozlov and Tkachenko, 1998; Grejner-Brzezinska et al., 2001; Berefelt et al., 2004), in this study, the positioning availability with multiple GNSS systems will be analyzed using a realistic Hong Kong 3D city model.

- Investigating ambiguity resolution performance with multiple frequency Galileo signals

With Galileo system, there are four frequency bands available, double the number of the frequency bands of current GPS and more number of frequency combinations can be formed. Undoubtedly this will provide more opportunities for fast ambiguity resolution. How to take advantage of the multiple Galileo frequency bands for ambiguity resolution is one main focus of current GNSS research. In this study, the current available methods will be compared first and a new algorithm will be then proposed.

- Studying ambiguity resolution validation methods

The search method is an important step for fast ambiguity resolution algorithms. Therefore, validation processing is crucial for any ambiguity resolution. Many different validation methods for ambiguity resolution have been proposed (Frei and Beutler, 1990; Landau and Euler, 1992; Euler and Schaffrin, 1991; Leick, 2003; Tiberius and De Jonge, 1995; Wang et al., 1998a; Han, 1997; Teunissen, 2004; Teunissen, 2005). But the reliability is not high enough to support navigation requirements. Currently, the carrier phase measurement is mainly used for surveying and some special applications where accuracy is a main concern. How to improve the reliability of ambiguity resolution is a major research focus of GNSS research, and in this study, the performance of existing validation methods will be analyzed and new algorithms will be proposed for improving ambiguity resolution reliability.

1.3 Dissertation Outline

This dissertation is organized in the following way. In Chapter 2, a brief description to recent developments on new GNSS systems is given. Then recent research on

multiple frequency ambiguity resolution, GNSS integrity issues and ambiguity resolution validation methods are reviewed. The GNSS data simulator developed in this project is described in Chapter 3, including the error models applied in the data simulator, the program structure and some examples. The point positioning issues with multiple GNSS systems are studied in Chapter 4. In this chapter, the navigation performance is first analyzed with pseudorange measurements. Special attention is paid to the performance improvements with multiple GNSS systems in an urban environment, in which GPS does not perform well due to signal obstructions. The ambiguity convergent time for the Precise Point Positioning (PPP) with multiple Galileo signals is also investigated in the chapter. In Chapters 5 and 6, the performance of ambiguity resolution is analyzed with multiple frequency Galileo signals and it is examined that if it is possible to resolve ambiguity reliably within a single epoch. In Chapter 5, the performances of two commonly used ambiguity resolution methods Cascading Ambiguity resolution (CAR) method and integer Least-Squares (ILS) method are compared. In Chapter 6, an improved ambiguity resolution method is proposed and the performance of this new method is evaluated with simulated Galileo data. The ambiguity resolution validation algorithm is a crucial part for any ambiguity resolution method. In Chapter 7, EIA method is analyzed. Then a new ambiguity resolution validation method is proposed. Based on the tests with real GPS observation data and simulated Galileo data, the new method is more reliable for ambiguity resolution than the traditional R-ratio and EIA method. Finally, the conclusions and recommendations are given in Chapter 8 of the dissertation.

Chapter 2 Recent developments in GNSS technologies

The development of Global Positioning System (GPS) has clearly demonstrated the advantages of satellite navigation systems over terrestrial navigation systems (i.e. Loran-C, DME/VOR). In recent years, we have witnessed rapid developments in satellite navigation. The US GPS system achieved its Full Operation Capacity (FOC) in 1995 and is currently improving through GPS modernization programme. Parallel to GPS, the Russian GLONASS also deployed full constellation in the late nineties. Due to an economic downturn and technical issues, the number of GLONASS satellites has reduced dramatically. Currently, the Russian government is implementing the GLONASS modernization programme and it is expected that the full GLONASS constellation will be available in the early 2010s. In addition, since early 1998, the European community (EC) has been planning to launch a similar global satellite navigation system, Galileo. Its first experimental satellite Giove-A was launched on 28 December 2005. Although there have been some problems with Galileo's development (funding and organizational) (Blair 2005), the system is expected to be operational in the 2010s as well. Meanwhile, China has indicated that it will expand its regional satellite navigation system into a global navigation system – BeiDou or Compass Navigation Satellite System (CNSS). Japan is also developing an ingenious satellite navigation augmentation system to the U.S. GPS under the QZSS programme and the Indian government is planning to build an independent satellite navigation system using home-grown components, called the Indian Regional Navigation System (RNSS).

All of these systems form the base of the new GNSS. This chapter will provide the background to the new GNSS. In addition the recent developments in GNSS research

relevant to this study will be reviewed.

2.1 Recent developments of the new GNSS

2.1.1 European Galileo system

In the early 1990s, the European Union (EU) began to conceive its own global satellite navigation system. The EC assumed political responsibility for Galileo and the European Space Agency (ESA) led the programme's development. In 1998, a series of studies were formally commissioned concerning the design of an independent, civil satellite navigation service. Three years later, a tentative Galileo frequency and signal plan was published. In 2002, the development phases of Galileo were finally decided in a meeting of the Transport Council of the EU. Taking into account the compatibility and interoperability with GPS, Galileo frequencies and signals were refined in the same year. In mid-2004, a few important changes were carried out in the waveforms on E1 and E6 as a consequence of the agreement made between the US and EU (USA and CE 2004). In addition, the orbit selection for the Galileo constellation was finalized. On 28 December 2005 the first experimental satellite Giove-A was launched (Oliver et al., 2006) and the system is expected to be operational in the 2010s.

Though similar to GPS in working principle, Galileo has its own unique features, which can be seen from its system architecture, the services to be provided and the integrity concept.

2.1.1.1 System architecture

The fundamental parts of Galileo's system architecture include the space segment, signal in space and ground segment (European Commission, Galileo Mission High Level Definition Document 2002).

- **Space segment**

The Galileo space segment will comprise a constellation of a total of 30 medium-Earth-orbit (MEO) satellites, 3 of which are spares, in a so-called Walker 27/3/1 constellation (Figure 2-1).

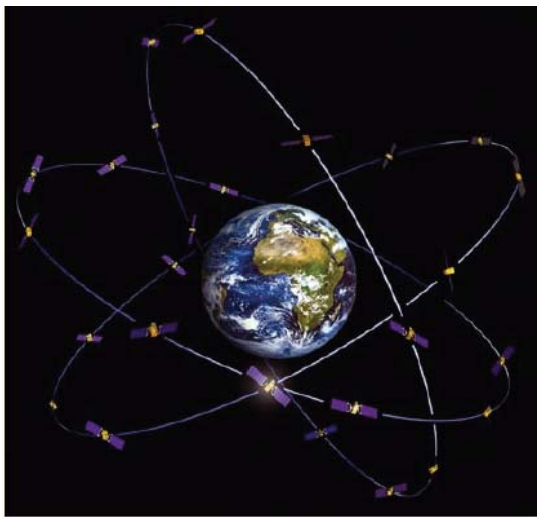

Figure 2-1 Galileo satellite constellation

The constellation has been optimized to the following nominal constellation specifications:

- circular orbits with a semi-major axis of 29,994 km
- orbital inclination of 56° (slightly larger than that of GPS (55°))
- three equally spaced orbital planes
- nine operational satellites equally spaced in each plane
- one spare satellite in each plane

The constellation provides better coverage over northern Europe, well suited for high latitude countries and offers improved visibility in towns and cities.

- **Signal in space (SIS)**

Ten navigation signals and one SAR signal are provided by Galileo (GAL OS SIS ICD 2006). In accordance with the ITU (International Telecommunication Union) regulations, Galileo navigation signals will be emitted in the RNSS allocated bands

and the SAR signal will be broadcast in one of the frequency bands reserved for the emergency services (1544-1545 MHz).

Figure 2-2 describes the Galileo navigation signals emission:

- 4 signals are transmitted in the frequency range 1164-1215 MHz (E5a-E5b)
- 3 signals are transmitted in the frequency range 1260-1300 MHz (E6)
- 3 signals are transmitted in the frequency range 1559-1591 MHz (L1)

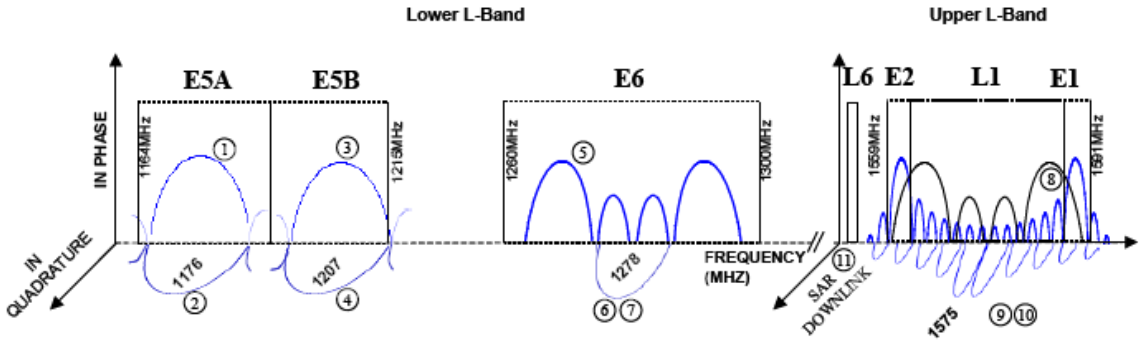

Figure 2-2 Galileo signal in space

Different signals are broadcast on the in-phase (I) and quadrature (Q) channels and, in the case of band 1164-1215MHz, different signals are provided in the upper (E5b) and lower (E5a) part of the band.

Table 2-1 is a summary of the primary Galileo navigation signal parameters and their mapping services (which are introduced in Section 2.1.1.2).

Table 2-1 Primary Galileo navigation signal parameters and mapping services

Signal name	Channel	Modulation type	Chip rate (Mcps)	Symbol rate (sps)	Reference service
E5	E5a data	AltBOC (15,10)	10.23	50	OS
	E5a pilot			N/A	
	E5b data			250	OS/SoL/CS
	E5b pilot			N/A	
E6	E6-B data	BPSK(5)	5.115	1000	CS
	E6-C pilot			N/A	
E1	E1-B data	BOC(1,1)	1.023	250	OS/SoL/CS
	E1-C pilot			N/A	

- **Ground segment**

The ground segment includes the Galileo control centre, Galileo sensor stations, Galileo uplink stations, mission uplink stations and a global area network.

The Galileo control centre is the heart of the system and includes all control and processing facilities. Its main functions include orbit determination, time synchronization, global satellite integrity determination, Galileo system time maintenance, satellite monitoring and control.

Galileo sensor stations collect navigation data from the Galileo satellites as well as meteorological and other required environmental information. This information is passed to the Galileo control centre for processing.

Galileo uplink stations include separate two-way tracking, telemetry and command stations in the S-band, specific Galileo mission related up-links in the C-band and Galileo sensor stations.

The global area network provides a communication network linking all system elements around the world.

2.1.1.2 Galileo services

The definition of the Galileo services is based on a comprehensive review and market analysis to cover the widest range of user needs, including professional users, scientists, mass-market users, safety of life and public regulated domains. There are some services resulting from the combined use of Galileo and other systems. There are also other services provided autonomously by Galileo which will be introduced as follows.

- **Open Service (OS)**

The Open Service results from a combination of open signals, free of user charges and

suitable for mass-market applications. The performance and features of the positioning, velocity and timing information it provides are summarized in Tables 2-2 & 2-3.

Table 2-2 Performance and features of Open Service (positioning)

Types of Receiver	Single Frequency	Dual-frequency
Ionospheric Correction	Based on simple model	Based on dual-frequency measurements
Coverage	Global	
Accuracy (95%)	H: 15m V: 35m	H: 4m V: 8m
Integrity	Not Applicable	
Availability	99.8%	

Table 2-3 Performance and features of Open Service (timing)

Carriers	Three-Frequency
Coverage	Global
Timing Accuracy w.r.t UTC/TAI	30nsec
Availability	99.8%

- **Safety of Life (SoL)**

The Safety of Life Service is for safety critical users, for example maritime, aviation and trains. It improves the open service performance by providing timely warnings to the user when it fails to meet certain margins of accuracy (integrity). Its performance and features are given in Table 2-4.

Table 2-4 Performance and features of Safety of Life Service

Types of Receiver		Three frequency	
Ionospheric Correction		Based on dual-frequency measurements	
Coverage		Global	
Accuracy (95%)		Critical level	Non-critical level
		H: 4m V: 8m	H: 220m
Integrity	Alarm Limit	H: 12m V: 20m	H: 556m
	Time-To-Alarm	6 seconds	10 seconds
	Integrity risk	$3.5\times10^{-7}/150s$	$10^{-7}/hour$
Continuity Risk		$10^{-5}/15s$	$10^{-4}/hour - 10^{-8}/hour$
Certification/Liability		Yes	
Availability of integrity		99.5%	
Availability of accuracy		99.8%	

- **Commercial Service (CS)**

Compared with Open Service, the Commercial Service (CS) will allow the development of professional applications, with increased navigation performance and added value data. It will be a controlled access service operated by Commercial Service providers.

- **Public Regulated Service (PRS)**

The Public Regulated Service (PRS) will be provided to specific users a higher level of protection against the threats to Galileo signals in space (SIS) than is available for OS, CS and SoL through the use of appropriate interference mitigation technologies.

The objective is to improve the probability of continuous availability of the SIS, in the presence of interfering threats, to those users with such a need. The use of PRS will be restricted to clearly identified categories of users authorized by the EU and participating states.

Its performance and features are shown in Table 2-5.

Table 2-5 Performance and features of the Public Regulated Service

Types of Receiver		Dual-frequency
Ionospheric Correction		Based on dual-frequency measurements
Coverage		Global
Accuracy (95%)		H: 6.5m V: 12m
Integrity	Alarm Limit	H: 6.5m V: 12m
	Time-To-Alarm	10 seconds
	Integrity risk	$3.5\times10^{-7}/150s$
Continuity Risk		$10^{-5}/15s$
Certification/Liability		Yes
Availability of integrity		99.5%
Timing Accuracy w.r.t UTC/TAI		100nsec

- **Search and Rescue Service (SAR)**

The Search and Rescue Service (SAR) broadcasts globally the alert messages received from distress emitting beacons. It will contribute to enhance the performance of the international COSPAS-SARSAT Search and Rescue system.

2.1.1.3 Galileo integrity concept

One main characteristic of the Galileo system is the provision of an integrity function for the global user. This means that the integrity performance must be achieved globally, keeping the Time-To-Alert within 6 seconds.

The Galileo integrity concept is to monitor each satellite itself and transmit the corresponding behaviour to the user. Taking all transmitted information into account the user can calculate the integrity risk and decide if he is allowed to start his operation.

The overall Galileo concept consists of a system alert mechanism, user integrity concept and the system allocation for integrity (Veit et al., 2004).

- **System alert mechanism**

Galileo has the capability to monitor the signal-in-space (SIS) through its complex global distributed ground network consisting of more than 30 ground sensor stations (GSSs). With the known positions of the GSSs, the actual position of the SV and maximum error on the range (the Signal-in-Space-Error, SISE) can be estimated.

The prediction of the SISE distribution can be over-bounded by a non-biased Gaussian distribution with the minimum standard deviation called Signal-in-Space-Accuracy (SISA).

The difference between the actual SISE and the estimated SISE (SISEest) can be described by a Gaussian distribution function with the standard deviation called Signal-in-Space-Monitoring-Accuracy (SISMA).

Within the Galileo integrity concept, the system estimates the SISE using the measurements of the GSSs to detect faulty satellites. If the estimated SISE for a SIS is larger than the integrity flag threshold, the integrity flag (IF) for this SIS is set to not ok and an alert will be sent to the user. The integrity flag threshold (TH) can be computed from the SISE distribution, the distribution of the difference between SISE and SISEest, and the allowed False Alarm probability.

According to the Galileo integrity concept, the following information will be disseminated to the user:

- Navigation Message: beside the normal navigation message content the message will include the SISA values and will be updated every 30 seconds;
- Integrity Message: the integrity message will be updated every 30 seconds, including the complete integrity table consisting of the SISMA value and IF for each SIS;
- Checksum and connectivity status: the integrity checksum and connectivity status (how integrity has been derived) will be updated every second;
- Alerts: if necessary alerts can be transmitted in real-time (every second).

- **User integrity concept**

Taking the disseminated integrity information into account (SISA, SISMA, IF) the user can derive its individual integrity risk.

The current Galileo system design uses four failure mechanisms: horizontal, vertical and for each of them a fault-free and an undetected error. The integrity risk is calculated for each failure mechanism at the alert limit to compare the sum of all four contributions with the required integrity risk.

Once the distribution of the error in the desired reference frame is known (SISMA), it is straightforward to derive the associated integrity risk. The error

distributions for the vertical (one dimensional Gaussian distribution) and horizontal (Chi-Squared distribution with two degrees of freedom) case need to be derived and the corresponding integrity risk can be easily computed by analyzing the integral for both distributions with the given limits (alert limits).

- **Integrity allocation**

An important part of the overall Galileo system integrity design is the allocation of the top level requirements down to the specific failure modes. This allocation for integrity is outlined in the so-called allocation tree. Figure 2-3 illustrates the high-level integrity allocation including the specific values.

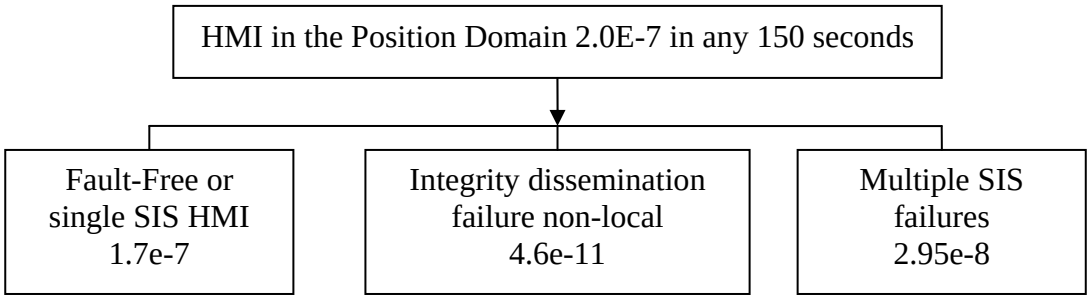

Figure 2-3 High-level integrity allocation

The left branch, fault-free or Single SIS HMI (HMI = Hazardous Misleading Information) represents the HMI situation created when either all the signals used in the position solution perform nominally or at most one signal affected by an undetected failure is used in the position solution.

The middle branch, integrity dissemination failure due to non-local effects covers all events where errors in the dissemination of integrity information result in an HMI in the position domain.

The right branch, multiple SIS failures represents the condition where at least one SIS is failing due to either navigation data determination failure or multiple independent signal failures.

2.1.1.4 Galileo pilot projects

To investigate the introduction and benefits of Galileo in safety of life applications, such as maritime, car navigation, railway etc., the European Commission launched several pilot projects.

- **GADEROS project**

The GADEROS project is a pilot project under the Growth thematic programme of the 5th RTD Framework Programme of the European Union. It forms part of ongoing research work for the Galileo programme and is managed by the Commission's Directorate-General for Energy and Transport.

GADEROS aimed at demonstrating the use of GNSS Safety-of-life features for defining a satellite-based system to perform train location for safe railway applications (Urech, 2002; GADEROS, 2002) that will be integrated into the ERTMS/ETCS (European Rail Traffic Management System/European Train Control System). The system will offer another technological approach for train location, mainly for conventional and low density traffic lines.

- **LOCOPROL project**

The LOCOPROL project intends to develop an innovative, cost-effective, satellite-based, vital, fail-safe train location system as the score of a train protection, control and command system (LOCOPROL 2002).

The four main objectives of the project are strongly interconnected:

- To define a new multi-technology train location system;
- To study its application to the ERTMS/ETCS;
- To study and prove its applicability in low density traffic lines (LDTL);
- To study and prove its application for workers' protection.

- **NAUPLIOS project**

NAUPLIOS is also a pilot project under the Growth thematic programme of the 5th RTD Framework Programme of the European Union.

The project will demonstrate the added value of Galileo positioning and SAR services for commercial shipping. It will make use of the EGNOS Test Bed and six vessels equipped with autonomous terminals - an EGNOS receiver, a satellite telecom link and an Automatic Identification System (AIS). NAUPLIOS Control Centres will monitor the results, which will be adapted in a geographical information system and formatted prior to being transmitted to several kinds of end users (Dick, 2004).

NAUPLIOS will demonstrate how monitoring and surveillance of European waters can be improved such that risks can be identified at an early stage and measures can be taken to avoid major pollution incidents (Jean, 2003; Jean, 2004).

- **GALLANT project**

GALLANT (Galileo for Safety of Life Application of driver Assistance in Road Transport) is also a pilot project under the Growth thematic programme of the 5th RTD Framework Programme of the European Union.

The main objectives of the GALLANT project focus on the integration of Galileo with an Advanced Driver Assistant System (ADAS) with ADAS onboard equipment to provide unprecedented support to the driver in avoiding accidents and to road mobility as a whole (GALLANT 2002).

The expected benefits include: Adaptive Cruise Control, Overtaking Warning, Vision Enhancement, Lane Warning and Keeping, Collision Warning and Avoidance, Automatic Guidance.

- **INSTANT project**

INSTANT (Infomobility services for safety-critical applications on land and sea based

on integrated GNSS terminals) addresses sustainable mobility and intermodality and focuses on the management of large-scale events and emergency situations (Luigi, 2004).

The objectives of the project are to accelerate the uptake of Galileo by the transport sector by exploiting and demonstrating the improved performance provided by EGNOS in targeted applications and to evaluate benefits and analyse economic viability from synergies with appropriate infrastructures and services, both terrestrial and space-based.

The expected benefits include more consistent and reliable route matching, an ability to give better route guidance and event monitoring - and integrity increases acceptability.

- **Polaris project**

Polaris is a software tool that allows the evaluation of navigation performance for different user applications in different environments. Its users include Galileo system engineers, navigation service providers and market analysts (Angel et al., 2004).

Polaris can model the four application domains that are most critical for mass-market application demonstrations: road, personal mobility, train and maritime. It will also provide a means for exploring new ideas for GNSS applications and demonstrating design feasibility to Galileo system designers.

2.1.2 GPS and its modernization

2.1.2.1 Current status of GPS

The Global Positioning System (GPS) is a space-based positioning, navigation and timing (PNT) system developed by the U.S. Department of Defense (DoD) in the

early 1970s and currently managed by the U.S. government through an interagency process that seeks to fuse civilian and military interests.

A combination of Block II, IIA, IIR and IIR-M satellites make up the current constellation. As of February 2007, there were 31 actively broadcasting satellites distributed among six orbital planes. The six planes have approximately 55 degree inclinations and are separated by 60 degree right ascension of the ascending node. Orbiting at an altitude of approximately 20,200 km, each satellite makes two complete orbits each sidereal day (Figure 2-4) (Global Positioning SPS Performance Standard 2001).

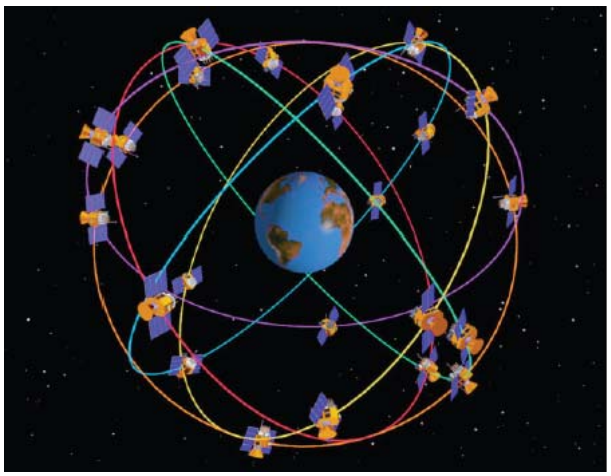

Figure 2-4 GPS satellite constellation

Current GPS uses two frequency bands: L1 and L2 with central frequencies of 1575.42MHz and 1227.60MHz respectively.

Two navigation signals are broadcast. The first one is the Coarse / Acquisition code (C/A) on L1, which is freely available to the public. The C/A code is a 1,023 bit long pseudo-random noise code broadcast at 1.023MHz. The second ranging signal Precision P(Y) code broadcast at 10.23MHz is reserved for military use.

2.1.2.2 GPS modernization

Since the President's decision on 1 May 2000 to "turn off" the capability to degrade

the civil signal, GPS modernization has begun to enhance both military and civil capabilities, including new signals for civil use and increased accuracy and integrity for all users, while maintaining backward compatibility with existing GPS equipment (Per Enge, 2003).

First, a third frequency L5=1175.45MHz will be broadcast beginning with the first IIF satellite and it can be used for safety-of-life aviation because it lies in the "Aeronautical Radionavigation Services" band. For precise applications, the third frequency will benefit ambiguity resolution.

Second, in the near future, GPS will provide an expanded signal set for both military and civil users.

The first new signal L2C signal has an overall chipping rate of 1.023MHz, the same as the C/A code, but with an increased length. This will reduce the probability of a false lock during signal acquisition especially when the desired signal is obstructed and also reduces the worst case effect of narrowband radio frequency interference (RFI) by 10dB (Spilker and Van derendonck, 2001). But unfortunately, the L2C signal does not fall in an Aeronautical Radio Navigation System band, and so it does not enjoy the same institutional protection as the L1 and L5 signals do.

The second new signal L5C is 10.23M chips long and the chipping rate will be 10.23 Megachips per second (Mcps), ten times faster than today's C/A code. This increase in speed will improve the noise performance of the GPS receivers and also make it easier for the receiver to resolve and mitigate the effects of multipath. Meanwhile the L5C will be significantly less vulnerable to RFI due to the tenfold increase in bandwidth and four times increase in power.

In addition, according to the agreement signed by the United States and the Member States of the European Union on GPS and Galileo, a compatible and interoperable signal on the L1 frequency L1C will be provided. It will be backwardly compatible with the current civil signal on L1, broadcast at a higher power level, and include an advanced design for enhanced performance.

Since 1 May 2000, a lot of modernization activities have been and will be carried out. See Table 2-6 for the time schedule.

GPS-III, which will incorporate the extra L2 and L5 signals of the Block IIR and Block IIF satellites are planned for launch from about 2013 until 2018.

In addition to the space segment, control segment modernization is also ongoing.

Table 2-6 GPS modernization plan

Activity	Implementation Date
SA set to zero	May 2000
GPS IIR-M enhancements (L2C)	1st satellite operational on Dec. 16, 2005 2nd launch 14 Sept. 2006
GPS IIF enhancements (L2C and L5C)	1st launch currently scheduled for May 2008
GPS III enhancements (L2C, L5C and new L1C)	1st launch ~ 2013
Control segment enhancements	Ongoing

2.1.3 GLONASS

GLONASS is another operational satellite navigation system. It was product of “cold war” and originally deployed as the former Soviet Union’s version of GPS. Today GLONASS is managed by the Commonwealth of Independent States (CIS) and especially the Russian Federation as the successor of the Soviet Union.

The full GLONASS space segment designed will consist of 24 satellites, distributed over three orbital planes. The longitude of ascending node differs by 120 degrees from plane to plane. Each plane comprises eight satellites, staggered by 45 degrees in argument of latitude. The arguments of latitude of satellites in equivalent slots in two different orbital planes differ by 15 degrees. Orbital and other parameters of the spacecraft are summarized and compared with GPS as in Table 2-7 (GLONASS ICD 2002; Rossbach U, 2000).

Table 2-7 Parameters of the GLONASS and GPS space segments

Parameter	GLONASS	GPS
Semi-major axis	25,510km	26,580km
Orbital height	19,130km	20,200km
Orbital period	11 h 15.8 min	11 h 58 min
Inclination	64.8°	55°
Eccentricity	≤ 0.01	≤ 0.1

Different from GPS, to distinguish between individual satellites, GLONASS employs different frequencies to broadcast their navigational information. Satellite frequencies are determined by the following equations:

$$f_{L_1} = 1602 + k \cdot 0.5625 \ \ MHz$$

$$f_{L_2} = 1246 + k \cdot 0.4375 \ \ MHz$$

Here, k means the frequency number of the satellite. Table 2-8 compares GLONASS and GPS. The frequency domain as specified in Table 2-8 is equivalent to the frequency numbers 0 – 24.

Table 2-8 Comparing frequency plans of GLONASS and GPS

Parameter	GLONASS	GPS
Differences between satellites	FDMA	CDMA
Frequency L1	1602 – 1615.5 MHz	1575.42 MHz
Frequency L2	1246 – 1256.5 MHz	1227.60 MHz
Signal polarization	RHCP	RHCP

In 2005, GLONASS frequencies was shifted to frequency numbers -7… +4, with +5 and +6 as technical frequencies. This equals a frequency domain of 1598.0625 – 1605.375 MHz in the L1 sub-band and 1242.9375 – 1248.625 MHz in the L2 sub-band.

Exactly as GPS, GLONASS uses a Coarse Acquisition (C/A) code and a Precision (P) Code. The L1 carrier phase band is modulated by both C/A and P code, whereas the L2 is modulated by the P code only.

GLONASS C/A code is 511 characters long at a clock frequency of 511KHz and P code is 33,554,431 characters long at a clock frequency of 5.11MHz.

The maintenance of the GLONASS system is affected by the continuing decline of the Russian Federation and especially its industries. See Figure 2-5 for the GLONASS constellation deployment history and future plan. Currently, there are 15 satellites in orbit, including 4 GLONASS-Ms. GLONASS is scheduled to reach a minimum constellation size (of 18 satellites) by 2007 and full constellation (24 satellites) by 2009.

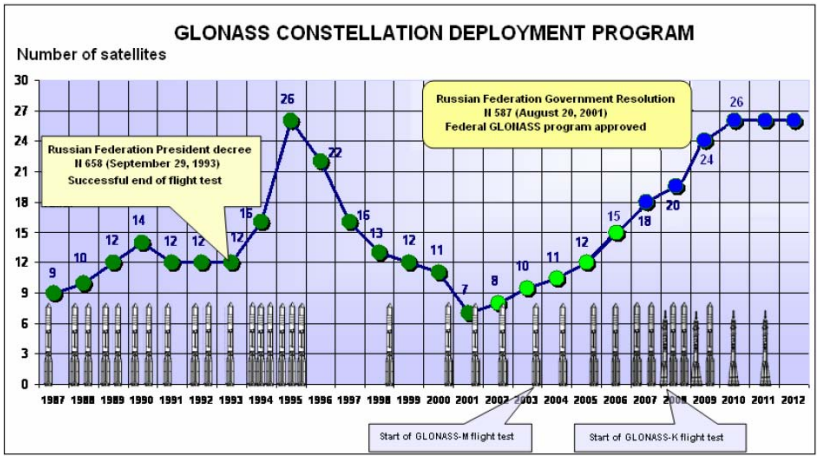

Figure 2-5 GLONASS constellation deployment history and future plan

2.1.4 Other GNSS systems

2.1.4.1 Chinese Beidou System

The BeiDou Navigation system or BeiDou Satellite Navigation and Positioning System, also known as Compass Navigation System (CNSS) by some western observers, is a project by China to develop an independent satellite navigation system (Elliott and Christopher, 2006).

Currently, BeiDou is in a semi-operational phase of BeiDou-1 with four satellites deployed in geostationary orbit over China, BeiDou 1A (See Figure 2-6), 1B, 1C and 1D. The latest BeiDou navigation satellite BeiDou 1D was successfully launched on 3 February 2007. See Table 2-9 for details of the first three satellites.

The official Chinese press has designated the constellation as the BeiDou Navigation Test System (BNTS). It supports two types of satellite navigation capabilities: Radio Determination Satellite Service (RDSS) (Figure 2-7) and Satellite Based Augmentation Systems (SBAS). The RDSS capability is operational with positioning accuracy between 20m and 100m (two-dimensional).

Figure 2-6 BeiDou 1A

Table 2-9 Parameters of BeiDou satellites

	BeiDou 1A	BeiDou 1B	BeiDou 1C
Launch Site	Xichang	Xichang	Xichang
Launch Vehicle	CZ-3A	CZ-3A	CZ-3A
Mass	2,200kg	2,200kg	2,200kg
Perigee	35,770km	35,773km	35,747km
Apogee	35,804km	35,801km	35,829km
Inclination	0.05°	0.07°	0.15°
Position	139.9° East	80.2° East	110.4° East

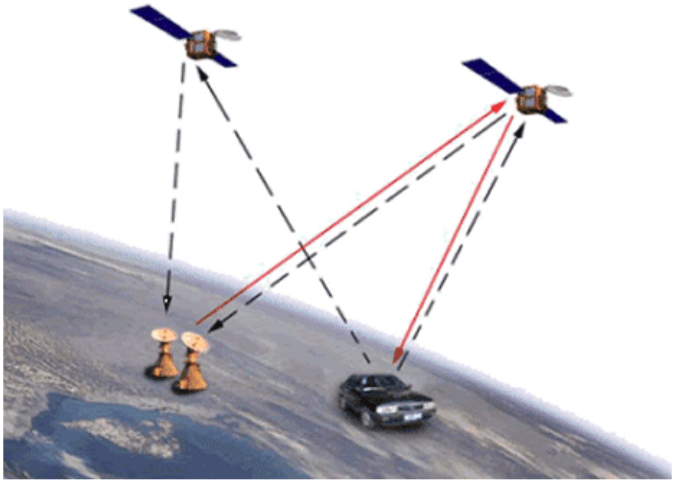

Figure 2-7 RDSS service

In addition to the BNTS RDSS service, the Chinese are in the process of establishing an ingenious SBAS system using the L-band transponder. The SBAS

service will likely share the GPS monitoring structure currently transmitting corrections via the S-band signals.

Beyond the current BeiDou-1 system, China is in the final stages of designing a follow-on system designated BeiDou-2. The new system will consist of 35 satellites, including 5 geostationary orbit satellites and 30 medium Earth orbit satellites, which will offer complete coverage of the globe. There will be two levels of service provided: a free service for those in China and licensed service for the military:

- The free service will have a 10-metre location-tracking accuracy, synchronized clocks with an accuracy of 50ns and measure speeds within 0.2m/s;
- The licensed service will be more accurate than the free service; it can be used for communication and can supply information about the system status to users.

2.1.4.2 Japanese QZSS

The Japanese are developing an ingenious satellite navigation augmentation to the U.S. GPS under the QZSS programme. Under current plans, the QZSS constellation will be designed to support both mobile communications and GPS augmentation services. Particularly, the Japanese intend the navigation services to address shortfalls in GPS satellite visibility in urban canyons and mountainous terrain (Elliott and Christopher, 2006).

To meet the requirements for having a system with satellites operating predominantly over Japan, an inclined geosynchronous or semi-synchronous orbit is being planned. A number of possible constellation designs have been considered. At the time of writing, the Japanese Aerospace Exploration Agency presented an updated concept for the QZSS constellation at an international conference. The agency

proposed a constellation of three distinct and separate inclined HEO orbits, complemented by a return to as many as five spacecraft at geostationary positions.

The overall satellite navigation service in Japan will be provided by 1,200 stations with the capability to receive GPS, the augmentation signals from QZSS and any future independent ranging signals that may be provided by QZSS satellites.

2.2 Navigation with new generation GNSS

Civilian uses of GNSS are growing rapidly due to the quality of the service that GNSS provides, ease of use and low user cost.

Although with the turn off of SA, navigation performance has been greatly improved with current GPS, it is still not sufficient to meet some requirements for safety-of-life navigation applications, especially the user integrity monitoring level in terms of RAIM availability.

Now Galileo is launching and GLONASS is under replenishment. In the near future there are likely three or more satellite-based navigation systems available simultaneously. Navigation with combined systems has attracted more research interest in recent years.

In this section, two aspects will be reviewed. One is the compatibility and interoperability issues between different GNSS systems. The other is the assessed navigation performance with combined GNSS.

2.2.1 Compatibility & interoperability issues

Compatibility is in this context understood as the assurance that one system will not degrade the stand-alone service of the other systems. Interoperability is the ability for the combined use of GNSSs to improve accuracy, integrity, availability and reliability through the use of a single common receiver design (McDonald, 2001).

The relationship among GNSS systems is not one of either cooperation or competition, but, rather, of degrees or levels of cooperation and competition. For joint use, compatibility and interoperability are very important issues.

In this part, only compatibility and interoperability issues among GPS, Galileo and GLONASS are addressed. Three topics are of primary importance: Signal in space, Geodetic coordinate reference frame and Time reference frame (Elliott and Christopher, 2006).

2.2.1.1 Signal-in-space

The ability to support different frequencies increases receiver cost and complexity, because extra or more complex antennas, filters and associated RF components are needed. Furthermore, processing two signals with different carrier frequencies may cause frequency biases in the navigation solution. In particular, the high-precision position solutions that use carrier phase data may be degraded in terms of accuracy.

Galileo/GPS interoperability is realized by a partial frequency overlap with different signal structures and/or different code sequences. At E5a (resp. L5) and E1 (resp. L1) Galileo and GPS signals are broadcast using identical carrier frequencies. At L1 spectral separation of GPS and Galileo signals is given by different modulation schemes. This will drastically simplify user receiver RF front-end design and also allows jamming of civil signals without affecting GPS M-code or the Galileo PRS service (Jeremie, 2003).

However, this simplification in RF frond-end design comes at the cost of mutual interference of both systems due to the overlapping of signal spectra. This so-called inter-system interference adds to the interference of navigation signals belonging to

the same system, called intra-system interference. Only the sum of both types of interference is relevant for determining receiver performance (Dennis et al., 2003).

Another area of interest for interoperability at signal level is the selection of the PRN code families. Currently, two Galileo safety of life signals on E5a and L1 have the same modulation and carrier frequency as the GPS L5 and modernized L1C signals (on GPS III), respectively. Having common code families could bring some more benefits to the user community.

Unlike GPS and Galileo with CDMA modulation, GLONASS employs FDMA technology (GLONASS ICD 2002; Rossbach U, 2000). The differences between FDMA and CDMA signals make combined GPS/GLONASS or Galileo/GLONASS receivers more complex and costly.

At the September 2006 meeting of the Institute of Navigation, Sergey Revnivykh, Deputy Director of the Mission Control Centre of the Central Research Institute of Machine Building of the Russian Federal Space Agency (RFSA) spoke of CDMA as an "option" for GLONASS and added that the system "probably will be able to implement CDMA signals" on the new third frequency, to be added on to GLONASS-K satellites during Phase 3 of GLONASS modernization and at L1 (Inside GNSS News, 2007). A GLONASS switch to CDMA would make manufacture of combined receivers far easier.

2.2.1.2 Coordinate reference frame

For the Galileo coordinate reference system, international civilian standards will be adopted. However, the realization of the Galileo coordinate reference frame should be based on stations different from those of GPS.

The Galileo Terrestrial Reference Frame (GTRF) shall be in practical terms an independent realization of the International Terrestrial Reference System (ITRS) established by the Central Bureau of the International Earth Rotation Service (IERS).

WGS 84 is the coordinate reference frame for GPS. The original WGS 84 realization essentially agrees with NAD 83 (1986). Subsequent WGS 84s, however, approximate certain ITRS realizations.

The differences between WGS84 and the GTRF are expected to be only a few cm. This implies for the interoperability of both GNSS systems that WGS84 and GTRF will be identical within the accuracy of both realizations (i.e. coordinate reference frames are compatible). This accuracy is sufficient for navigation and most other user requirements. Besides, transformation parameters can be provided by a Galileo external Geodetic Reference Service Provider and mapping between the two systems can readily be accomplished in the receiver.

Coordinate reference frames often include Earth gravity models. For example, the WGS-84 uses a spherical harmonic expansion of the gravity potential up to the order and degree of 360. For Galileo, a similar model must be considered.

The coordinate system used by GLONASS is PZ 90. Though the definitions of WGS 84 and PZ 90 sound similar, due to different realizations, there are differences in origin, orientation and scale. Therefore, in order to get meaningful results when combining GPS/GLONASS or Galileo/GLONASS measurements, a coordinate transformation is needed.

2.2.1.3 Time reference frame

The Galileo System Time (GST), modulo 1 second, is planned to be steered to a prediction taken from a number of UTC laboratories obtained through an external Galileo time service provider. GST is specified to be kept to within 50ns (95%) of

International Atomic Time (TAI) over any 1-year time interval. The offset between TAI and GST will be known with a maximum uncertainty of 28ns (2 sigma), assuming the estimation of TAI six weeks in advance. Users equipped with a Galileo timing receiver will be able to predict UTC to 30ns for 95% of any 24 hours of operation.

GPS System Time is the internal GPS navigation time scale, which is not adjusted for leap seconds and which is steered to UTC (USNO) modulo 1 second. GPS System Time is specified to be maintained to within one microsecond modulo integral seconds, and for the past eight years it has been maintained to within +/-25ns of this goal.

GLONASS System Time is maintained by the GLONASS Central Synchronizer by means of a set of hydrogen masers. It is closely coupled to UTC, but with a constant offset of three hours plus a fractional part in the order of microseconds. Therefore, GLONASS system time also considers leap seconds. But The GLONASS ephemeris is referenced to UTC (GL). UTC (GL) is a discontinuous time scale, with leap seconds introduced on 30 June or 31 December as needed. With GPS, the integer second difference between GPS time and UTC is transmitted within the GPS navigation message.

When using a combined GNSS positioning, navigation and timing service there are two options for obtaining the system time offset:

- The user is able to determine the system time offset in the position and navigation processing at the expense of one additional satellite tracked.

- ❖ The offset could be measured by traditional time transfer techniques or precisely estimated in near real time at the monitoring station of the systems using a combined receiver.

The latter option was adopted as part of the EU-U.S. agreement on Galileo/GPS interoperability. The accuracy of this time offset modulo 1 second is specified to be less than 5ns with a 2-sigma confidence interval over any 24-hour period.

The Russian Military Space Forces as the operator of the GLONASS system are planning to include the time difference between GLONASS system time and GPS system time in the navigation message of GLONASS-M spacecraft.

In addition to the system time offset between these systems, there is another problem when using combined navigation services. Future receivers may have the same or different receiver clocks for different system signals, so one more clock parameter may be introduced in the navigation mathematical model.

2.2.2 Navigation with new GNSS

Combinations with the new GNSS systems will provide more than 100 satellites, with multiple frequency band navigations signals. A number of studies has been carried out to evaluate navigation performance by integrating these systems (Hein et al., 1997; Ryan and Lachapelle, 2000; Kyle, 2001; O'Keefe, 2001; Verhagen, 2002; Ochieng and Sauer, 2001; Ochieng et al., 2002; Blomenhofer et al., 2004; Lee, 2004; Daghay et al., 2005; Hewitson et al., 2004). Based on the simulated performance of GPS, Galileo, and combined GPS and Galileo, the following conclusions can be made:

- Although the additional satellites available in a combined constellation clearly improve the accuracy performance, it is of limited significance especially in the horizontal direction (Ochieng and Sauer, 2001);

- Using a combined GPS and Galileo system can clearly improve the availability performance, especially in extreme masking environments, where navigation with GPS only is very difficult (Kyle, 2001);
- There is a significant improvement in integrity using a combined Galileo/GPS system compared to the performance using the Galileo system alone. The use of a combined constellation can either reduce the minimum position shift that can be detected at a given probability level or can increase the probability with which a blunder of a given size will be detected overall (Daghay et al., 2005; Hewitson et al., 2004; Ochieng et al., 2002).

2.3 High precision relative positioning with new GNSS

The Global Navigation Satellite Systems (GNSS) provide two main types of measurements: pseudorange and carrier phase. The main differences between them are measurement precision (metre vs millimetre) and integer ambiguity associated with carrier phase. If we can reliably resolve the carrier phase ambiguity, then the carrier phase measurement can be conceptually turned into a high-precision range observation and positioning accuracy at the centimetre level could be achieved every epoch. This can benefit an large number of scientific applications.

Ambiguity resolution has been a continuing challenge and a rich source of research over the last decade. From the first demonstration of the use of the GPS carrier phase observations for sub-centimetre-level precision positioning and surveying, to the latest development of the instantaneous ambiguity resolution on-the-fly (OTF) techniques, from zero-distance baseline to long baseline more than 1,000km, from a single frequency band of GPS to multiple frequency bands of new GNSS

systems, a lot of ambiguity resolution techniques has been proposed by many groups from all over the world.

Ambiguity validation is equally important in order to ensure reliable ambiguity resolution. Ambiguities cannot be fixed if there is not enough confidence. A lot of validation criteria or tests or methods have been proposed over the last decade. And obviously it is still an open problem.

Three aspects are summarized and discussed here, including ambiguity resolution over short, long-distance baselines and ambiguity validation.

2.3.1 Ambiguity resolution over a short baseline

- **Ambiguity resolution with current GPS**

In the past, various ambiguity resolution algorithms have been developed for different applications such as rapid static positioning, kinematic or real-time navigation, etc. Generally these techniques can be classified according to how they attempt to make use of the information contained within the receiver measurements.

The first class includes the very first ambiguity resolution technique developed, namely the Ambiguity Function Method (AFM) (Counselman and Gourevitch, 1981; Remondi, 1984; Han and Rizos, 1996a). This technique uses only the fractional value of the instantaneous carrier phase measurement and hence the ambiguity function values are not affected by the whole-cycle change of the carrier phase or by cycle slips. Generally it provides relatively poor computational efficiency and consequently is of little importance other than of historical interest (Kim and Langley, 2000).

The second class comprises the most abundant group of techniques which are based on the theory of integer least-squares (ILS) (Teunissen, 1993). Parameter estimation under the theory is carrier out in three steps – the float solution, the integer ambiguity estimation and the fixed solution. Each technique makes use of the

variance-covariance matrix obtained at the float solution step and employs different ambiguity search processes at the integer ambiguity estimation step. The following are some representative techniques in this class: the Least-Squares Ambiguity Search Technique (LSAST) (Hatch, 1990); the Fast Ambiguity Resolution Approach (FARA) (Frei and Beutler, 1990); the modified Cholesky decomposition method (Euler and Landau, 1992); the Least-Squares AMBiguity Decorrelation Adjustment (LAMBDA) (Teunissen, 1994; Teunissen, 1995); the null space method (Martin-Neira et al., 1995); the Fast Ambiguity Search Filter (FASF) (Chen and Lachapelle, 1995); and the Optimal Method for Estimating GPS Ambiguities (OMEGA) (Kim and Langley, 1999).

The second class – ILS, can be divided into two categories. The first category takes advantage of both pseudorange and carrier phase measurements, so the observation model is full rank; the second category uses only carrier phase ones, so its observation model is rank defect. Though the former one generally takes less time, the latter has its own advantages, that is, it is free from the effects of big multipath in pseudorange measurements.

In addition to the above developments trying to solve full ambiguities, a partial solution concept has been proposed (Teunissen, 1998; Teunissen et al., 1999). The idea of partial ambiguity resolution is based on the fact that the success rate will generally increase when fewer integer constraints are imposed. Due to its higher reliability, if the accuracy provided can meet navigation requirements, a partial solution can improve navigation continuity.

However with current GPS, both the efficiency and reliability of ambiguity resolution is not high (Chen, 1992) even for short baselines. Fewer available carrier phase frequency bands (only L1, L2) is an important limitation factor.

- **Ambiguity resolution with modernized GPS and Galileo**

In the future, both modernized GPS and Galileo are expected to have at least three carrier phase frequencies. With more carrier phase data available, more frequency combinations with longer equivalent wavelengths can be formed. This will provide more opportunities for fast and reliable ambiguity resolution.

In recent years, studies on fast ambiguity resolution with new GNSS have been carried out by many researchers (Hatch et al., 2000, Tiberius et al., 2002; Vollath et al., 1998; Zhang et al., 2003; Werner and Winkel, 2003; Schlotzer and Martin, 2005; Zhang, 2005). A new kind of ambiguity resolution method class has been developed. Instead of estimating all ambiguities at one time, this class solves ambiguities step by step from the easiest ones to the most difficult. They are specially designed for multiple frequency bands of modernized GPS and Galileo by taking advantage of inter-frequency carrier phase linear combinations. Representative techniques in this class include: three-carrier ambiguity resolution (TCAR) (Forsell et al., 1997), Integrated TCAR (ITCAR) (Vollath et al., 1998) and Cascade Integer Resolution (CIR) (Jung et al., 2000). They share a similar basic approach and can all be called the Cascading Ambiguity Resolution (CAR) method.

This class can be divided into two categories. The first category is the simplest ambiguity resolution technique and is called geometry-free which determines the carrier phase ambiguity directly with pseudorange measurement. The second category is geometry-based, in which satellite geometry strength is taken advantage of. Generally the second category performs better than the first one, but with a heavy computational burden.

However two problems are left open with modernized GPS and Galileo. The first is how to select optimal combinations for CAR. The second is which ambiguity

resolution method is best compared with ILS. These two problems are important for fast and reliable ambiguity resolution.

2.3.2 Ambiguity resolution over a long baseline

Unlike short baselines, due to weakened spatial correlation, the remaining atmospheric effect of long baselines (> 10 or > 30km) cannot be neglected after double differencing, especially ionospheric ones.

With current GPS, if without external ionospheric information, traditionally, there are two methods to deal with ionosphere-delay: ionosphere-delay float and ionosphere-free.

With the first method, ionosphere delay is parameterized in the mathematical model and assumed to be invariant with time. This method can easily lead to wrong ambiguity resolutions when there are active solar activities.

With the second method, the integer property of ambiguities is lost due to only two frequency bands being available.

So with current GPS, ambiguity resolution is not an easy task and a fast static ambiguity resolution is almost impossible. The traditional approach has been long static occupation allowing time for the ambiguities to converge to integers. Typical occupation time can be hours, depending on baseline length and atmospheric conditions, and is far too restrictive for many applications.

In recent years, much research work has been carried out to investigate ambiguity resolution performance over long baselines with new GNSS. Generally, the CAR method is used (Zhang et al., 2003; Zhang, 2005) with the remaining ionospheric effect just ignored. This is only feasible for ambiguity resolution of combinations with long wavelength when the baseline is not very long (e.g. < 100km). When the baseline grows longer, ambiguity resolution reliability becomes questionable.

2.3.3 Ambiguity validation

To ensure reliable ambiguity resolution, ambiguity validation is an important step. Several validation methods have been proposed over the last decade and the following are some representative methods: the F-ratio (Frei and Beutler, 1990; Landau and Euler, 1992), R-ratio (Euler and Schaffrin, 1991; Leick, 2003), difference-test (Tiberius and De Jonge, 1995), projector test (Wang et al., 1998a; Han, 1997) and W-test (Wang et al., 1998a).

In recent years, another class of validation methods called Integer Aperture (IA) estimators (Teunissen, 2003) has been proposed. It provides a theoretically sound, overall approach to the problem of integer estimation and validation and the user has control over the fail rate and thus also over the amount of discernibility. With the concept of integer aperture estimation, three possibilities are distinguished: the success rate, the fail rate and the undecided rate. To guarantee that the probability of fixing incorrectly is low enough, a fixed fail rate is generally chosen as the decision parameter. Among the IA class, the Ellipsoidal Integer Aperture (EIA) estimator (Teunissen, 2005) is an outstanding one with an easy-to-evaluate fail-rate.

Analysis (Teunissen and Verhagen, 2004; Verhagen, 2005) has shown that the F-ratio, R-ratio, projector test and difference-test all belong to the IA estimator class.

In the W-test, the test statistic W is assumed to have the t-distribution. However, analysis (Verhagen, 2005) has shown that this is not true.

In spite of the above developments, ambiguity validation is far from being resolved.

Chapter 3 GNSS Data Simulator

A GNSS data simulator has been developed in this research, as the Galileo system is not yet fully operational. The simulator is able to simulate pseudorange and carrier phase measurements in different frequency bands from various satellite systems including GPS, GLONASS, and Galileo.

The radio frequency bands for these systems are all in L band. Thus the error models used in the simulator are based on detailed GPS satellite signal error behaviour and realistic GPS error models, including orbit errors, satellite and receiver clock errors, propagation errors (ionosphere, troposphere), multipath and measurement noise.

In this chapter, the data models used for the GNSS data simulator are presented and the positioning results from simulated Galileo data show that the error models applied in the GNSS simulator are realistic.

3.1 Data models for GNSS simulator

3.1.1 Satellite constellations

The constellations considered in the GNSS simulator include Galileo, GPS and GLONASS.

- **Galileo**

The Walker 27/3/1 constellation (European Commission, Galileo Mission High Level Definition Document 2002) is adopted for Galileo data simulation. A simplified circular orbit with an orbit height of 24,000km is used in the simulation.

- **GPS**

GPS constellation (28 satellites) and orbit parameters on January 3rd, 2004 are adopted (Table 3-1 gives satellite orbit plane locations) for GPS data simulation.

Table 3-1 Parameters of the GPS constellation

Block sequence	SVN	PRN	Orbit Plane
II-2	13	02	B-5
II-5	17	17	D-6
II-9	15	15	D-5
II-10	23	23	E-5
II-11	24	24	D-6
II-12	25	25	A-2
II-14	26	26	F-2
II-15	27	27	A-4
II-16	32	01	F-6
II-17	29	29	F-5
II-19	31	31	C-3
II-20	37	07	C-5
II-21	39	09	A-1
II-22	35	05	B-4
II-23	34	04	D-4
II-24	36	06	C-1
II-25	33	03	C-2
II-26	40	10	E-3
II-27	30	30	B-2
II-28	38	08	A-3
IIR-2	43	13	F-3
IIR-3	46	11	D-2
IIR-4	51	20	E-1
IIR-5	44	28	B-3
IIR-6	41	14	F-1
IIR-7	54	18	E-4
IIR-8	56	16	B-1
IIR-9	45	21	D-3

- **GLONASS**

For the GLONASS constellation, the full constellation (with 24 satellites in three orbital planes) (GLONASS ICD 2002; Rossbach, 2000) is used in the simulation. Similar to Galileo constellation simulation, a simplified circular orbital model is adopted for convenience.

3.1.2 Reference frames

- **Coordinate reference frames**

The coordinate reference frames for different satellite GNSS systems are maintained by different system operators, i.e. WGS84 for GPS, PZ90 for GLONASS and GTRF for Galileo. For GPS and Galileo, in practice the reference frames are the realization of the International Terrestrial Reference Frame (ITRF) to an accuracy of a few centimetres (Elliott and Christopher, 2006). For GLONASS, the transformation between PZ90 and the ITRF has been good (Rossbach, 2000). Therefore, in the GNSS simulator, the differences of the reference frames will not be considered with different GNSS systems and a unified ITRF is adopted for all GNSS systems in the simulation. With this approach, the performance analysis from a single GNSS system will not be affected. With the integration of a number of GNSS systems, the effects of reference frame differences are within a few centimetres.

- **Time reference frames**

The time standards of different GNSS systems are maintained by different system operators. Therefore, there are time offsets among different GNSS systems. With current technology, the time synchronization accuracy between two time references of 5ns can be achieved (Elliott and Christopher, 2006), which will lead to a range error of less than one and half a metre. Both Galileo and GLONASS systems plan to

broadcast their system time offsets compared to GPS time reference (GLONASS interface control document version 5.0).

In the GNSS simulator, one time offset can be set for each GNSS system or a common time reference can be applied for all GNSS systems.

3.1.3 Error models

The pseudorange and carrier phase measurements from GNSS systems are affected by many error sources, i.e. clock errors, propagation errors, orbit errors, antenna offset and phase centre errors, inter-channel biases, relativity effects, multipath, etc. (Elliott and Christopher, 2006). As the signals of the three GNSS systems considered in this study are all in the L band, the error models which have been widely applied in GPS positioning will be adopted for the GNSS simulator.

In the simulator, the main error models include orbital error and satellite clock error, measurement noise, multipath effect, receiver clock error and ionospheric and tropospheric delays.

- **Satellite clock**

The satellite clock error is simulated in two ways. The first method models the satellite clock error by a second-order polynomial to count for the specific offset relative to the reference time, including systematic clock errors (bias, drift and acceleration) and thermal noise errors. Although the random atomic clock errors should be modeled by coloured noise models (Stephen and Willy, 1989), in this simulator, a simple Gaussian white noise model is adopted. The sizes of systematic and random clock errors are user configurable.

The second method directly simulates satellite clock errors based on GPS satellite broadcast clock errors, which can be obtained by comparing the satellite clock errors computed from broadcasting navigation messages and those computed from the precise clock error estimates from the International GNSS Service (IGS) products.

- **Satellite orbit**

Similar to GPS, the future Galileo navigation message also gives the Keplerian parameters to compute the satellite coordinates. The GLONASS broadcasts the satellite coordinates at different time epochs. As the orbit determination methods for different GNSS systems are similar, the orbital error behaviour is expected to be similar to GPS. The orbit errors used in the simulator are obtained from the differences from the orbit computed from the broadcast ephemeris and the precise ephemeris from the IGS products. The precise orbit will be used to generate the measurements while the orbits with errors will be used for positioning computation.

- **Ionosphere delay**

In the simulator, ionosphere delay for different frequencies can be simulated using two methods and is user configurable. The first method applies the Klobuchar Model (Klobuchar, 1987) to simulate the vertical ionospheric delays. Then a mapping function is applied to convert it to the slant delays. The second method is to interpolate the ionsopheric delay based on the IGS global ionosphere model (Final Ionospheric TEC grid) (Joachim, 2003). For different frequency bands, only the first-order ionospheric delay is simulated and the higher-order part is not considered.

Figures 3-1 to 3-5 are samples of zero-differenced, single-differenced and double-differenced ionospheric delays for one satellite simulated using the Klobuchar Model. From the figures we can see that the zero-differenced ionospheric delays are in the range of 15-24m for a particular set of Klobuchar model parameters broadcast from a

GPS satellite. The differential process can significantly reduce the effects of ionospheric delays. The ionospheric residuals for relative positioning are increased with baseline distance. For a very short baseline (i.e. 1km), the ionospheric delay residuals between two stations are very small and can be ignored. When the distance of baseline exceeds one thousand kilometres, the ionospheric delay residuals can reach several metres.

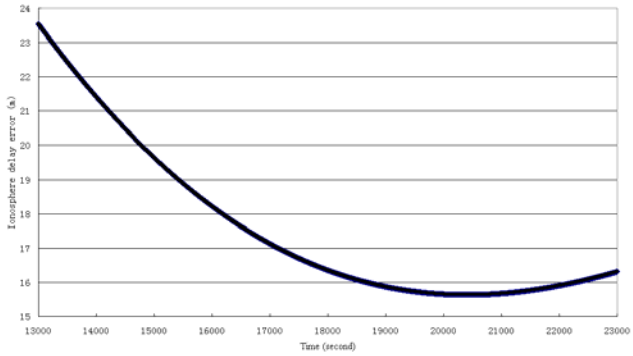

Figure 3-1 Simulated zero-differenced ionospheric delays

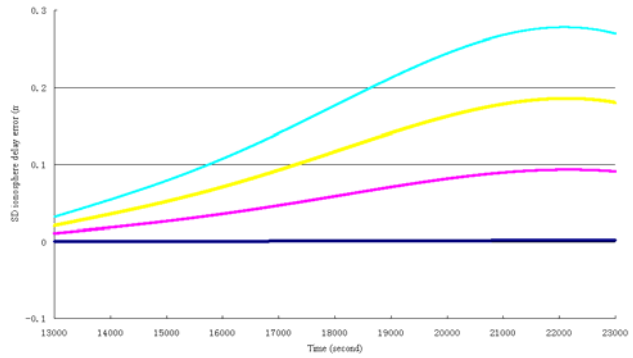

Figure 3-2 Simulated single-differenced ionospheric delays of different baselines (1km, 45km and 90km from bottom to top)

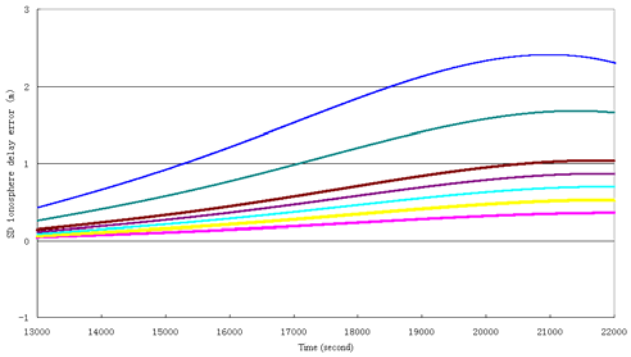

Figure 3-3 Simulated single-differenced ionospheric delays of different baselines (170, 260, 345, 430, 520 & 860km from bottom to top)

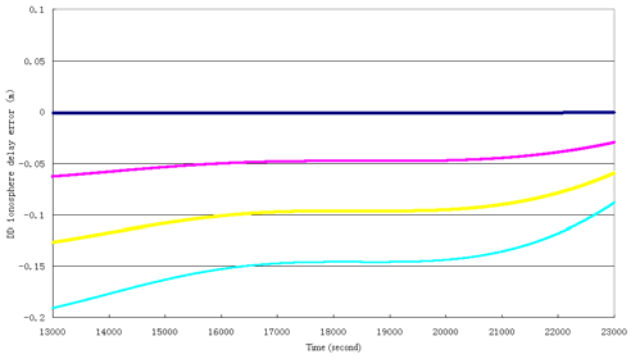

Figure 3-4 Simulated double-differenced ionospheric delays of baselines (1km, 45km and 90km from top to bottom)

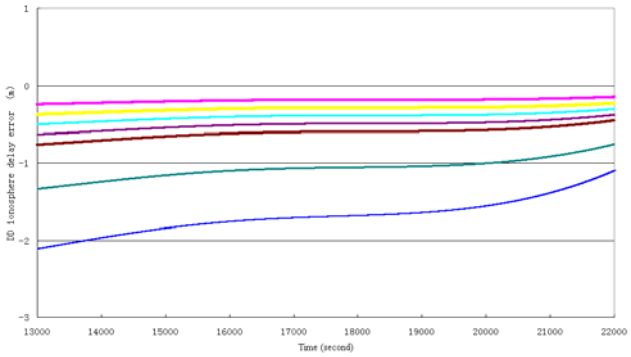

Figure 3-5 Simulated double-differenced ionosphere delays of different baselines (170, 260, 345, 430, 520 and 860km from top to bottom)

- **Troposphere delay**

There are a number of models available for tropospheric delays, i.e. Saastamoinen model (Saastamoinen, 1973), Hopfield model (Hopfield, 1969), etc. In the data

simulator, troposphere delay is simulated using the Modified Hopfield Model (Goad and Goodman, 1974).

The effects of tropospheric delays on zero-differenced, single-differenced, double-differenced observables are plotted in Figures 3-6 to 3-10.

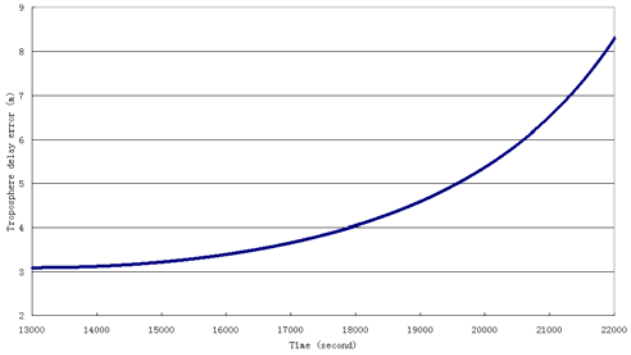

Figure 3-6 Troposphere delays for one satellite

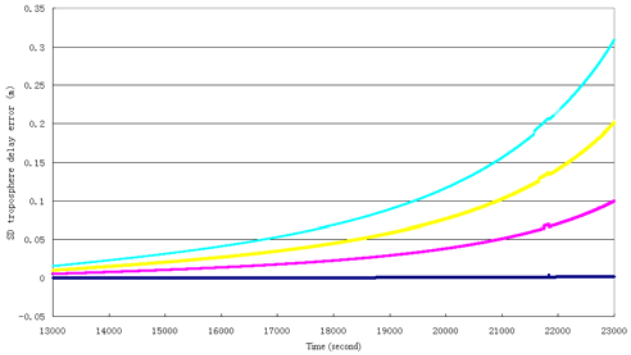

Figure 3-7 Single-differenced troposphere delay residuals for different baselines (1km, 45km and 90km from bottom to top)

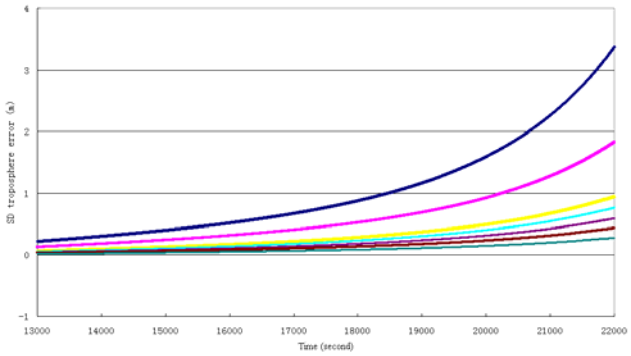

Figure 3-8 Single-differenced troposphere delay residuals for different baselines (170, 260, 345, 430, 520 & 860km from bottom to top)

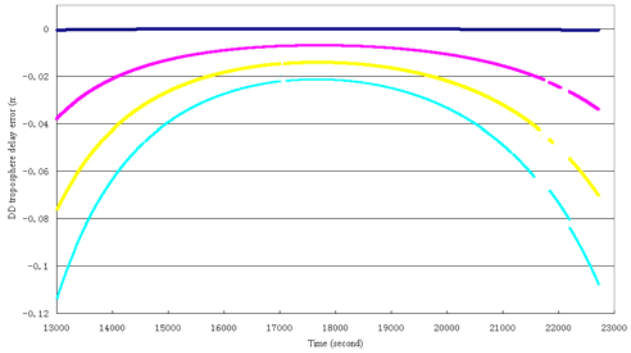

Figure 3-9 Double-differenced troposphere delay residuals for different baselines (1km, 45km and 90km from top to bottom)

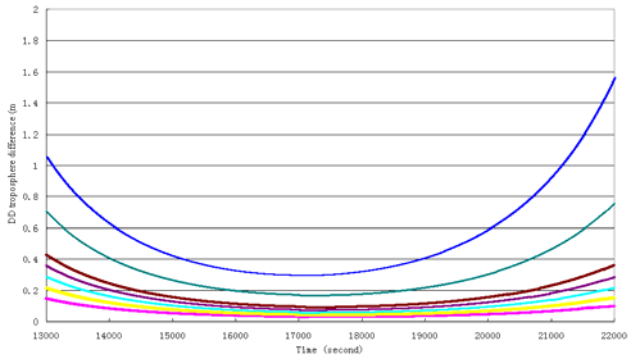

Figure 3-10 Double-differenced troposphere delay residuals for different baselines (170, 260, 345, 430, 520 & 860km from bottom to top)

- **Receiver clock**

The receiver clock is modelled as a specific offset relative to the reference time, including: systematic clock errors (bias, drift and acceleration) and thermal noise errors. White noise is used to represent the clock random errors.

- **Measurement noise**

Code and carrier phase observation noises are simulated according to Gaussian normal distribution model (Parkinson, 1996). Their sizes are user configurable.

- **Multipath effect**

The code range error E_{mr} and carrier phase range error E_{mp} due to the multipath effect are simulated according to the following formula (Galileo System Simulation Facility – Algorithms and Models 2005):

$$E_{mr} = A_{br} + A_r K_{env} K_{rec} K_{ran} \sin(\omega * Elev) \quad (3\text{-}1)$$

$$E_{mp} = A_{bp} + A_p K_{env} K_{rec} K_{ran} \sin(\omega * Elev) \quad (3\text{-}2)$$

Where A_r and A_p are the amplitude of the multipath effects respectively, A_{br} and A_{bp} are corresponding random residual multipath bias terms (mean = 0), K_{rec} is the receiver sensibility factor (0 to 1), ω is the multipath frequency and *Elev* is the elevation angle of the transmitter relative to the receiver. K_{ran} is a time-correlated Gaussian distribution noise with a mean of 0. K_{env} depends on the receiver environment characteristics. Table 3-2 lists typical K_{env} values in different environments (Galileo System Simulation Facility – Algorithms and Models 2005).

Table 3-2 K_{env} values

Value	Environment
0	No fading or reflections
0.25	Rural area, fading only
0.5	Urban area, fading and one specular reflection only
1	Urban area, fading and multiple reflections
10	Excessive multipath

Figures 3-11 to 3-15 give the multipath errors of code observations using different environmental values K_{env}. The sigma value of A_{br} is set to 0.2m.

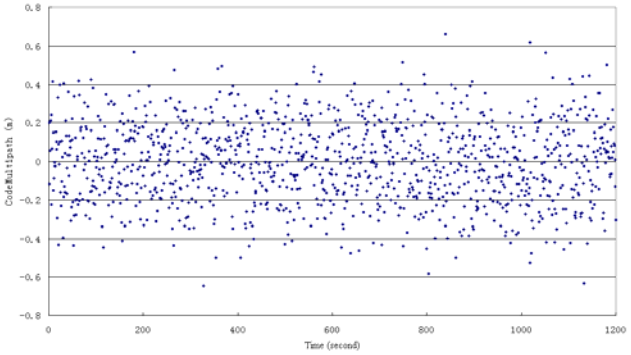

Figure 3-11 E1/L1 code Multipath error when K_{env}=0

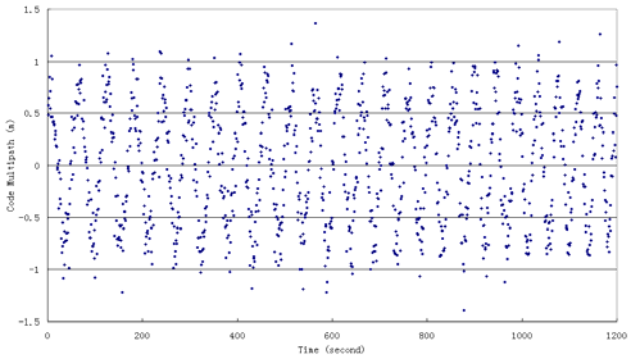

Figure 3-12 E1/L1 code Multipath error when K_{env} =0.25

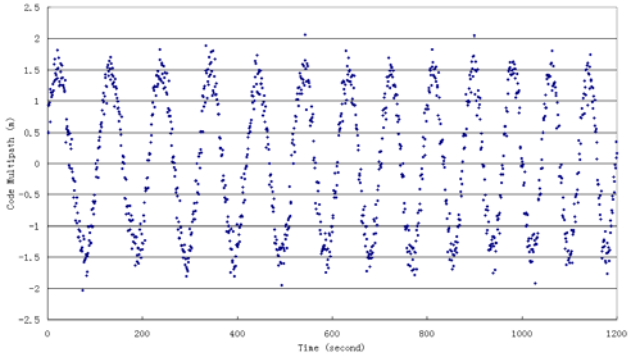

Figure 3-13 E1/L1 code Multipath error when K_{env} =0.5

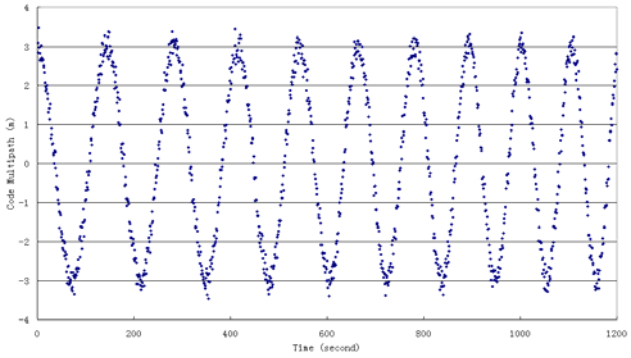

Figure 3-14 E1/L1 code multipath error when K_{env} =1

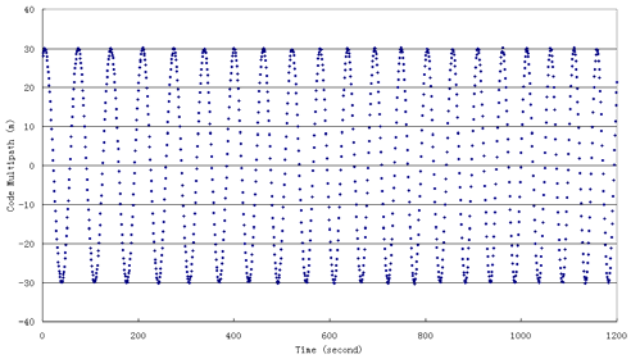

Figure 3-15 E1/L1 code multipath error when K_{env} =10

These figures show that when K_{env} becomes bigger, the code multipath error increases from less than one metre to about thirty metres, the error characteristics change from random (i.e. K_{env} =0) to approximately periodical (i.e. K_{env} =10).

Figure 3-16 is a sample of carrier phase multipath error when K_{env} =0.5 and sigma of A_{bp} = 0.01. The errors are approximately randomly distributed and the magnitudes do not exceed one quarter of the wavelength.

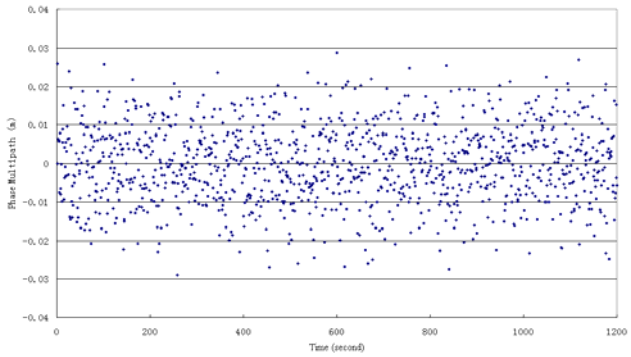

Figure 3-16 E1/L1 phase multipath error when K_{env} =0.5

3.2 Program structure

The program's structure of the simulator can be seen in Figure 3-17.

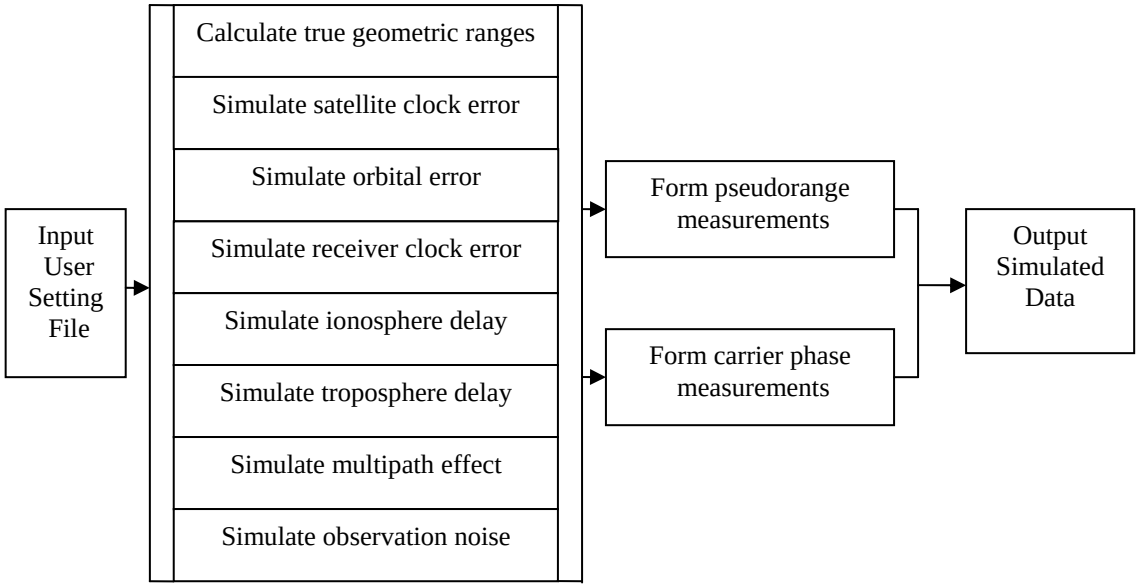

Figure 3-17 Programme structure of the simulator

User setting file consists of all user configurable parameters, including output file name, station(s) name(s) and coordinates, broadcast ephemeris and/or precise ephemeris file, the starting time and the ending time of observations, data sampling interval, the sizes for the satellite clock and receiver clock noises, the sizes for pseudorange and carrier phase measurement noises and the cutoff elevation angle. Users can also select whether to simulate cycle slips.

Based on the station coordinates and ephemeris file, the true geometric ranges from the station to satellites at any epoch can be calculated. Then the main error sources listed in Figure 3-17 are simulated, including satellite clock error, orbital error, receiver clock error, ionosphere and troposphere delays, multipath effect and observation noise. Afterwards pseudorange and carrier phase measurements are formed separately by combining the true receiver with satellite distances and all simulated errors together. Finally pseudorange and carrier phase measurements are output to the user indicated file.

3.3 Validation test

In the simulator, the clock errors of both satellite and receiver are modeled as having a specific offset relative to the reference time. The clock offset includes: systematic clock errors (bias, drift and acceleration) and thermal noise errors. There are generally five sources of clock noises that can be present:

- Random walk on frequency
- White noise on frequency
- Flicker noise on frequency
- White noise on phase
- Flicker noise on phase

In the simulator, only the white noise on frequency is implemented, since it is the basic noise classically associated with atomic clocks. This is also the model used in Galileo System Simulation Facility (GSSF) officially developed by VEGA for Galileo system design (Galileo System Simulation Facility – GSSF Models and Algorithms, 2005).

For orbital error simulation, the differences between precise orbit provided by IGS and broadcast orbit are adopted. Since the accuracy of the precise orbit can reach up to 5cm, the orbital error in simulated measurement is very similar to practical one of GPS.

Since the final ionosphere TEC grid provided by IGS can be as precise as to 2-8 TECU, the ionosphere delay simulated by interpolating the TEC grid will be similar to practical one with expected TEC difference less than 10 TECU generally.

For troposphere delay, the modified Hopfield model appears to predict the tropospheric effects by 92% to 95% depending on the amount of atmospheric information available to the user (Wells et al., 1987). So the simulated tropospheric

delay is almost the same to the practical one with the difference less than 2dm generally.

Observation noise sources include analogue-to-digital quantization, and tracking loop design. Most of these noises are essentially white in nature and can be modeled by a Gaussian normal distribution.

The model used in the simulator for multipath effect represents a parameterization of the observations and conclusion drawn from the reference: Global Positioning System: Theory and Applications, Vol. I, B.W. Parkinson, J.J. Spilker, AIAA, Chapter 14 Multipath Effects.

To validate the suitability of the error models applied in the GNSS data simulator, the 'receiver' positions is determined by using the simulated pseuodrange measurements and then compared with the inputted "true position" to examine the size of the positioning errors. The point positioning method is used because the positioning errors will be affected by all the simulated errors. The simulated errors include orbital error, satellite clock error, receiver clock error, tropospheric delay, ionospheric delay, pseudorange measurement noise and multipath. The IGS precise ephemeris is used to simulate satellite's orbit. Ionospheric delay errors are simulated using the IGS global ionosphere maps. Tropospheric delay error is simulated with modified Hopfield model. The parameters for measurement noise and multipath are given in Table 3-3.

Table 3-3 Data Simulation for Point Positioning

Error source	Error size
Code observation noise	0.5 m
Code multipath error	Sigma of A_{br} = 0.2m; K_{env} =0.25

In data processing, the broadcast ephemeris is used for positioning computations. The ionospheric delay errors are corrected by the Klobuchar Model and the tropospheric delay errors are corrected using the dry part of Modified Hopfield Model only.

Figures 3-18 and 3-19 are the horizontal and vertical positioning errors from the simulated data.

It can be seen from the two figures that the horizontal positioning errors are in the range of 2 to 6m, while the vertical errors are up to 20m, which is what we expected from GNSS positioning (Global Positioning SPS Performance Standard 2001). Thus the error models used in the GNSS simulator reasonably represent the real situation.

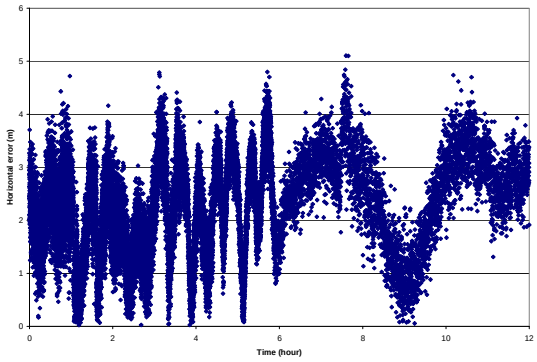

Figure 3-18 Horizontal position error of point positioning with Galileo

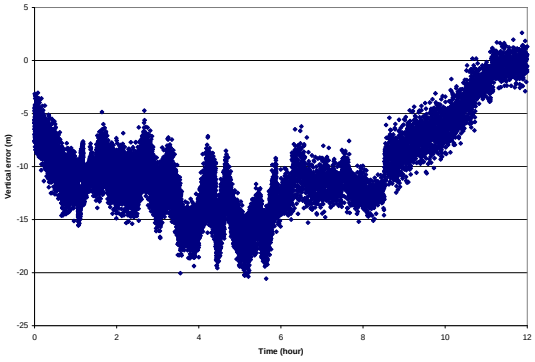

Figure 3-19 Vertical position error of point positioning with Galileo

Chapter 4 Point Positioning Performance Analysis with New GNSS Systems

Point positioning is the basic positioning mode for GNSS systems and has been widely used in navigation, which utilizes a single GNSS receiver to determine the absolute position of a point. Both pseudorange and carrier phase measurements can be used for point positioning. Pseudorange measurement is commonly used due to its robustness for positioning computations. The point positioning accuracy with pseudorange measurement is around 10m. In recent years, the Precise Point Positioning (PPP) technique has been developed which utilizes carrier phase measurement and can achieve centimetre level positioning accuracy (Kouba and Heroux, 2001; Bisnath and Langley, 2001a; Bisnath and Langley, 2001b; Bock et al., 2002; Colombo et al.,; 2004; Chen et al., 2004).

For navigation applications, any navigation system needs to fulfil certain required navigation performance factors, i.e. accuracy, integrity, availability continuity and coverage (Federal Radionavigation Plan 2005). It is well known that GPS alone cannot satisfy navigation requirements for some specific applications, i.e. civil aviation (Civil Aviation Authority 2004). The development of the US WAAS and the European EGNOS systems (Gauthier et al., 2001) is an important step to provide augmentation systems to further improve navigation performances of GNSS, particularly accuracy, integrity and coverage (Mohamed et al., 2000).

In the near future, a number of GNSS systems will be available, including modernized GPS, Galileo, GLONASS and Chinese BeiDou systems. Integrating these systems, undoubtedly, will improve navigation performance, due to the fact that more measurements and frequency bands are available (Hewitson and Wang, 2004). Of

course, the compatibility and interoperability issues have to be taken into account when integrating these systems, which have been discussed in Chapter 2 of this dissertation.

In this chapter, the navigation performance improvements is analyzed by integrating different systems together, using simulated data. Except some general analyses in the accuracy and RAIM performance improvements by combining GPS/Galileo, this study concentrates on the performance improvements in urban environments, where GPS alone is particularly vulnerable (Miller et al., 1995; Kozlov and Tkachenko, 1998; Grejner-Brzezinska et al., 2001; Berefelt et al., 2004). Also, the Precise Point Positioning performance with combined GPS and Galileo is investigated in this chapter.

4.1 Accuracy improvement with GPS/Galileo integration

4.1.1 Mathematical models of GPS and Galileo integration

Both GPS and Galileo establish their coordinate and time references independently. To process measurements from GPS and Galileo together, the time and coordinate systems have to be synchronized first. As both GPS and Galileo systems have in practice adopted the ITRF as the reference frame, the coordinate frame errors caused by different realizations of the ITRF by the two systems are expected to be within the centimetre level (Elliott and Christopher, 2006), which will not significantly affect positioning accuracy when the two systems are integrated. On the other hand, the absolute clock errors for GNSS is in the order of 10-20ns (Elliott and Christopher, 2006), which is equivalent to a range error of around 5m. Thus, there exists a system time offset between GPS and Galileo. Techniques have been developed to synchronize different time reference frames using GNSS measurements with the

accuracy of sub-ns (Píriz et al., 2006) and the Galileo system plans to estimate the time offset between GPS and Galileo and broadcast it to users (European Commission 2002). Alternatively, users may estimate this time offset by using an additional measurement. Moreover, the integrated receivers may use one or two receiver clocks in future GPS/Galileo receivers. Then the receiver clock errors have to be estimated separately if two receiver clocks are used. In general, the clock errors may be described by the following four cases, which require different mathematical models:

Case 1: same receiver clock without a system time offset

Case 2: same receiver clock with a system time offset

Case 3: different receiver clocks with a system time offset

Case 4: different receiver clocks without a system time offset

The mathematical models corresponding to each of the above cases will be discussed separately.

- **same receiver clock without a system time offset**

This case is the simplest one and the mathematical model is the same as a single system (Leica, 2004) which is:

$$AX + Bt_R = L \tag{4-1}$$

where t_R is receiver clock error and X is position parameters. A and B are corresponding coefficient matrices and L is the observation vector.

- **same receiver clock with a system time offset**

In this case, the time offset between GPS and Galileo has to be estimated, together with other parameters in Eq. (4-1). The mathematical model for GPS measurement is the same as Eq. (4-1), while the observation equation for Galileo measurement is

$$AX + Bt_R + Ct_S = L \tag{4-2}$$

where t_S is the system time offset between GPS and Galileo and C is the corresponding coefficient matrix.

- **different receiver clocks with a system time offset**

This is the most complicated case and the mathematical model is:

$$AX + B_{Galileo}t_{Galileo} + B_{GPS}t_{GPS} + Ct_S = L \tag{4-3}$$

where, $t_{Galileo}$ is the receiver clock error for Galileo, t_{GPS} is the receiver clock error for GPS. A, $B_{Galileo}$, B_{GPS} and C are corresponding coefficient matrices.

B_{GPS} is 0 (a Galileo measurement) or 1 (a GPS measurement).

$B_{Galileo}$ is 0 (a GPS measurement) or 1 (a Galileo measurement).

C is 0 (a GPS measurement) or 1 (a Galileo measurement).

Actually, for single epoch point positioning, $B_{Galileo}$ and C have the same values and can be combined together. Therefore, the mathematical model can be simplified as:

$$AX + B_{Galileo}t_{Galileo} + B_{GPS}t_{GPS} = L \tag{4-4}$$

where $t_{Galileo}$ is the sum of the Galileo receiver clock error and the system time offset between GPS and Galileo.

- **different receiver clocks without a system time offset**

The mathematical model for this case is:

$$AX + B_{Galileo}t_{Galileo} + B_{GPS}t_{GPS} = L \tag{4-5}$$

which has the same form as Eq. 4-4 for case 3.

4.1.2 Global PDOP Analysis

Position Dilution Of Precision (PDOP) is an important factor to quantify GNSS positioning accuracy (Leica, 2004) and the positioning error can be expressed as:

$$\delta = PDOP\,\delta_0 \tag{4-6}$$

In the above equation, δ_0 denotes the standard deviation of the observations and δ is an one-number representation of the standard deviation of position. PDOP is a factor related to visible satellite geometry. With a low PDOP value, navigation solutions can be expected to be more precise.

By giving satellite constellations, we are able to calculate the PDOP values at any location on the earth. Figures from 4-1 to 4-3 are three global PDOP maps of GPS alone, Galileo alone and GPS + Galileo. Ideally, one should estimate the PDOP values for every point on the earth and over the whole period of satellite navigation. For simplicity, here the PDOP values in a global distribution is showed only at a particular epoch. In the computation, snapshots of PDOP values are taken around the world ($1^\circ \times 1^\circ$) with a masking angle of 15°. Based on the computation, we can summarize below:

1. With GPS or Galileo alone:
   - All PDOP values are bigger than 1.0.
   - Most places have values between 1.0 and 5.0.
   - There are a few places where PDOP values are bigger than 5, even 10.
- With GPS + Galileo:
   - There are many places with values between 0.5 and 1.0.
   - Most places have values between 0.5 and 1.5.
   - All PDOP values are less than 4.0.

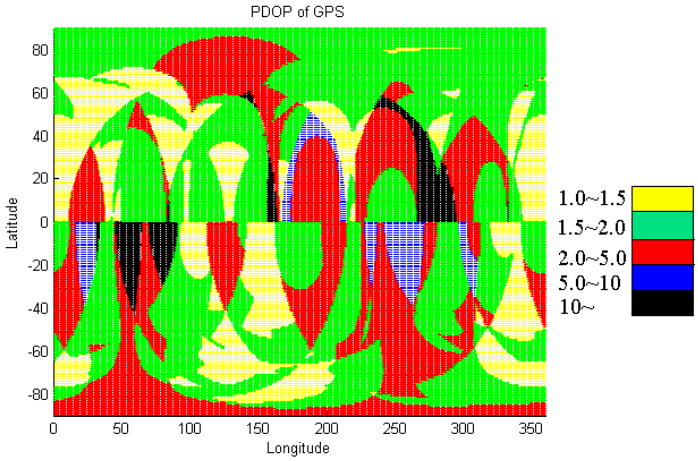

Figure 4-1 Global PDOP with GPS alone

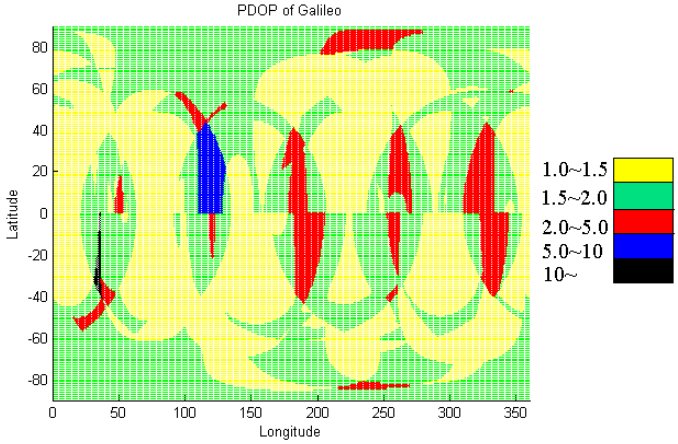

Figure 4-2 Global PDOP with Galileo alone

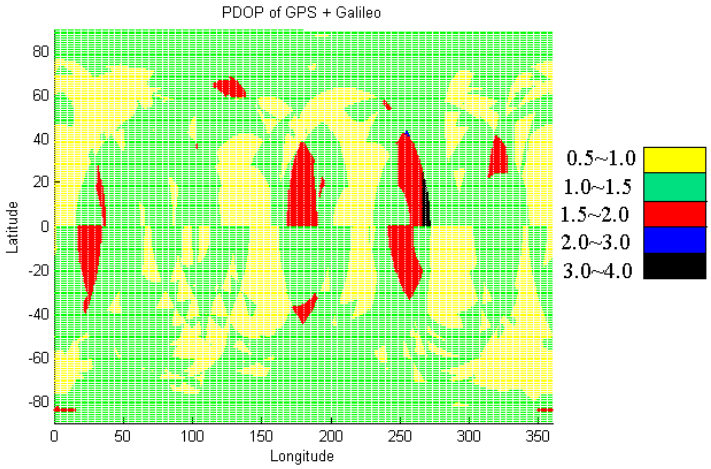

Figure 4-3 Global PDOP with GPS + Galileo

With the integration of GPS and Galileo, the PDOP values are decreased compared with GPS or Galileo alone, due to more satellites being available.

Particularly, the maximum PDOP values are significantly reduced with the integration of GPS and Galileo. Therefore, the position errors have less dependence on location and time with the integration.

4.1.3 Accuracy evaluation based on simulated data

To further evaluate the positioning accuracy with GPS/Galileo integration, the positions are estimated based on simulated measurements, using a GNSS data simulator developed in this study (Chapter 3) and then the estimations are compared with the simulated truth.

In data simulation, both GPS and Galileo pseudorange measurements are simulated based on the models described in Chapter 3 at a point in Hong Kong. The errors considered here are receiver clock errors, tropospheric and ionospheric delays, orbit error, pseudorange observation noise and multipath. Table 4-1 gives the parameters and models for the error simulation.

The precise orbit is used to generate measurements, while the broadcast ephemeris is used for position computation. In data processing, ionospheric delay error is corrected using the Klobuchar model and tropospheric delay error is corrected using only the dry part of the modified Hopfield model.

Table 4-1 Simulated errors

Error source	UERE* (sigma) or Model
Code observation noise	0.5m
Code multipath error	Sigma of A_{br} = 1m; K_{env} =0.5
Tropospheric delay	Modified Hopfield Model
Ionospheric delay	IGS ionosphere map model

*** UERE – User equivalent range error**

In position computations, for a single system (either Galileo or GPS), the following model is used with only one receiver clock parameter:

$$AX + Bt = L \tag{4-7}$$

For integration of GPS and Galileo, two receiver clocks are estimated separately using the model used in Eq. (4-4).

Figures 4-4 to 4-6 show the horizontal positioning errors of 30,000 samples with Galileo, GPS and Integration of Galileo and GPS. Figures 4-7 to 4-9 show the vertical positioning errors with Galileo, GPS, and integration of Galileo and GPS respectively. With GPS and Galileo alone, the RMS values of the horizontal position errors are 1.5m and 1.3m respectively. With integration of Galileo and GPS, the RMS value of the horizontal position errors is about 1.2m. For vertical positioning errors, the RMS values are 4.7m, 3.0m and 2.8m for GPS, Galileo and integration of GPS and Galileo respectively. From these tests, we can see that the navigation accuracy (RMS values) with the integration of GPS and Galileo is only slightly improved compared with GPS or Galileo alone. However, the maximum position errors with the integration of GPS and Galileo are significantly reduced, particularly for the vertical component (Figure 4-9).

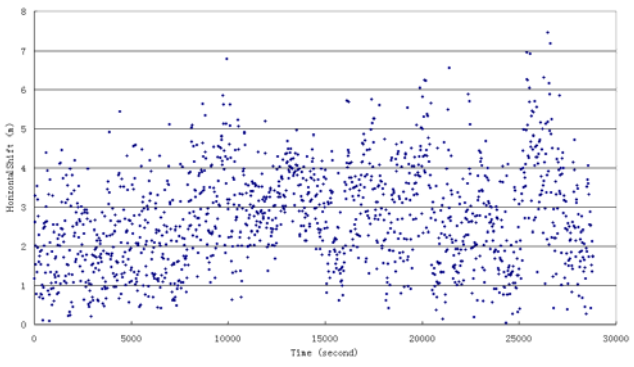

Figure 4-4 Horizontal error with Galileo alone

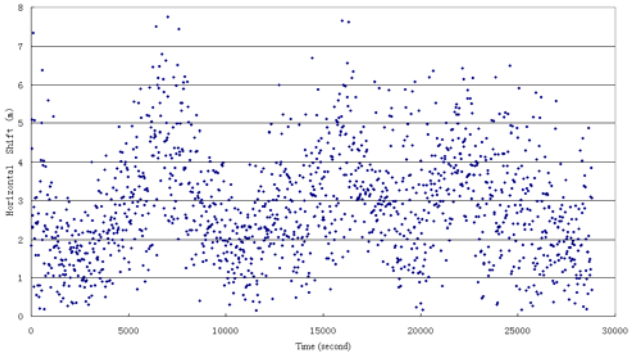

Figure 4-5 Horizontal error with GPS

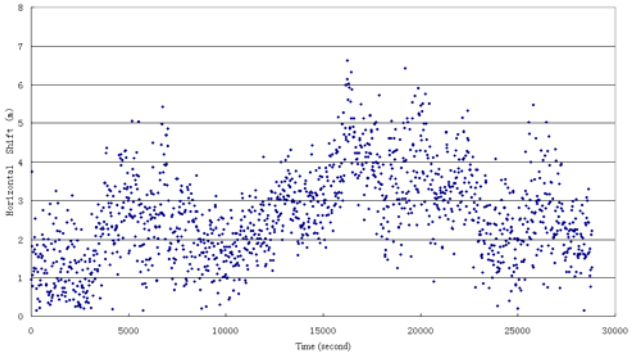

Figure 4-6 Horizontal error with Galileo + GPS

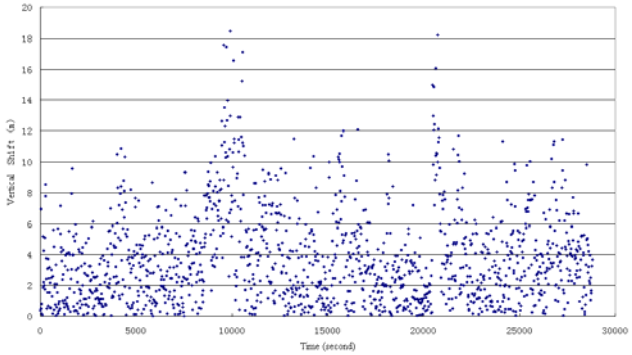

Figure 4-7 Vertical error with Galileo

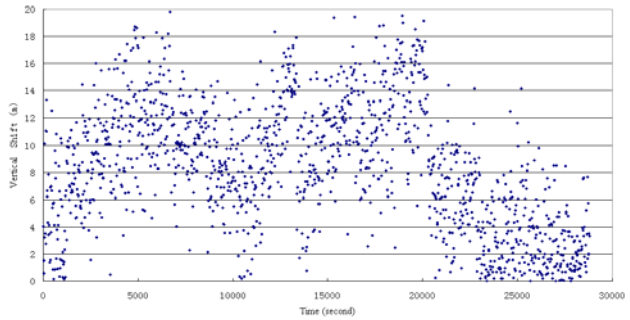

Figure 4-8 Vertical error with GPS

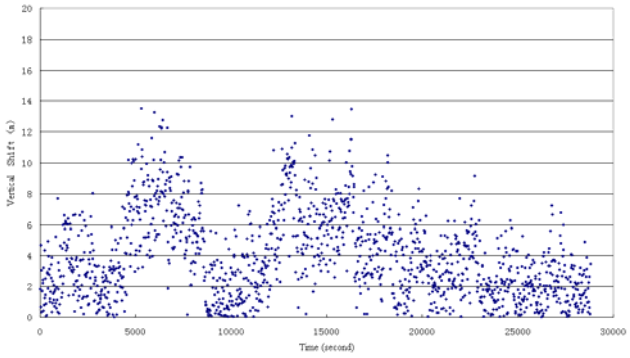

Figure 4-9 Vertical error with GPS + Galileo

4.2 RAIM performance analysis

Integrity is the ability of a navigation system to provide timely warnings to users when the system fails to meet the navigation requirements, which is very important for safety-of-life navigation. In general, there are two main approaches for GNSS integrity monitoring, including network integrity monitoring and Receiver Autonomous Integrity Monitoring (RAIM). The network integrity monitoring method utilizes an independent integrity monitoring station to estimate the size of measurement errors and to broadcast integrity information through a dedicated Ground Integrity Channel (GIC). The RAIM method checks the consistency of measurements made from different satellites to estimate the quality of the resulting positions.

In this section, the RAIM performances with various constellations are mainly analyzed. The reliability theory developed by Baarda (1968) is adopted in this study, which analyzes the effects of Marginal Detectable Bias (MDB) on position error estimation.

4.2.1 RAIM algorithm

4.2.1.1 Outlier detection and identification

The linearized observation equation can be expressed as:

$$Ax = l + v \tag{4-8}$$

where A is the $n \times m$ design matrix; x is a vector of m parameters; l is a vector of n measurements and v is the measurement error vector. The stochastic variance covariance (VCV) matrix of measurements is Q_l.

Define:

$$P = Q_l^{-1} \tag{4-9}$$

the estimation of x and residual are:

$$\hat{x} = (A^T PA)^{-1} A^T Pl \tag{4-10}$$

$$v = A\hat{x} - l \tag{4-11}$$

where $\hat{x}$ is the least squares estimates of x and v is the vector of residuals.

The variance factor is determined as:

$$\hat{\delta}_0^2 = \frac{v^T Pv}{n - m} \tag{4-12}$$

The variance factor can be tested against the two-tailed limits derived from the Chi-squared distribution:

$$\frac{\chi^2_{1-\alpha/2,n-m}}{n-m} \le \hat{\delta}_0^2 \le \frac{\chi^2_{\alpha/2,n-m}}{n-m} \tag{4-13}$$

where $n - m$ is the degree of freedom and α is the significance level of the test.

If the variance factor exceeds the test limit (critical value), either the statistical model is not correct or there exist outliers in the measurements.

Assuming that an outlier ∇S_i exists, the linearized adjustment model can be formed as:

$$A\hat{x} + e_i \nabla S_i = l + v \tag{4-14}$$

$$e_i = [0 \quad 0 \quad \ldots \quad 1 \quad 0]^T$$

A least squares estimation of the magnitude of the outlier ∇S_i can be determined as:

$$\nabla \hat{S}_i = -(e_i^T P Q_v P e_i)^{-1} e_i^T P v \tag{4-15}$$

with a variance of:

$$\delta^2_{\nabla \hat{S}_i} = (e_i^T P Q_v P e_i)^{-1}$$

The w-test (Baarda, 1968; Cross et al., 1994; Teunissen, 1998b) can be used to identify an outlier:

$$w_i = \frac{-e_i^T P v}{\sqrt{e_i^T P Q_v P e_i}} \tag{4-16}$$

For the situation where:

$$|w_i| > N_{1-\alpha/2}(0,1)$$

The ith measurement is identified as an outlier.

4.2.1.2 Internal reliability

The measure of internal reliability is quantified as MDB which is indicated by the lower bound for detectable outliers. The MDB is the magnitude of the smallest error that can be detected for a specific level of confidence and is determined by (Baarda, 1968; Cross et al., 1994):

$$\nabla_0 S_i = \frac{\delta_0}{\sqrt{e_i^T P Q_{\hat{v}} P e_i}} \tag{4-17}$$

where δ_0 is the non-centrality parameter which depends on the given Type I and Type II errors (α_0 and β_0).

4.2.1.3 External reliability

External reliability of the system is characterized by the effects of the MDB on the estimated parameters. External reliability measures are evaluated as (Baarda, 1968; Cross et al., 1994):

$$\nabla_0 \hat{x} = Q_x A^T P e_i \nabla_0 S_i \tag{4-18}$$

4.2.2 RAIM test based on simulated data

Based on the above theory, the RAIM performance is able to be analyzed with different satellite constellations. In the tests, the following parameters are adopted in the computation (Ochieng et al., 2001). Table 4-2 lists the parameter values for probabilities of Missed Detection and False Alarm and Table 4-3 provides the UERE budgets.

Table 4-2 Parameter values of Probabilities of Missed Detection and False Alarm

β	α
0.999	0.9998

Table 4-3 UERE budgets

Elevation angle (Degree)	10	30	50	70	90
UERE (m, 1σ)	5.23	2.77	2.28	2.25	2.27

Internal reliability

Using Eq. 4-17, the MDB values are able to be calculated for any satellite observed for different satellite constellations. As an example, the MDB values for one Galileo

satellite are calculated over a 5-hour period, with Galileo only and GPS and Galileo constellations. The results are shown in Figures 4-10 and 4-11 respectively. With the integration of GPS and Galileo (Figure 4-11), the MDB values are slightly smaller than that from the Galileo system alone (Figure 4-10). The average values of MDB are 17.5m and 14.8m for Galileo alone and GPS/Galileo combined constellations respectively.

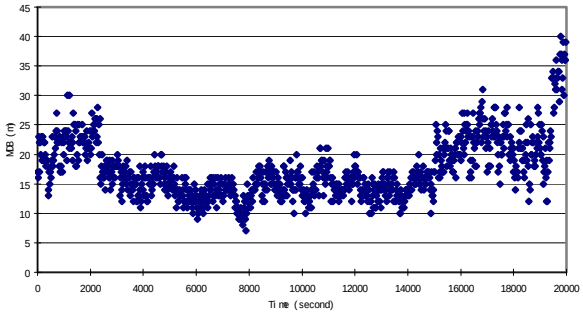

Figure 4-10 MDB of satellite No. 14 using Galileo alone

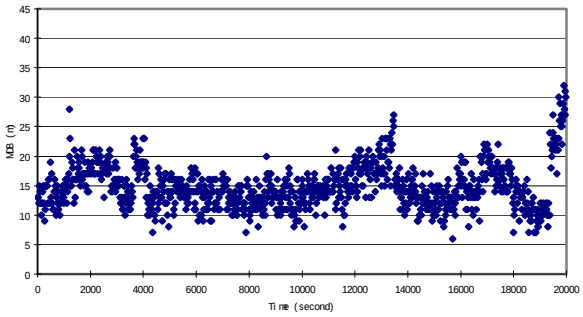

Figure 4-11 MDB of satellite No. 14 using Galileo + GPS

External reliability

External reliability indicates the effects of the MDB on the position errors. Figures 4-12 to 4-15 are maximum horizontal and vertical position error due to the MDB with Galileo alone and Galileo/GPS constellations for a period of 5 hours, which are the maximum value of Eq. 4-18 for all satellites.

This example clearly demonstrates the advantage of the integrated GPS/Galileo constellation. With Galileo alone, the RAIM protection levels for horizontal and vertical errors are 30m and 70m respectively. On the other hand, with the GPS/Galileo constellation, the protection levels for horizontal and vertical errors reduce to less than 15m and 25m respectively.

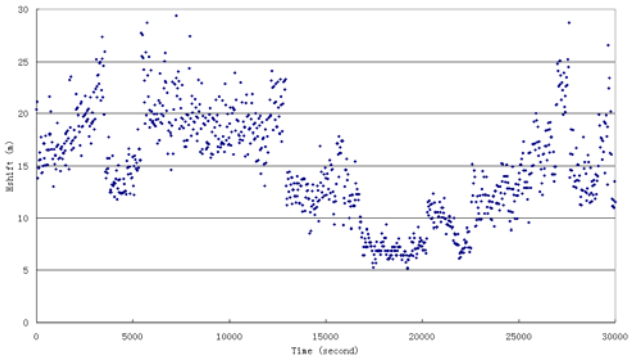

Figure 4-12 Maximum horizontal errors due to MDB of Galileo alone

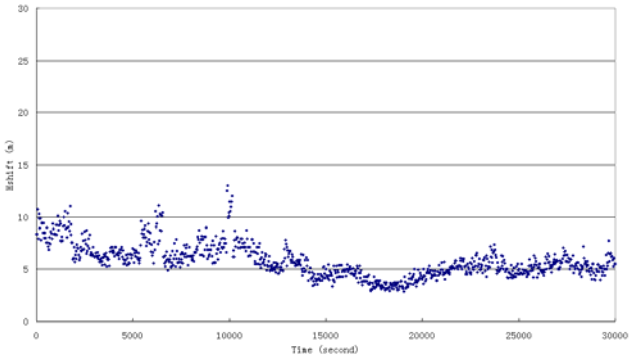

Figure 4-13 Maximum horizontal errors due to MDB of Galileo + GPS

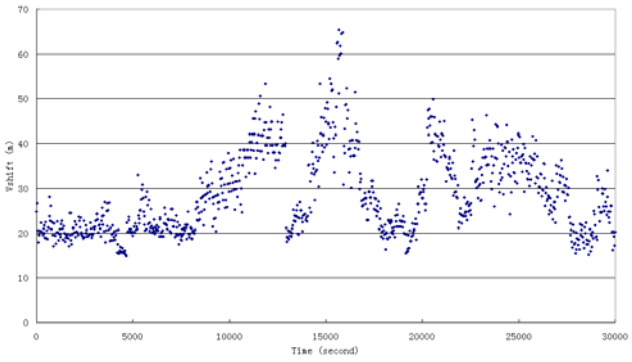

Figure 4-14 Maximum vertical errors due to MDB of Galileo alone

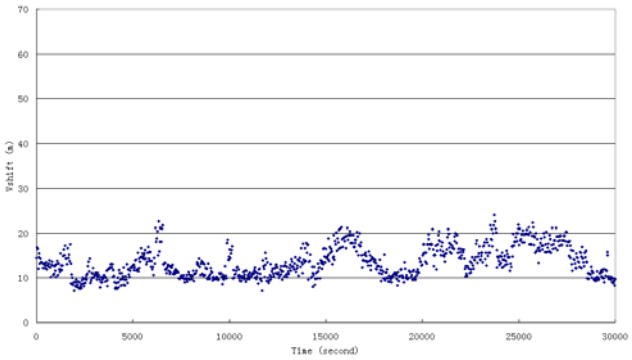

Figure 4-15 Maximum vertical errors due to MDB of Galileo + GPS

4.3 Navigation performance analysis with new GNSS in urban environments

It is well known that GNSS navigation performance in urban areas is significantly degraded due to signal blockage by buildings and multipath effects (Klukas et al., 2003). For example, GPS availability in Hong Kong urban streets is less than 30% (Yu et al., 2006). With more satellites available for various GNSS systems (i.e. GPS, Galileo and GLONASS), GNSS navigation performance should be improved. However, how much it can be improved still is a question to be answered. In this section, the improvement is quantified by analyzing the navigation performance in Hong Kong urban areas by using a 3D building model. Three satellite constellations (GPS, GLONSS and Galileo) and their combinations are considered in the study.

4.3.1 Method to analyze GNSS positioning availability in urban areas

To evaluate GNSS satellite availability in urban areas, the 3D building model has to be taken into account. For a point in the street, the heights of surrounding buildings will be used to calculate the minimum elevation angles in all azimuth directions (360 degrees). For example, as shown in Figure 4-16, a range of 200m is selected to cover a point in a street. Within this range, the minimum elevation angle will be calculated

for satellite availability in all azimuth directions (using 5 degree intervals) using surrounding building heights (as shown in Figure 4-17 as an example) and only satellite elevation angles larger than the minimum elevation angle at a specific azimuth direction can be observed by the GNSS receiver in the street.

The positioning availability of a point is considered as the percentage of time when there are at least four satellites to be seen and the HDOP value is less than 10, over a 24-hour period. The time interval of 15 minutes. is adopted in the analysis.

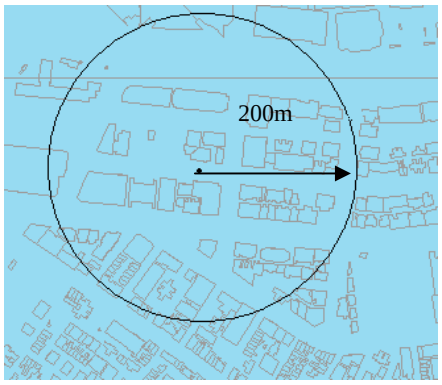

Figure 4-16 Close View of a Sample Point

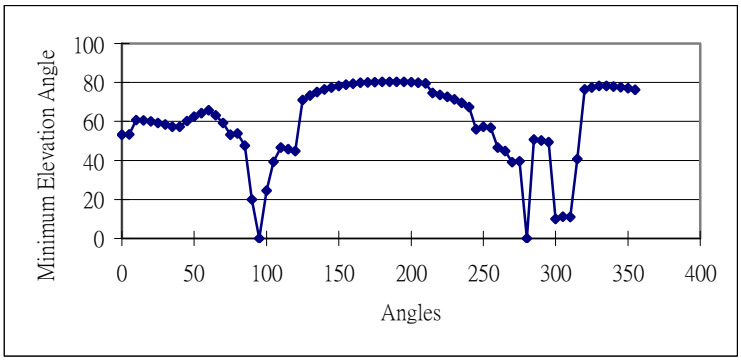

Figure 4-17 Minimum elevation angle for the point

As an example, the availabilities of three typical points are calculated in Hong Kong streets, namely a main road (road wider than 20m), narrow road (road width is less than 20m) and junction area point (as shown in Figure 4-18).

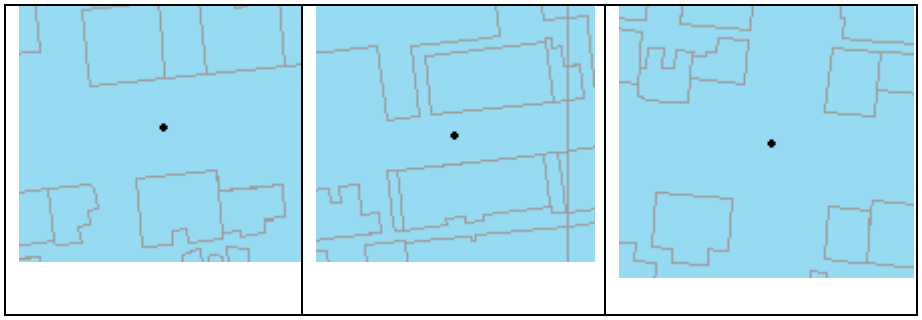

Figure 4-18 Points in Major road, Minor road and Junction area

[from left to right]

Table 4-4 Availability in Different Urban Environments

	GPS	GPS + GLONASS	GPS + Galileo	GPS + GLONASS + Galileo
Major Road point	1%	6%	17%	44%
Minor Road point	1%	1%	1%	3%
Junction Area point	5%	28%	63%	84%

Table 4-4 gives the positioning availabilities for these three points with different satellite constellations. With only one system (i.e. GPS), the availability is very low (only a few percent) for all three points. With a three-system constellation (GPS, GLONASS and Galileo), the positioning availabilities increase to 44% and 84% for the main road and junction area points, but it is still very low for narrow road points (3%).

4.3.2 GNSS positioning availability in Hong Kong urban areas

To evaluate GNSS positioning availability in Hong Kong urban areas, 189 sample points are selected in Hong Kong, almost evenly spaced in urban areas of Hong Kong Island covering Wan Chai, Causeway Bay, Sheung Wan and Central (see Figure 4-19).

The positioning availability analysis results are summarized in Figure 4-20. The horizontal axis shows the percentage of time availability over a 24-hour period and the vertical axis shows the percentage of points (out of 189 points). The different

colours in the figure demonstrate different satellite constellations. For example, the figure shows that there are 60% of points with positioning availability larger than 10% and 40% points with positioning availability larger than 30% for the three systems (GPS, Galileo and GLONASS) constellation.

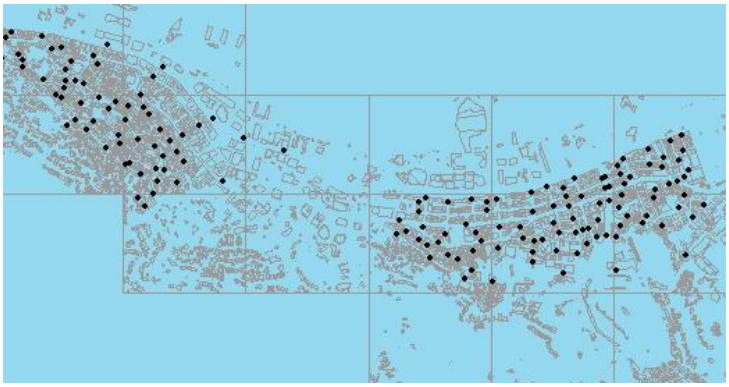

Figure 4-19 Study site to evaluate coverage performance

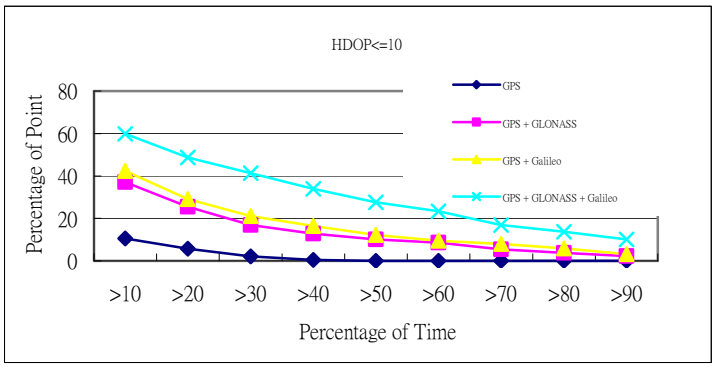

Figure 4-20 Availability performance analysis

In general, with a single system (i.e. GPS only), the positioning availability is extremely low in Hong Kong urban areas and that is the main restriction for the navigation applications of GNSS in Hong Kong. With more satellites available (combined constellations), the positioning availability improves significantly. However, even using three systems, the positioning availability is still very low - only 10% of points have a positioning availability larger than 90%. Thus GNSS alone cannot satisfy the navigation requirements in dense urban areas such as Hong Kong.

4.3.3 GNSS positioning discontinuity analysis in Hong Kong urban areas

In urban navigation, GNSS is normally integrated with other navigation systems (i.e. Dead Reckoning, DR) (Vlcek, 1993; Lachapelle and Mezentsev, 2005). However, a DR system is subject to large drift errors and GNSS positioning is crucial for providing calibration for the DR errors (Yu et al., 2006). Although GNSS alone cannot satisfy the navigation requirements in urban areas (as discussed before), can it provide sufficient positioning fixes for the DR calibration? To answer this question, we need to analyze the discontinuity of GNSS positioning in urban areas. Here the discontinuity is defined as mean or maximum distance in streets where no GNSS positioning fixes are available.

To evaluate the discontinuity of GNSS positioning in Hong Kong, a simulated vehicle route of approximate 8,000 metres is selected in Wan Chai and Causeway Bay on Hong Kong island (Figure 4-21). The vehicle speed is set to 20km/hour. Then a large number of points (187 points) are sampled approximately equally spaced along the route (Figure 4-21) to test the GNSS positioning availability along the route. To count the constellation changes with time, we simulate the run at 7 different start times with 3-hour intervals. If there is a point where GNSS positioning is available and at the next point GNSS positioning is not available, it is counted as a positioning discontinuity. Finally the mean and maximum discontinuity distances are used along the route to quantify the GNSS positioning quality along the route. As GPS availability is very poor in this region, the discontinuity can reach more than 5km. In the following discussion, the single system analysis results will not be included.

Figures 4-22 and 4-23 show the mean and maximum GNSS discontinuity distances for various combined GNSS constellations at different start times. For two system combinations (i.e. GPS/GLONASS or GPS/Galileo) the mean discontinuity

distance is in the range of 80 to 140m and the maximum discontinuity is in the range of 400m to 1,000m. With three systems combined (GPS/Galileo/GNSS), the mean discontinuity is less than 80m and the maximum discontinuity is slightly over 400m.

Figure 4-21 Sample Points along a simulated Route

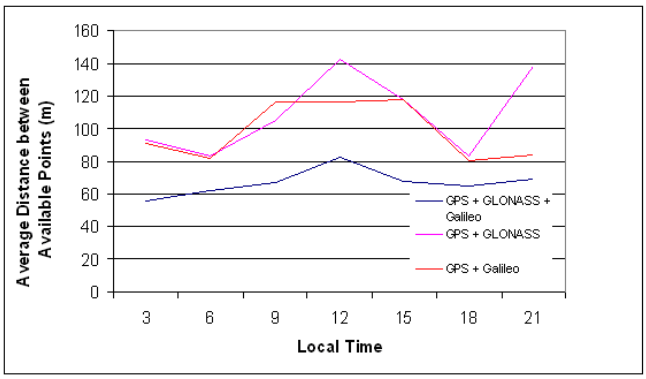

Figure 4-22 Average discontinuity Distance

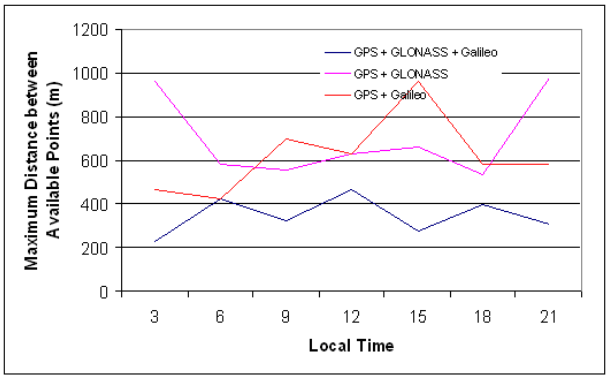

Figure 4-23 Maximum discontinuity distance

4.4 Precise Point Positioning with GPS and Galileo Constellations

4.4.1 The basic concepts of PPP positioning

With the advent of precise ephemeredes and satellite clock corrections from IGS and several other organizations, it is possible to conduct high precision GPS positioning with carrier phase observations with just one receiver. This positioning method is known as Precise Point Positioning (PPP).

PPP research began around 1997 before Selective Availability (SA) was turned off and it has attracted much attention in recent years. Previous research work has shown that centimetre accuracy positioning can be reached in a static mode.

In the implementation of PPP, generally both code and phase observations from a dual-frequency receiver are used as basic observables. When forming observation equations, generally ionosphere free pseudorange and carrier phase combinations (Zumberge et al., 1997; Kouba and Heroux, 2001; Bisnath and Langley, 2001a; Bisnath and Langley, 2001b; Bock et al., 2002; Colombo et al., 2004; Chen et al., 2004;) are used as follows:

$$\phi_{IF} = \frac{f_1^2 \cdot \phi(L_1) - f_2^2 \cdot \phi(L_2)}{f_1^2 - f_2^2} = \rho - cdT + d_{trop} + \frac{f_1^2 \lambda_1 N_1 - f_2^2 \lambda_2 N_2}{f_1^2 - f_2^2}$$

$$+ \frac{f_1^2 \lambda_1}{f_1^2 - f_2^2}(\phi_r(t_0, L_1) - \phi^s(t_0, L_1)) + \frac{f_1^2 \lambda_1}{f_1^2 - f_2^2}(\phi_r(t_0, L_2) - \phi^s(t_0, L_2))$$

$$+ d^s_{hd(\phi(L_1,L_2))} - d^r_{hd(\phi(L_1,L_2))} + d_{mult/\phi(L_1,L_2)} + \varepsilon(\phi(L_1, L_2)) \quad (4\text{-}19)$$

$$P_{IF} = \frac{f_1^2 \cdot P(L_1) - f_2^2 \cdot P(L_2)}{f_1^2 - f_2^2} = \rho - cdT + d_{trop}$$

$$+ d^s_{hd(P(L_1,L_2))} - d^r_{hd(P(L_1,L_2))} + d_{mult/P(L_1,L_2)} + \varepsilon(P(L_1, L_2)) \quad (4\text{-}20)$$

Where

ϕ_{IF}, P_{IF} -ionosphere-free carrier phase and pseudorange measurements

ρ -true geometric range

c -speed of light

dT -receiver clock error

d_{trop} -tropospheric delay

$d^{s}_{hd(\phi(L_1,L_2))}$ -satellite carrier phase hardware bias after ionosphere-free combination

$d^{r}_{hd(\phi(L_1,L_2))}$ -receiver carrier phase hardware bias after ionosphere-free combination

$d^{s}_{hd(P(L_1,L_2))}$ -satellite pseudorange hardware bias after ionosphere-free combination

$d^{r}_{hd(P(L_1,L_2))}$ -receiver pseudorange hardware bias after ionosphere-free combination

$\phi_r(t_0, L_i)$ -initial phase of receiver oscillator

$\phi^s(t_0, L_i)$ -initial phase of satellite oscillator

$d_{mult/P(L_1,L_2)}$ -multipath effect in the ionosphere-free pseudorange measurement

$d_{mult/\phi(L_1,L_2)}$ -multipath effect in the ionosphere-free carrier phase measurement

$\varepsilon(\cdot)$ -measurement noise

In equation (4-19), the ionosphere-free ambiguities ($\frac{f_1^2\lambda_1 N_1 - f_2^2\lambda_2 N_2}{f_1^2 - f_2^2}$) are calculated as a lumped term and treated as a float number. Hence there is one float ambiguity parameter for each satellite.

Another way to form observation equations, averaged pseudorange and carrier phase observations on the two GPS frequencies in addition to the ionosphere free carrier phase combination (Gao and Shen, 2001) are used as follows:

$$P_{P_i,\phi_i} = 0.5(P_{SM}(L_i) + \phi(L_i)) \tag{4-21}$$

$$P_{(P_1,\phi_1)} = \rho - cdT + d_{trop} + 0.5\lambda_1 N_1$$

$$+0.5\lambda_1(\phi_r(t_0,L_1)-\phi^s(t_0,L_1))+0.5(d^s_{hd/P(L_1)}+d^s_{hd/\phi(L_1)}-d^r_{hd/P(L_1)}-d^r_{hd/\phi(L_1)})$$

$$+0.5(d^s_{Interfreq/P(L_1)}+d^s_{Interfreq/\phi(L_1)}-d^r_{Interfreq/P(L_1)}-d^r_{Interfreq/\phi(L_1)})$$

$$+d_{mult/(\phi(L_1,P(L_1))}+\varepsilon(\phi(L_1,P(L_1)) \quad (4\text{-}22)$$

$$P_{(P_2,\phi_2)}=\rho-cdT+d_{trop}+0.5\lambda_2N_2$$

$$+0.5\lambda_2(\phi_r(t_0,L_2)-\phi^s(t_0,L_2))+0.5(d^s_{hd/P(L_2)}+d^s_{hd/\phi(L_2)}-d^r_{hd/P(L_2)}-d^r_{hd/\phi(L_2)})$$

$$+0.5(d^s_{Interfreq/P(L_2)}+d^s_{Interfreq/\phi(L_2)}-d^r_{Interfreq/P(L_2)}-d^r_{Interfreq/\phi(L_2)})$$

$$+d_{mult/(\phi(L_2,P(L_2))}+\varepsilon(\phi(L_2,P(L_2)) \quad (4\text{-}23)$$

Where

P_{P_i,ϕ_i} -average of pseudorange and carrier phase observations

$P_{SM}(L_i)$ -ionosphere-free smoothed pseudorange measurement

$P_{(P_1,\phi_1)}$ -average of pseudorange and carrier phase observations on L1

$P_{(P_2,\phi_2)}$ -average of pseudorange and carrier phase observations on L2

$d^s_{Interfreq/P(L_i)}$ -satellite pseudorange inter-frequency bias on Li

$d^s_{Interfreq/\phi(L_i)}$ -satellite carrier phase inter-frequency bias on Li

$d^r_{Interfreq/P(L_i)}$ -receiver pseudorange inter-frequency bias on Li

$d^r_{Interfreq/\phi(L_i)}$ -receiver carrier phase inter-frequency bias on Li

Hence the model allows for the estimation of two float ambiguity parameters (on L1 and L2) for each satellite.

When implementing PPP, except for the errors listed in the above equations, several other error sources should be taken into consideration, including satellite antenna phase centre offset, and errors from phase wind up, solid earth tides, ocean loading, atmosphere loading, etc.

For PPP, either zero or single-differenced (between satellites) observations can be used. The latter can make observation equations simpler by cancelling receiver related parameters.

Ever since its introduction, PPP has shown its potential to become a high precision technology. Unfortunately, the ambiguity terms are no longer integers as they are corrupted by fractional initial phase biases in the GPS satellites and receivers. This makes the ambiguity parameters only estimable as float numbers in PPP. A long initialization time, typically more than 20 minutes, is necessary before a converged position solution can be obtained.

With the combination of GPS and Galileo constellations, the number of satellites is doubled and satellite geometry is greatly improved (Feng et al., 2006). Moreover, there are a total of four independent ionosphere-free carrier phase combinations that can be formed. Therefore, it is expected that the PPP convergence time will be decreased.

In this section the convergence time improvement is investigated from the combination of GPS and Galileo constellations.

The PPP ionosphere-free observation equation for carrier phase measurements can be expressed as (Holfman-Wellenhof et al., 2002; Kouba et al., 2001; Han et al., 2001):

$$\varphi_{ij} = \frac{f_i^2}{f_i^2 - f_j^2}\varphi_i - \frac{f_j^2}{f_i^2 - f_j^2}\varphi_j = \rho + c(dt_r - dt) + \lambda_{ij}N_{ij} + md_{trop} + \varepsilon \qquad (4\text{-}24)$$

where

φ_{ij} - ionosphere-free carrier phase observation of frequency band i and j (m);

f_i, f_j - carrier phase frequencies of band i and j respectively;

φ_i, φ_j - carrier phase observation ranges of frequency band i and j respectively;

λ_{ij} - wavelength of ionosphere-free carrier phase combination of frequency band i and j;

ρ - geocentric topocentric distance from receiver r to satellite;

N_{ij} - real valued ionosphere-free carrier phase ambiguity;

$dt_r(t)$ - clock error of receiver r;

$dt(t)$ - satellite clock error;

$d_{trop}(t)$ - zenith tropospheric delay;

t - epoch time;

m - tropospheric mapping function, e.g. Neil mapping function (Niell, 1996);

c - speed of light;

r - subscript for receiver station identifier;

ε - observation noise.

And

$$N_{ij} = c\frac{f_i N_i - f_j N_j}{f_i^2 - f_j^2}$$

where, N_i, N_j - ambiguity of carrier phase frequency bands i and j respectively;

For GPS, only one ionosphere-free combination between L1 and L2 can be formed; while for the Galileo system, a maximum of three independent ionosphere-free combinations between two frequency bands can be formed from four frequency bands (E1, E6, E5a and E5b).

In PPP data processing, precise satellite orbital and clock error data from IGS are used. Some other errors which are not considered in relative positioning such as errors caused by earth rotation (McCarthy D.D., 1996), earth body tide, ocean loading, phase wind-up effects and satellite antenna offset (Wu J.T. et al., 1993) have to be corrected

with models. Detailed data processing methods can be found (Chen et al., 2004) and will not be discussed here.

When combining GPS and Galileo systems, a time offset between GPS and Galileo has to be considered. Also, receiver clock errors for GPS and Galileo will be considered separately. The receiver clock errors are time-dependent unknown parameters and different for every epoch. Single-difference between satellites can be formed to cancel out the receiver clock errors.

4.4.2 Data simulation and analysis

In this study, the GPS data is observed in Hong Kong by a Leica SR530 dual frequency GPS receiver in a static positioning mode, from 11 o'clock (UTC) on 9 December to 7 o'clock (UTC) on 10 December, 2004. The data interval is 1 second. The precise satellite orbit and clock products are downloaded from the CODE Analysis Centre of the IGS.

As Galileo is not available yet, the Galileo measurements are simulated using a data simulator developed for this study (Chapter 3). In the simulation, the receiver position and tropospheric delays are obtained from GPS data processing. The receiver clock errors are simulated with a second order polynomial with white noise. The ionospheric delay is simulated with a Klobuchar model. As in the PPP data processing, the ionosphere-free observables are used; the ionosphere model error will not affect the results. The measurement noise is simulated with normal distributed noise with the standard errors of 1.5m and 3mm for the pseudorange and carrier phase respectively.

In data processing, the ambiguity is regarded as convergent if the position error is less than 20cm. To count for the effects of satellite constellation difference at different

times, the data is processed every hour. Table 4-5 gives the ambiguity convergence time for GPS alone and GPS/Galileo integration.

Table 4-5 Convergence time

Starting Time		Convergence Time (seconds)	
		Case I	Case II
December 9	11:12	1,683	862
	12:12	3,121	1,150
	13:12	>7,200	685
	14:12	>7,200	360
	15:12	6,441	320
	16:12	1,385	1,264
	17:12	1,380	575
	18:12	1,259	460
	19:12	2,201	740
	20:12	900	1,730
	21:12	>7,200	1,420
	22:12	1,681	1,428
	23:12	4,356	1,780
December 10	00:12	592	330
	01:12	869	1,465
	02:12	>7,200	483
	03:12	7,008	370
	04:12	1,567	1,120
	05:12	3,570	575
	06:12	1,714	547
*Average Time		3,426	883

*Note: if convergence time exceeds 7,200 seconds, it is regarded as 7,200 seconds when computing average time.

For GPS alone, the ambiguity convergence time varies significantly at different times, from 592s to over 7,200s, with an average time of 3,426s. On the other hand, with the GPS/Galileo constellation, the ambiguity convergence time is in the range of 330s to 1,780s, with an average time of 883s, which is much more stable.

4.5 Summary

In this chapter, the positioning performance improvements have been analyzed by using the combined GNSS constellations from (GPS, Galileo and GLONASS). Based

on the studies, we can summarize as follows:

a) Integration of multiple GNSS constellations does not significantly improve positioning accuracy. However, the RAIM performance is significantly improved. The simulation study shows the RAIM position protection levels reduce dramatically from 30m and 70m with GPS only for the horizontal and vertical components to 15m and 25m with GPS/Galileo constellations.

b) For urban applications, combined constellations can improve the positioning availability in streets. However, it still does not satisfy the requirement for vehicle navigation in urban areas. On the other hand, the discontinuity distances are significantly reduced with the combined constellations. Therefore, it is possible to use cheaper DR systems to bridge the gaps of GNSS positioning, with high accuracy.

c) For PPP data processing, the combined constellation with GPS/Galileo can significantly reduce the ambiguity convergence time, from an average time of around 1 hour (3,400s) with GPS alone to less than 15 min (880s) with GPS/Galileo combination.

Chapter 5 Performance analysis of ambiguity resolution with Galileo multiple frequency carrier phase measurements

The Global Navigation Satellite Systems (GNSS) provide two main types of measurements: pseudorange and carrier phase. The main differences between them are measurement precision (metre vs. millimetre) and integer ambiguity associated with carrier phase. If we can reliably resolve the carrier phase ambiguity, the carrier phase measurement is conceptually turned into high-precision range observation and positioning accuracy at centimetre level can be achieved.

Ambiguity resolution has been a continuing challenge in GNSS research and a large number of ambiguity resolution techniques have been proposed by many different research groups (Counselman and Gourevitch, 1981; Remondi, 1984; Han and Rizos, 1996a; Teunissen, 1993; Teunissen, 1994; Teunissen, 1995; Hatch, 1990; Frei and Beutler, 1990; Euler and Landau, 1992; Martin-Neira et al., 1995; Chen and Lachapelle, 1995; Kim and Langley, 1999). Even if the ambiguities for all satellites cannot be fixed at the same time, a partial ambiguity-fixed solution is also useful for improving GNSS navigation performance (i.e. accuracy and continuity) (Teunissen, 1998; Teunissen et al., 1999).

Reliable and fast ambiguity resolution is affected by many factors, such as the number of satellites observed, the sizes of errors, the observation time and the number of signal frequencies. For example, it has been demonstrated that more satellites are helpful for ambiguity resolution in Chapter 4 of this dissertation.

Galileo will provide navigation signals in more frequency bands (up to four frequency bands). With more carrier phase data available, more frequency

combinations with longer equivalent wavelengths can be formed. This will provide more opportunities for fast and reliable ambiguity resolution.

In recent years, studies on fast ambiguity resolution using multiple frequencies from new GNSS have been carried out by many researchers (Hatch et al., 2000; Tiberius et al., 2002; Vollath et al., 1998; Zhang et al., 2003; Werner and Winkel, 2003; Schlotzer and Martin, 2005), predominantly based on triple frequencies of Galileo, namely E1, E5b and E5a. The Cascading Ambiguity Resolution (CAR) method is mostly used in these studies.

In this chapter, the performance of ambiguity resolution will be studied using a multiple frequency Galileo system. Two different algorithms, including the CAR method and the Integer least-squares (ILS) method, are used in the study for comparison. Particularly, we are interested in studying the possibility of single epoch ambiguity resolution using a multiple frequency Galileo system.

5.1 Mathematic models for CAR and ILS algorithms

The linearized double-differenced Galileo pseudorange and carrier phase measurements for frequency band i (i=1, 2, 3, 4) can be expressed as:

$$\begin{aligned} AX &= L_{code} + n_p \\ AX + \lambda_i N_i &= L_i + n_i \end{aligned} \tag{5-1}$$

where X is a position parameter; N_i is an ambiguity parameter of frequency band i; L_{code} and L_i are pseudorange and carrier phase measurements respectively; n_P and n_i are measurement noises for pseudorange and carrier phase measurements respectively; A is the linear coefficient matrix related to position parameters; and λ_i is the wavelength of carrier L_i.

Using observations from all four frequencies, we are able to solve for X and ambiguities by least squares:

$$\begin{pmatrix} X \\ N \end{pmatrix} = (B^T Q_L^{-1} B)^{-1} B^T Q_L^{-1} L \tag{5-2}$$

where B is the design matrix, L is the vector of pseudorange and carrier phase measurements, and Q_L is the variance-covariance matrix of measurements.

The variance-covariance matrix of the estimated unknowns X and N can be written as:

$$Cov(X, N) = (B^T Q_L^{-1} B)^{-1} = \begin{pmatrix} Q_X & Q_{XN} \\ Q_{NX} & Q_N \end{pmatrix} \tag{5-3}$$

Normally the estimated float ambiguities N are strongly correlated. Teunissen (1995) applied an integer transformation Z which de-correlates the variance-covariance matrix Q_N, as follows:

$$z = Z^T N \tag{5-4}$$

where Z is an integer transformation and all the elements in Z are integers, and det(Z)= ±1. Therefore, z is also an integer with the variance-covariance matrix:

$$Q_z = Z^T Q_N Z \tag{5-5}$$

This integer transformation provides an effective way to reduce ambiguity search range and to improve ambiguity resolution performance.

The CAR method tries to form longer equivalent wavelengths using GNSS multiple frequency signals and to resolve for ambiguities one by one. The mathematical model of the CAR method can be expressed as:

$$\begin{cases} AX = L_{code} + n_p \\ AX + \lambda_{W1} N_{W1} = L_{W1} + n_{W1} \end{cases} \tag{5-6}$$

$$\begin{cases} AX = L_{W1} - \lambda_{W1} \breve{N}_{W1} + n_{W1} \\ AX + \lambda_{W2} N_{W2} = L_{W2} + n_{W2} \end{cases} \tag{5-7}$$

$$\begin{cases} AX = L_{W2} - \lambda_{W2} \breve{N}_{W2} + n_{W2} \\ AX + \lambda_{W3} N_{W3} = L_{W3} + n_{W3} \end{cases} \tag{5-8}$$

$$\begin{cases} AX = L_{W3} - \lambda_{W3} \breve{N}_{W3} + n_{W3} \\ AX + \lambda_{W4} N_4 = L_{W4} + n_{W4} \end{cases} \tag{5-9}$$

where, X is a position parameter; λ_{W1}, λ_{W2}, λ_{W3} and λ_{W4} are wavelengths of selected independent combinations W1, W2, W3 and W4; N_{W1}, N_{W2}, N_{W3} and N_{W4} are corresponding double-differenced unknown ambiguity parameters; $\breve{N}_{W1}$, $\breve{N}_{W2}$, and $\breve{N}_{W3}$ are corresponding fixed double-differenced ambiguities; n_{W1}, n_{W2}, n_{W3} and n_{W4} are the noises of the combinations; L_{W1}, L_{W2}, L_{W3} and L_{W4} are corresponding double-differenced measurements; L_{code} and n_p are double-differenced measurements and noise of pseudorange measurement respectively; A is the linear coefficient matrix related to position parameters.

5.2 Optimal Galileo frequency combinations for the CAR method

5.2.1 Linear combination of Galileo frequency bands

The Galileo system will provide four frequency bands for navigation (GAL OS SIS ICD 2006) with central frequencies at:

E1: $f_1 = 1575.42$ MHz, E6: $f_2 = 1278.75$ MHz

E5b: $f_3 = 1207.14$ MHz, E5a: $f_4 = 1176.45$ MHz

The general form for a combination of the four frequencies (Liu and Wang, 2003) is:

$$N_c = iN_1 + jN_2 + kN_3 + mN_4 \tag{5-10}$$

$$\lambda_c = \frac{\lambda_1\lambda_2\lambda_3\lambda_4}{i\lambda_2\lambda_3\lambda_4 + j\lambda_1\lambda_3\lambda_4 + k\lambda_1\lambda_2\lambda_4 + m\lambda_1\lambda_2\lambda_3} \tag{5-11}$$

$$f_c = if_1 + jf_2 + kf_3 + mf_4 \tag{5-12}$$

$$L_c = \alpha L_1 + \beta L_2 + \gamma L_3 + \delta L_4 \tag{5-13}$$

where N_c, λ_c, f_c, and L_c are ambiguity, wavelength, frequency and observable of the combination respectively. We further have:

$$\alpha = i\lambda_c / \lambda_1,\ \beta = j\lambda_c / \lambda_2,\ \gamma = k\lambda_c / \lambda_3,\ \delta = m\lambda_c / \lambda_4,\ \ \alpha + \beta + \lambda + \delta = 1.$$

In the above equations, i, j, k and m are integers so that the integer property of the ambiguity for the new combination is preserved.

The combinations are affected by the same tropospheric delay as are E1, E6, E5b or E5a observables. But the ionospheric delay I_c and observation noise σ_c are different:

$$I_c = R_{i,j,k,m} I_1 \tag{5-14}$$

$$\sigma_c = A_{i,j,k,m}\sigma_0 \tag{5-15}$$

where

$$R_{i,j,k,m} = \frac{i + jf_1/f_2 + kf_1/f_3 + mf_1/f_4}{i + jf_2/f_1 + kf_3/f_1 + mf_4/f_1}$$

$$A_{i,j,k,m} = \sqrt{\alpha^2 + \beta^2 + \gamma^2 + \delta^2}$$

The symbol σ_0 denotes the measurement noise level of the original frequencies (assuming E1, E6, E5b or E5a have the same observation noise) and I_1 is the ionospheric delay at E1 frequency.

With different values assigned to i, j, k and m, different combinations can be formed. Thus, it is necessary to find optimal criteria to select four independent combinations which are optimal for ambiguity resolution. Combinations proposed by

different researchers are often based on longer equivalent wavelengths or larger wavelength-to-noise ratio (Zhang et al., 2003; Zhang, 2005; Wang et al., 2004).

Table 5-1 lists the top five combinations with largest wavelength-to-noise ratio. They have one common feature, i.e. i + j + k + m = 0. Therefore, only three independent combinations can be selected from Table 5-1. Table 5-2 lists the top five combinations with the largest wavelength-to-noise ratio and independent from those in Table 5-1. They have one common feature: i + j + k + m = 1. Apart from the combinations listed in Table 5-1 and 5-2, there are other combinations with longer wavelengths and reasonable wavelength-to-noise ratio. They are listed in Table 5-3.

Table 5-1 Top five combinations with largest wavelength-to-noise ratios

No.	i	j	k	m	λ_c (m)	$R_{i,j,k,m}$	$A_{i,j,k,m}$	i+j+k+m	$\lambda_c / A_{i,j,k,m}$
1	0	0	1	-1	9.76	-1.74	54.92	0	0.18
2	0	1	-1	0	4.18	-1.6	24.55	0	0.17
3	0	1	0	-1	2.93	-1.64	16.98	0	0.17
4	1	-1	0	0	1.01	-1.23	6.84	0	0.15
5	1	0	-1	0	0.81	-1.31	5.39	0	0.15

Table 5-2 Top five combinations with largest wavelength-to-noise ratio which are independent from those in Table 5-1

No.	i	j	k	m	λ_c (m)	$R_{i,j,k,m}$	$A_{i,j,k,m}$	i+j+k+m	$\lambda_c / A_{i,j,k,m}$
1	-1	0	1	1	0.37	3.21	2.85	1	0.130
2	-2	1	1	1	0.59	5.77	7.41	1	0.078
3	-2	0	1	2	0.73	7.63	10.05	1	0.072
4	-2	1	0	2	0.62	6.25	8.60	1	0.072
5	-2	0	2	1	0.68	6.98	9.41	1	0.072

Table 5-3 Combinations with longer wavelength and reasonable wavelength-to-noise ratios

No.	i	j	k	m	λ_c (m)	$R_{i,j,k,m}$	$A_{i,j,k,m}$	i+j+k+m	$\lambda_c / A_{i,j,k,m}$
1	0	1	-3	2	29.3	-0.77	440.27	0	0.066
2	-1	4	0	-3	29.3	-13.77	626.69	0	0.047
3	0	1	-2	1	7.32	-1.5	72.69	0	0.10
4	1	-4	2	1	5.86	0.66	117.07	0	0.05

The question is how to select four independent combinations that will lead to an easier ambiguity resolution. Obviously, different optimal criteria will lead to different selections. For example, if we only consider the effects of measurement noise, the wavelength-to noise ratio may be a good selection. On the other hand, if we consider long baselines which have to take the ionospheric delay into account, the size of coefficient $R_{i,j,k,m}$ for the ionospheric term in Eq. 5-9 will also need to be balanced.

5.2.2 Optimal Galileo frequency combinations for the CAR method

One method to express the quality of ambiguity resolution is the success rate of fixing all ambiguities to their integers (Teunissen, 1998), which indicates the probability of correct integer ambiguity estimation. The success rate can be computed from the simulated data. Thus the success rate expresses the probability of ambiguity fixing given the satellite geometry distribution and the assigned statistical errors of the measurements. In this section, the success rate will be used as the criterion for the selection of independent combination for the CAR method. The success rate is calculated based on the following formula (Teunissen, 2003):

$$P_S \approx (2\Phi(\frac{1}{2ADOP}) - 1)^n \tag{5-16}$$

where, $ADOP = \sqrt{|Q_N|^{\frac{1}{n}}}$, Q_N is the variance-covariance matrix of float ambiguity vector and

$$\Phi(X) = \int_{-\infty}^{X} \frac{1}{\sqrt{2\pi}} \exp\left\{-\frac{1}{2}v^2\right\} dv \tag{5-17}$$

First combination

From Tables 5-1, 5-2 and 5-3, we can see that different combinations have different wavelengths and wavelength-to-noise ratios. When selecting the first combination for Eq. 5-6, should we select the longest wavelength (the first row in

Table 5-3) or the largest wavelength-to-noise ratio (the first row in Table 5-1)? Table 5-4 gives these two combinations for comparison. Figure 5-1 shows the success rate calculated based on different pseudorange and carrier phase noise levels for the combinations of Com0 and Com1 listed in Table 5-4. It can be seen that the success rate is related to the measurement noise level. For the same combination, a larger noise level will lead to a lower success rate. Also, the success rate of Com0 is always larger than that of Com1 for the same code and phase noise levels. Thus, the first optimal combination for the CAR method should be Com0.

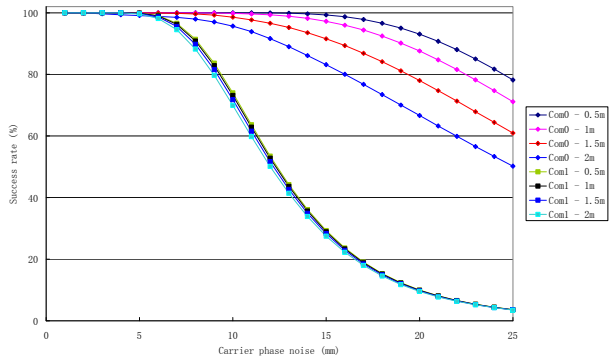

Figure 5-1 The success rates of Com0 and Com1

Table 5-4 Candidates for the first combination

Name	i	j	k	m	λ_c (m)	$R_{i,j,k,m}$	$A_{i,j,k,m}$	i+j+k+m	$\lambda_c / A_{i,j,k,m}$
Com0	0	0	1	-1	9.76	-1.74	54.92	0	0.18
Com1	0	1	-3	2	29.3	-0.77	440.27	0	0.066

Second combination

After the first optimal combination is determined, we can find three independent combinations from Tables 5-1, 2, 3 which are possible for the second combination for Eq. 5-7, as shown in Table 5-5.

Table 5-5 Candidates for the second combination

Name	i	j	k	m	λ_c (m)	$R_{i,j,k,m}$	$A_{i,j,k,m}$	i+j+k+m	$\lambda_c / A_{i,j,k,m}$
Com1	0	1	-3	2	29.3	-0.77	440.27	0	0.066
Com2	0	1	-1	0	4.18	-1.60	24.55	0	0.17
Com3	0	1	-2	1	7.32	-1.50	72.69	0	0.10

Figure 5-2 shows the success rate for the three combinations with different carrier phase noise levels. It is clear the success rate of combination Com2 is larger than the other two. Thus the combination Com2 is selected as the second optimal combination.

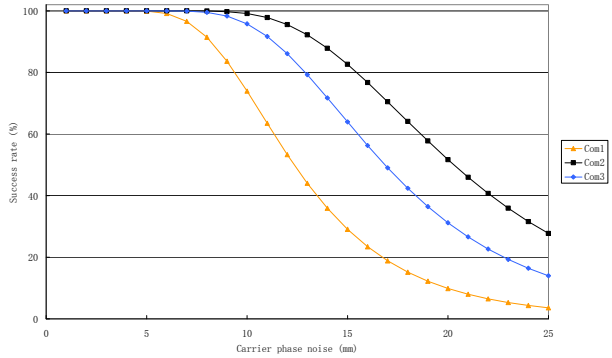

Figure 5-2 Approximate success rates of Com1, Com2 and Com3

Third combination

In Eq. 5-8, when solving for N_{W3}, the ambiguity fixed in the second step is usually used as a constraint. Thus the noise level of the second combination Com2 will affect the success rate of the N_{W3} resolution.

In fact, as the com0 and com2 ambiguities in steps 1 and 2 have been fixed to their integers, we can use a combination of the two to form a new combination with minimum noise level as the constraint for solving N_{W3}. Table 5-6 gives this combination (called Trans3).

Table 5-6 Combination used as unambiguous measurement in the third step

Name	i	j	k	m	λ_c (m)	$R_{i,j,k,m}$	i+j+k+m	$A_{i,j,k,m}$
Trans3	0	5	-1	-4	0.62	-1.64	0	16.7

Similarly the candidates for the third combinations are those with reasonable wavelength-to-noise ratio and independent of Com0 and Com2. Table 5-7 shows a list of possible candidates for the third combination. The success rates for these combinations are shown in Figure 5-3. It is obvious that combination Com4 should be selected as it is associated with a larger success rate.

Table 5-7 Candidates for the third combination

Name	i	j	k	m	λ_c (m)	$R_{i,j,k,m}$	$A_{i,j,k,m}$	i+j+k+m	$\lambda_c / A_{i,j,k,m}$
Com4	1	-1	0	0	1.01	-1.23	6.84	0	0.15
Com5	1	-4	2	1	5.86	0.66	117.07	0	0.05
Com6	-1	4	0	-3	29.3	-13.77	626.69	0	0.047

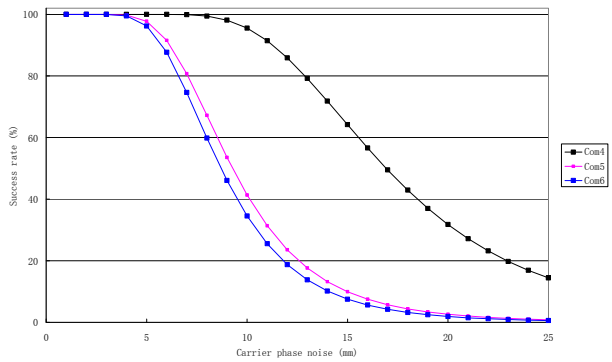

Figure 5-3 Approximate success rates of Com4, Com5 and Com6

The fourth combination

Similar to the way to find the third combination, we will use a combination of Com0, Com2, and Com4 which has a minimum noise level, to constrain the solution of N_{W4}. Table 5-8 shows the combination (called Trans4).

The candidates for the fourth combination are listed in Table 5-9 and the success rates for these combinations are shown in Figure 5-4. Obviously, the fourth

combination should be E5a, which corresponds to the larger success rate.

Table 5-8 Combination used as unambiguous measurements in the fourth step

Name	i	j	k	m	λ_c (m)	$R_{i,j,k,m}$	$A_{i,j,k,m}$	i+j+k+m
Trans4	5	0	-2	-3	0.155	-1.32	4.64	0

Table 5-9 Candidates for the fourth combination

Name	i	j	k	m	λ_c (m)	$R_{i,j,k,m}$	$A_{i,j,k,m}$	i+j+k+m	$\lambda_c / A_{i,j,k,m}$
Com7	-1	0	1	1	0.37	3.21	2.85	1	0.130
Com8	-2	1	1	1	0.59	5.77	7.41	1	0.078
Com9	-2	0	1	2	0.73	7.63	10.05	1	0.072
E5a	0	0	0	1	0.255	1.79	1	1	0.255

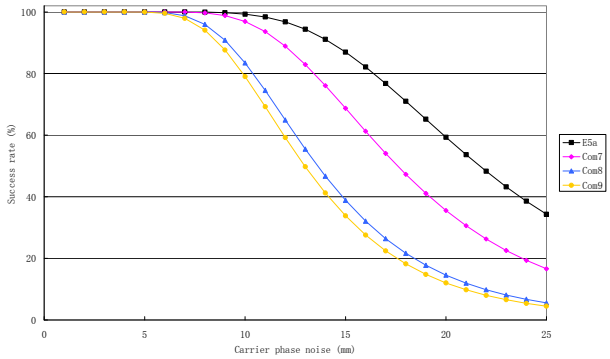

Figure 5-4 Approximate success rates of Com7, Com8, Com9 and E5a

Finally, the optimal combinations for the CAR method based on the success rate criterion are listed in Table 5-10; the two unambiguous combinations with minimum noises for the third and fourth steps are listed in Table 5-11.

Table 5-10 Optimal combinations

Name	i	j	k	m	λ_c (m)	$R_{i,j,k,m}$	$A_{i,j,k,m}$
Com0	0	0	1	-1	9.76	-1.74	54.92
Com2	0	1	-1	0	4.18	-1.6	24.55
Com4	1	-1	0	0	1.01	-1.23	6.84
E5a	0	0	0	1	0.25	1.79	1

Table 5-11 Two unambiguous combinations for the third and fourth steps

Name	i	j	k	m	λ_c (m)	$R_{i,j,k,m}$	$A_{i,j,k,m}$
Trans3	0	5	-1	-4	0.62	-1.64	16.7
Trans4	5	0	-2	-3	0.155	-1.32	4.64

5.2.3 Comparison with combinations proposed by previous research

Different combinations for the CAR method have been proposed by previous research. Table 5-12 and Table 5-13 give two examples with three frequencies (except E6) and four frequencies for Galileo signals (Zhang et al., 2003; Wang et al., 2004). For convenience, they are named Group 1 and Group 2 separately; the optimal combinations selected in this section (Tables 5-10 and 5-11) are named Group 3 in the following context. The success rates for these three groups of combinations are shown in Figure 5-5. The success rate with Group 3 is the largest. From Figure 5-5, it is also shown that more frequency bands will be very useful for ambiguity resolution as the success rate with four frequency combinations is higher than that of three frequency combinations.

Table 5-12 Group 1 combinations

i	j	k	m	λ_c (m)	$R_{i,j,k,m}$	$A_{i,j,k,m}$
0	0	1	-1	9.76	-1.74	54.92
1	0	-1	0	0.81	-1.31	5.39
1	0	0	0	0.19	1	1

Table 5-13 Group 2 combinations

i	j	k	m	λ_c (m)	$R_{i,j,k,m}$	$A_{i,j,k,m}$
0	0	1	-1	9.76	-1.74	54.92
0	1	0	-1	2.93	-1.64	16.98
1	-1	0	0	1.01	-1.23	6.84
0	0	0	1	0.25	1.79	1

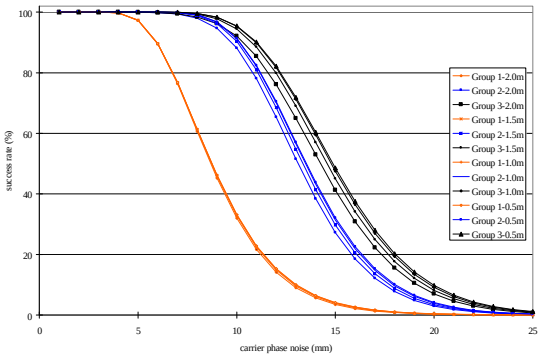

Figure 5-5 The success rates of the three groups of combinations

5.3 Ambiguity resolution performance analysis using ILS and CAR methods

In this section, ambiguity resolution performances with CAR and ILS methods are investigated and compared. Two different methods are used for the evaluation. The first method analyzes the success rate of ambiguity resolution. This provides the answer to the question: is the geometry of Galileo able to support reliable single epoch ambiguity resolution, given a certain measurement noise level and desired success rate? The second method evaluates the actual ambiguity resolution performance based on simulated Galileo observations.

5.3.1 Comparison of CAR and ILS methods based on success rate

The success rate can be used to evaluate the performance of ambiguity resolution of different methods. The success rate is based on *a priori* information of measurement models and provides an expected probability of the ambiguity solution. The lower-bound approximation of the success rate can be calculated as (Teunissen and Odijk, 1997; Teunissen, 1998; Verhagen, 2005):

$$Ps \geq P_{s,B} = \prod_{i=1}^{n} (2\Phi(\frac{1}{2\sigma_{i|I}}) - 1) \qquad (5\text{-}18)$$

where, $\sigma_{i|I}$ is the standard deviation of the i-th ambiguity obtained through a previous i = 1, …, (i – 1) ambiguities. These sequential conditional standard deviations follow from the diagonal elements of the diagonal matrix D, whereby LDL^T is the decomposition to the variance covariance matrix of the float ambiguities Q_N .

For the CAR method, the lower bound success rate to fix carrier phase ambiguities is obtained from the following formula:

$$P_{s,B} = P_{s,B,1} * P_{s,B,2} * P_{s,B,3} * P_{s,B,4} \tag{5-19}$$

where $P_{s,B,i}$ is the lower bound success rate for each step derived from the variance-covariance matrix of float ambiguities.

In this study a success rate threshold of 99.9% is used to assure reliable geometrical strength for ambiguity resolution. This means an ambiguity solution is considered to be a fixed integer only when the lower bound success rate is greater than 99.9%.

The Ambiguity-Fix Rate (AFR) is used to quantify the performance of ambiguity resolution methods in a 24-hour period:

$$AFR = \frac{Number\ \ of\ \ eopch\ with\ success\ rate\ > 99.9\%}{Total\ \ number\ of\ \ epochs\ in\ \ 24\ \ hour} \tag{5-20}$$

Table 5-14 lists the AFR values for the CAR and ILS methods when carrier phase noise is 3mm (1σ). Different pseudorange noise levels from 0.5m to 2m (1σ) are used in the test. For the ILS method, the AFR reaches 100% with single epoch data, independent of pseudorange noise levels. For the CAR method, 100% of AFR can be achieved with single epoch data only when the pseudorange noise levels are less than 1m. The single epoch AFRs for the CAR method drop to 93% and 80% for pseudorange noises of 1.5m and 2.0m respectively. Two epochs of data are required for the CAR method to achieve 100% of AFR.

Table 5-14 AFR for CAR and ILS (phase noise: 3mm)

Time to Fix (second)	AFR (%)							
	Code Noise (m)							
	0.5		1.0		1.5		2.0	
	CAR	ILS	CAR	ILS	CAR	ILS	CAR	ILS
1	100	100	100	100	92.9	100	79.9	100
2	-	-	-	-	100	-	100	-

Table 5-15 shows the AFR values for the CAR and ILS methods when the carrier phase noise level increases to 6mm (1σ). For ILS, the AFR can reach 100% with single epoch data. For the case where the code noise level is 2.0m, the AFR is slightly reduced to 99.6%. For CAR, the AFR is affected by the pseudorange noise level. When the code errors are less than 1m, the AFR can reach 100% with single epoch data. However, when the code noise level increases to 2m, it requires three epochs to reach 100% of AFR.

Table 5-15 AFR for CAR and ILS (phase noise: 6mm)

Time to fix (second)	AFR (%)							
	Code Noise (m)							
	0.5		1.0		1.5		2.0	
	CAR	ILS	CAR	ILS	CAR	ILS	CAR	ILS
1	100	100	100	100	65.42	100	37.6	99.58
2	-	-	-	-	100	-	88.19	100
3	-	-	-	-	-	-	100	-

By further increasing the carrier phase noise level to 12mm, the AFR values significantly reduce for both CAR and ILS methods. The AFR values are 0% for single epoch data with both CAR and ILS methods (as shown in Table 5-16), i.e. no ambiguity solution is able to be fixed with a success rate greater than 99.9%. It requires 3 to 4 epochs to achieve 100% of AFR for both methods, depending on code noise levels.

From the success rate analysis in this section, we find that the single epoch ambiguity resolution is possible for both CAR and ILS methods if the carrier phase noise level is low (< 6mm, 1σ), even with a very high success rate threshold of 99.9%. The ILS method, in general, performs better than the CAR method. The performance of the CAR method is strongly affected by the pseudorange noise level. When the code noise level is larger than 1.5m, the single epoch AFR reduces significantly to less than 93%. Both methods are very sensitive to carrier phase noise level. Four epochs are needed to achieve 100% of AFR for both methods when the carrier phase noise level is 12mm.

Table 5-16 AFR for CAR and ILS (phase noise: 12mm)

Time to fix (second)	AFR (%)							
	Code Noise (m)							
	0.5		1.0		1.5		2.0	
	CAR	ILS	CAR	ILS	CAR	ILS	CAR	ILS
1	0	0	0	0	0	0	0	0
2	0	81.11	0	68.58	0	47.78	0	42.22
3	67.78	100	67.78	100	67.78	99.86	67.78	97.91
4	100	-	100	-	100	100	100	100

5.3.2 Comparison of CAR and ILS methods based on the simulated data

5.3.2.1 Data simulation

To investigate ambiguity resolution performance over short baselines, Galileo measurements are simulated at two stations around Hong Kong - A (114.19^{o}, 22.23^{o}, 11.19m) and B (114.196^{o}, 22.236^{o}, 0.97m). The baseline distance of AB is about 860m.

A 27/3/1 Walker constellation of thirty satellites (27 satellites + 3 operational in-orbit spares) is adopted for the simulated Galileo constellation (GAL OS SIS ICD 2006). The satellites are distributed in three planes in medium Earth orbit (about

24,000km above the Earth's surface). The orbital inclination is 56°. For convenience circular orbits are assumed with a radius of 29,994km.

Gaussian noise is assumed for both carrier phase and pseudorange measurements. Different noise levels (1σ error) have been simulated, as shown in Table 5-17. Tropospheric and ionospheric delays are based on the Hopfield and Klobuchar models (Xu, 2003). Twenty-four hour Galileo measurement data is simulated with epoch intervals of one second, with a total of 86,400 epochs.

Table 5-17 Observation noise levels

observation type and noise level		observation noise (sigma)
carrier phase	Level 1	3mm
	Level 2	6mm
	Level 3	12mm
code	Level 1	0.5m
	Level 2	1.0m
	Level 3	1.5m
	Level 4	2.0m

5.3.2.2 Numerical results of ambiguity resolution performance

Based on the success rate analysis it has been shown above that it is possible to fix ambiguity with single epoch Galileo data, if the carrier phase noise level (1σ) is less than or equal to 6mm. In this section, the performance of the CAR and ILS methods will be examined based on simulated Galileo measurements described in section 5.2.3.1. For ambiguity resolution, the discrimination test is very important. It is dangerous to fix ambiguity if two ambiguity candidates cannot be separated statistically, even when the ambiguity resolution success rate is as high as 100%. In this study, a simple ratio test is used for ambiguity fixing (Euler et al., 1991; Leick, 2004):

$$\frac{R_S}{R} \geq k \tag{5-21}$$

where, R and R_S are the smallest and second smallest sum of residuals for fixed ambiguities respectively; k is an empirically chosen critical value.

Different thresholds have been used by different authors based on their experience, e.g. 1.5 (Han and Rizos, 1996b), 2 (Wei and Schwarz, 1995) and 3 (Leick, 2004). Though not an optimal test, the theoretical foundation of the ratio test has been studied by Teunissen (Teunissen and Verhagen, 2004; Teunissen, 2005). In this study the value 2 is used.

Also the Ambiguity-Fix Rate (AFR) is used to quantify the quality of ambiguity fixing with different methods, but with a slightly different definition.

$$AFR = \frac{Number\ \ of\ \ eopch\ ambiguity\ \ fixed\ to\ integers}{Total\ \ number\ of\ \ epochs\ in\ 24\ \ hour} \tag{5-22}$$

Table 5-18 shows the AFR values for both CAR and ILS, with carrier phase noise of 3mm (1σ). For the ILS method we can achieve 100% single epoch AFR with 24-hour simulated data. For the CAR method, the single epoch AFR can reach 100% when the pseudorange noise level is less than 1.0m. When the code noise increases to 2m, the single epoch AFR reduces slightly to 98.7%; ambiguity resolution can be achieved 100% within three epochs.

Table 5-18 AFR for CAR and ILS (phase noise: 3mm)

Time to fix (second)	AFR (%)							
	Code Noise (m)							
	0.5		1.0		1.5		2.0	
	CAR	ILS	CAR	ILS	CAR	ILS	CAR	ILS
1	100	100	100	100	99.91	100	98.7	100
2	-	-	-	-	100	-	99.95	-
3	-	-	-	-	-	-	100	-

When the carrier phase noise level increases to 6mm, it requires two epochs to fix ambiguities 100% of the time. On the other hand, the single epoch ambiguity fix percentage is still very high with ILS, in fact more than 99.58% (Table 5-19). The

performance of CAR is slightly worse than that of the ILS method. It requires three epochs of data to achieve 100% of AFR.

Table 5-19 AFR for CAR and ILS (phase noise: 6mm)

Time to fix (second)	AFR (%)							
	Code Noise (m)							
	0.5		1.0		1.5		2.0	
	CAR	ILS	CAR	ILS	CAR	ILS	CAR	ILS
1	99.2	99.68	99	99.63	97.9	99.72	94.7	99.58
2	100	100	100	100	100	100	99.7	100
3	-	-	-	-	-	-	100	-

If carrier phase noise level increases to 12mm, the single epoch AFR is low for both CAR and ILS - only around 30% and 47% respectively (Table 5-20). Again, the ILS method performs better that the CAR method. The latter requires five to six epochs to achieve 100% of AFR.

One of the criteria to evaluate ambiguity resolution methods is the missed-fix rate, which is the percentage of solutions fixed to wrong ambiguity integers. Out of a total of 86,400 epochs for a day, the percentages of missed-fix rate based on our simulated Galileo data are shown in Figure 5-6. The missed-fix rate for CAR is around 2 to 3% or around 2,000 epochs out of 86,400 epochs in a day. It is much lower for the ILS method, with a rate less than 0.05%, or less than 43 epochs out of 86,400 epochs.

Table 5-20 AFR for CAR and ILS (phase noise: 12mm)

Time to fix (second)	AFR (%)							
	Code Noise (m)							
	0.5		1.0		1.5		2.0	
	CAR	ILS	CAR	ILS	CAR	ILS	CAR	ILS
1	35.8	50.2	35.4	47.8	32.7	47.2	29.5	44.1
2	88.4	92.4	89.8	92.1	88.8	90.9	86.8	91.8
3	98.2	99.0	98.0	99.1	98.2	98.8	97.8	99.1
4	99.5	99.9	99.8	99.9	99.6	99.8	99.7	99.8
5	99.9	100	100	100	99.9	100	99.9	100
6	100	-	-	-	100	-	100	-

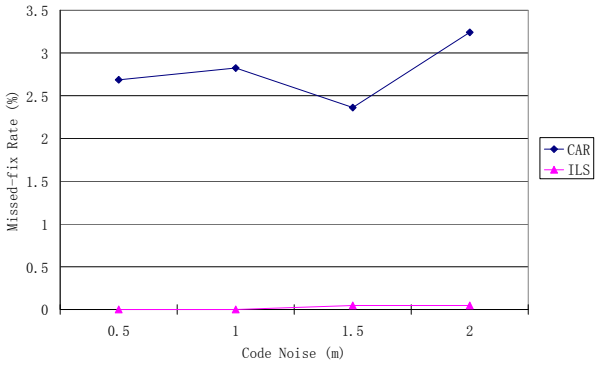

Figure 5-6 Mis-fixed rate for ILS and CAR

In section 5.1.4, it has been demonstrated that the optimal combinations (Group 3, Tables 5-10 and 5-11) for the CAR method have higher success rates than the combinations proposed by previous research: Group 1 (Table 5-12) and Group 2 (Table 5-13). Here the performance of these three groups of combinations will be examined based on simulated Galileo data. Figure 5-7 shows the AFR values for the three groups. Noise levels of 12mm and 1.5m are used for carrier phase and pseudorange measurements respectively. It shows again that the optimal combinations proposed in this paper perform better. To achieve 100% AFR one needs 6 epochs for Group 3 but 9 epochs for Group 1.

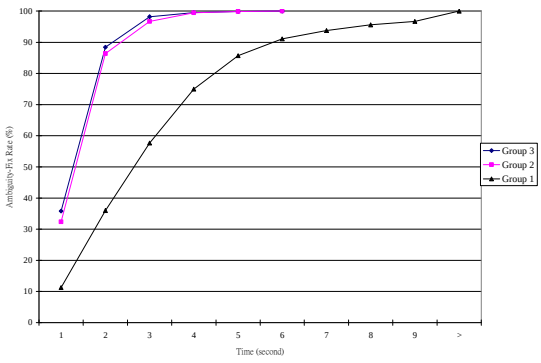

Figure 5-7 Comparison of three groups of combinations for the CAR method

5.3.2.3 Performance of single epoch ambiguity resolution with Galileo

A question we try to answer relates to the possibility of reliably fixing ambiguities from single epoch Galileo observations. For any ambiguity resolution algorithms the discrimination test is based on carrier phase residuals. Therefore, in this study we will check if the single epoch minimum sum of residuals $V^T PV$ corresponds to the correct ambiguities. The results are obtained based on the simulated Galileo data, assuming carrier phase and pseudorange noises obeying a zero-mean Gaussian distribution. The results are shown in Figure 5-8 for the CAR and ILS methods. When the carrier phase noise level is 3mm, for 100% of epochs the minimum sum $V^T PV$ corresponds to the correct ambiguities. At the level of 6mm, the percentage of correct matches is still high - more than 99.7% for both methods. However, when the carrier phase noise level increases to 12mm, there are more than 20% of epochs where the minimum sum of residuals do not correspond to the correct ambiguities, which will lead either to no ambiguity fixing solutions or wrong fixes. The ILS method performs slightly better with the success rate ranging between 92% and 98%, depending on the quality of the pseudorange.

Figure 5-9 gives the mean success rates calculated for every epoch in a day (86,400 epochs), with different carrier phase and pseudorange noise levels for CAR and ILS respectively. It can be seen that the mean success rates are very high if the carrier phase noise level is less than 6mm - more than 99% for both methods - while the ILS method has slightly higher success rates, especially when the pseudorange noise level is larger (2m). When the carrier phase noise level increases to 12mm, the mean success rates reduce significantly for both methods - to 77-82% for CAR and 90-97% for ILS.

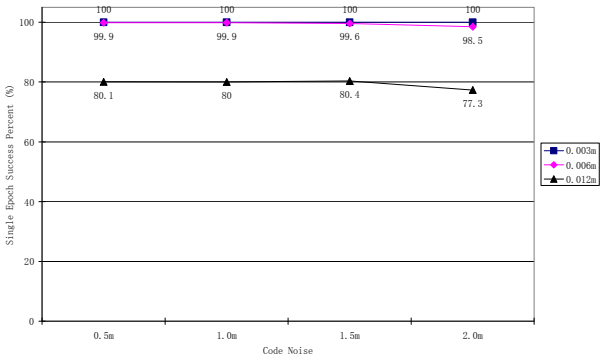

a) CAR method

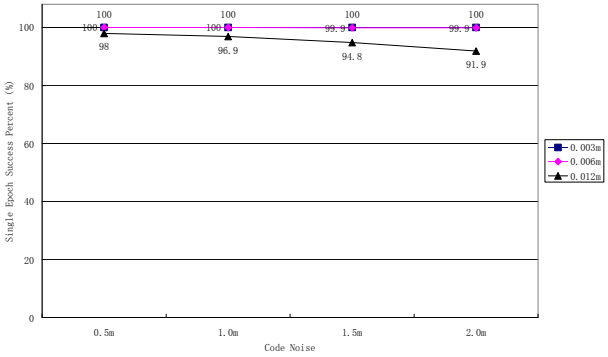

b) ILS Method

Figure 5-8 The Percentage of Epochs for the single epoch $V^T PV$ corresponding to correct ambiguities

Figure 5-10 gives the percentage of epochs in which the ambiguities can be fixed to the correct integers using the test ratio method (k=2) for both methods. For the ILS method the ambiguities can be fixed to integers for 100% of the epochs when the carrier phase noise level is 3mm, or 99.6% of the epochs with a carrier phase noise level of 6mm. However, the ambiguity fixing rate drops to about 50% if the carrier phase noise level increases to 12mm. For the CAR method, the ambiguity fixing rate is less than that of the ILS method. However, 100% of epochs ambiguity fixing can still be achieved if the carrier phase and pseudorange noise levels are low (i.e. 3mm and 0.5m respectively). The CAR method is more sensitive to pseudorange errors; as

the pseudorange errors level increases, the percentage of epochs of ambiguity fixing reduces.

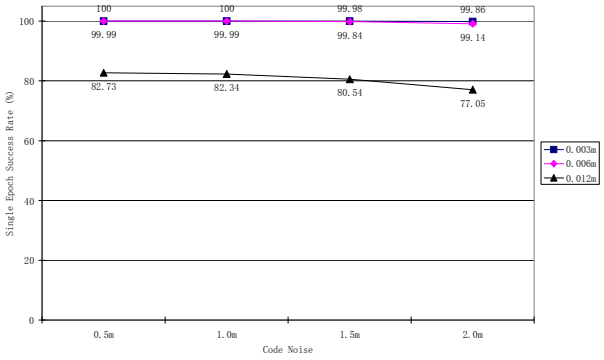

a) CAR method

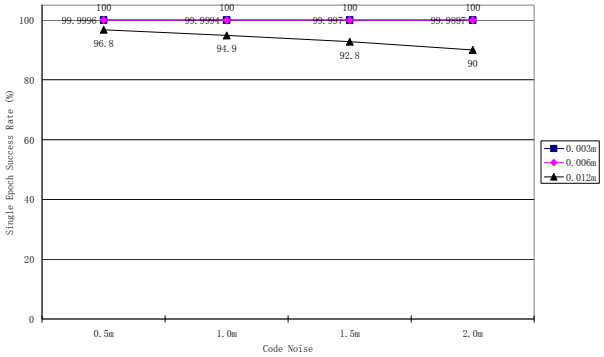

b) ILS method

Figure 5-9 The single epoch success rate for CAR and ILS Methods

The ratio test method (k=2) is a very conservative method, especially when the carrier phase noise level is large (i.e. 12mm). Comparing Figures 5-8b and 5-10b, for over 90% of epochs, the minimum sum of residuals correspond to the correct ambiguities, but only for around 50% of epochs can the ambiguities be fixed to their integers by the ratio test method.

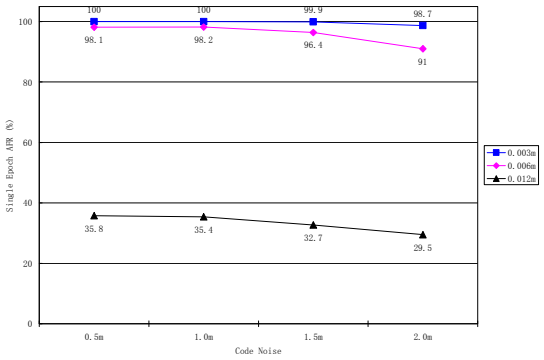

a) CAR Method

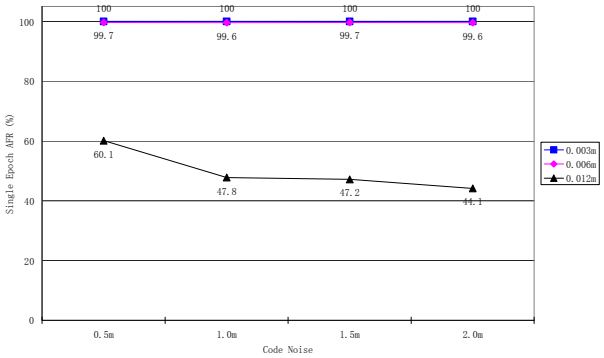

b) ILS method

Figure 5-10 Percentage of single epoch ambiguity fix with CAR and ILS Methods

5.4 Single epoch positioning performance with partial ambiguity resolution

From the test results in the above sections, we can see that when the carrier phase noise is as small as 3mm, all ambiguities may be fixed with 1 epoch; when noise increases to as large as 12mm, single-epoch performance is degraded significantly. Therefore navigation continuity would be greatly affected by carrier phase positioning when large observation noises or outliers occur.

Centimetre positioning accuracy can be reached once all ambiguities are fixed. But this precision level is not necessary for many navigation applications. A partial solution concept has been proposed as another alternative for carrier phase positioning (Teunissen, 1998; Teunissen et al., 1999) in case of failing to fix all ambiguities.

In this section, single-epoch positioning performance with partial ambiguity resolution is investigated with Galileo alone and Galileo and modernized GPS constellations.

5.4.1 Partial ambiguity resolution concept

When it is not possible to resolve the complete vector of ambiguities with sufficient confidence, as an alternative, one may consider resolving only a subset of the ambiguities. Then the receiver position will be estimated by fixing the subset of ambiguities to their integers, while leaving the remaining ambiguities as a float solution.

The bootstrapped probability of partial ambiguity resolution can be calculated according to the following formula (Teunissen, 1998; Teunissen et al., 1999):

$$P_{partial} = \prod_{i=1}^{m} (2\Phi(\frac{1}{2\sigma_{\bar{a}_{i|I}}}) - 1) > P_{\bar{a}} = \prod_{i=1}^{n} (2\Phi(\frac{1}{2\sigma_{\bar{a}_{i|I}}}) - 1) \qquad (5\text{-}27)$$

where $P_{partial}$ is the probability of resolving a subset of m ambiguities and $P_{\bar{a}}$ is the probability of resolving all n ambiguities.

The partial solution success rate (Eq. 5-27) has a design-stage meaning and is highly dependent on the correctness of stochastic models. In this section, a practical method is proposed to select the subset of ambiguities which can be fixed to integers. Firstly the float ambiguity resolution is calculated and also the corresponding variance-covariance matrix for the combinations Com0, Com2, Com4 and E5a (table 5-10). Then the ambiguity combinations that cannot be distinguished by the Ratio test will be selected for further investigation. In other words, all ambiguity candidates are selected if their corresponding sums of residuals R meet the following requirement:

$$\frac{R_i}{R_{\min}} \le k \qquad (5\text{-}28)$$

where $R_{\min}$ is the minimum sum of residuals, R_i is the value corresponding to i-th ambiguity candidate and k is a predefined threshold.

If there are any ambiguities which are common in the selected ambiguity combinations, those ambiguities will be considered as able to be fixed. Finally after fixing those ambiguities, the receiver position will be estimated again as the partial ambiguity fixing solution.

5.4.2 Simulation study

To assess real-time positioning continuity and accuracy, single-epoch ambiguity resolution performance based on partial ambiguity resolution with Galileo alone and modernized GPS + Galileo are investigated and compared. The data used for the investigation are simulated as discussed in Section 5.2.3.1.

Similar to Galileo, optimal combinations of modernized GPS (three frequency bands, L1, L2 and L5) have been selected based on the success rate, as listed in Table 5-21 and 5-22. Combination Trans1 in Table 5-25 is similar to Trans3 and Trans4 in Table 5-11.

Table 5-21 Optimal combinations of modernized GPS

Name	j_1	j_2	j_3	λ_c (m)	R	A
Com1	0	1	-1	4.19	-1.61	24.56
Com2	1	-1	0	1.01	-1.23	6.84
L5	0	0	1	0.25	1.79	1

Table 5-22 Combination formed from Com0 and Com1

Name	j_1	j_2	j_3	λ_c (m)	R	A
Trans1	3	-1	-2	0.29	-1.28	5.28

5.4.2.1 Single-epoch full ambiguity resolution performance

Firstly, the single-epoch performance to fix all ambiguities is investigated. Table 5-23

shows the AFR values for both Galileo and GPS/Galileo constellations, with different carrier phase and pseudorange noise levels (1σ), based on 24-hour simulated data with a sample rate of 1 second.

Table 5-23 The single epoch AFR (%) for Galileo and GPS/Galileo constellation

Carrier phase noise (mm)	Code Noise (m)							
	0.5		1.0		1.5		2.0	
	Galileo	GPS/Galileo	Galileo	GPS/Galileo	Galileo	GPS/Galileo	Galileo	GPS/Galileo
3mm	100	100	100	100	100	100	100	100
6mm	99.7	100	99.6	100	99.7	100	99.6	100
12mm	50.2	74.6	47.8	69.9	47.2	54.7	44.1	48.6

From table 5-23, it can be seen that when the carrier phase noise level is 3mm, the ambiguity can be fixed to their integers 100%, based on the simulated data for both constellations. On the other hand, if the noise level increases to 12mm, ambiguities can be fixed to their integers with only around 50% of epochs. Therefore for the rest of the epochs, the positioning accuracy would reduce to a metre level (differential pseudorange positioning).

5.4.2.2 Partial ambiguity resolution performance

For those epochs in which the ambiguities cannot be fixed for all satellites, can we fix a subset of the ambiguities to improve positioning accuracy? In this investigation, the method proposed in section 5.4.1 is used to estimate receiver position with partial ambiguity resolution. Particularly, we are interested in whether we can determine the receiver position with an accuracy of less than 10cm.

Table 5-24 summarizes the positioning results with a partial ambiguity resolution method, with larger carrier phase noise levels (6mm and 12mm). Based on the simulated data, the positioning errors are less than 10cm for 100% of epochs if the carrier phase noise level is 6mm for both Galileo alone and GPS/Galileo constellations. However, if the carrier phase noise level increases to 12mm, there is no significant improvement in positioning accuracy using the partial ambiguity resolution

for Galileo only constellation and only a few percent more epochs can reach the positioning accuracy of less than 10cm. On the other hand, by increasing the number of satellites (GPS/Galileo constellation), the number of epochs for which positioning errors are less than 10cm increases to over 90% from around 50% for full ambiguity resolution. Also, the maximum positioning errors of the partial ambiguity resolution method are examined within the one-day simulated data. It is shown that the maximum errors for the case of Galileo only (carrier phase and pseudorange errors are 12mm and 2m respectively) can reach up to several metres (differential pseuodrange performance), while it is 0.6m for the GPS/Galileo constellation under the same noise levels.

Table 5-24 Percentage of epochs with a positioning error of less than 10cm

Carrier phase noise	Code Noise (m)							
	0.5		1.0		1.5		2.0	
	Galileo	GPS/Galileo	Galileo	GPS/Galileo	Galileo	GPS/Galileo	Galileo	GPS/Galileo
6mm	100	100	100	100	100	100	100	100
12mm	58.6	99.1	55.9	98.1	54.2	94.5	51.7	90.6

5.5 Summary

In this chapter, the performance of ambiguity resolution has been investigated using multiple frequency data from the Galileo system. An optimal frequency combination has been proposed based on the success rate analysis. Two algorithms (CAR and ILS) are compared for the efficiency of ambiguity resolution based on theoretical analysis (success rate) and simulation studies. Particularly, the possibility of ambiguity resolution with single epoch Galileo data is studied. Based on this study, we can summarize as follows:

- With four frequency Galileo data, it is highly possible to achieve reliable single epoch ambiguity resolutions, when the carrier phase noise level is

reasonably low (i.e. less than 6mm). This has been confirmed by both the success rate analysis and simulation study.

- Carrier phase noise level is an important factor for successful single epoch ambiguity resolution. If the carrier phase noise level increases to 12mm, the performance of single epoch ambiguity resolution degrades significantly. The pseudorange noise levels do not affect ambiguity resolution performance of the ILS method very much, but have strong effects on the CAR method.
- Two ambiguity resolution methods are compared in this study. In general, the ILS method performs better than the CAR method on single epoch ambiguity resolution, based on both the success rate analysis and simulation study.
- A group optimal frequency combination is proposed based on the success rate criterion for the CAR method. The test shows that the optimal combination performs better than the combinations proposed in previous studies which are based on wavelength-to-noise ratio.
- The success rate analysis method is a very powerful tool for studying the performance of ambiguity resolution. The ambiguity resolution performance obtained from the success rate analysis is very close to the simulation results.
- With the simulated Galileo data, the ratio test with a critical value of 2 seems to be too conservative.
- With the Galileo constellation only, the positioning accuracy does not improve significantly with partial ambiguity resolution. By increasing the number of satellites (GPS/Galileo), positioning error can be significantly reduced. Over 90% of epochs (out of 86,400), the positioning errors are less than 10cm and the maximum error is less than 0.6m.

Chapter 6 An improved CAR method for multiple frequency ambiguity resolution

From the simulation studies in Chapter 5, it is shown that ambiguity resolution performance of the ILS method is slightly better than that of the CAR method. By comparing these two methods, we can find several differences:

- ILS uses original carrier phase measurements, while the CAR method uses those of carrier phase combinations which generally have larger noise levels.
- The effects of code measurements in CAR method is larger than that in the ILS method due to larger measurements of noise of long wavelength combinations used in the CAR method. Thus, the CAR method can be more easily affected by large code noise.
- The CAR method fixes ambiguities step by step (bootstrap) after every step. By fixing a subset of ambiguities, the unambiguous measurement is helpful for resolving the rest of the ambiguities.
- The CAR method applies an optimal ambiguity combination based on the success rate, while ILS uses an approximate orthogonal combination.

In this section, an improved CAR is proposed which includes the advantages of both ILS and CAR. Like ILS, the new algorithm uses original carrier phase measurement, instead of those of the combinations used in the CAR method. Meanwhile, the optimal ambiguity combination based on the success rate and the bootstrap algorithm are adopted in the new algorithm.

Similar to Chapter 5, the performance of the new algorithms will be studied using simulated multiple frequency Galileo data.

6.1 Mathematical models of the improved CAR method

The linearized double-differenced Galileo pseudorange and carrier phase measurements for frequency band i (i=1, 2, 3, 4) can be expressed as:

$$\begin{aligned} AX &= L_{code} + n_p \\ AX + \lambda_i N_i &= L_i + n_i \end{aligned} \tag{6-1}$$

where X is a position parameter; N_i is an ambiguity parameter of frequency band i; L_{code} and L_i are pseudorange and carrier phase measurements respectively; n_P and n_i are measurement noises for pseudorange and carrier phase measurements respectively; A is the linearised coefficient matrix related to the position parameters; and λ_i is wavelength.

Firstly, an optimal combination of different frequencies will be identified based on the success rate (i.e. in Chapter 5). Then the original ambiguity vector N will be mapped to the combination N_{com}, to let $N=CN_{com}$. Finally the ambiguity will be solved using the bootstrap approach similar to the CAR method used in Chapter 5. The improved CAR method can be described in the following mathematical model:

$$\begin{cases} AX = L_{Code} \\ AX + \lambda CN_{Com} = L \end{cases} \tag{6-2}$$

$$\begin{cases} AX = L_{Com1} - \lambda_{Com1}\breve{N}_{Com1} \\ N_{Com1} = \breve{N}_{Com1} \\ AX + \lambda CN_{Com} = L \end{cases} \tag{6-3}$$

$$\begin{cases} AX = L_{Trans3} - \lambda_{Trans3}\breve{N}_{Trans3} \\ N_{Com1} = \breve{N}_{Com1} \\ N_{Com2} = \breve{N}_{Com2} \\ AX + \lambda CN_{Com} = L \end{cases} \tag{6-4}$$

$$\begin{cases} AX = L_{Trans4} - \lambda_{Trans4}\breve{N}_{Trans4} \\ N_{Com1} = \breve{N}_{Com1} \\ N_{Com2} = \breve{N}_{Com2} \\ N_{Com3} = \breve{N}_{Com3} \\ AX + \lambda CN_{Com} = L \end{cases} \quad (6\text{-}5)$$

where, L is the measurement vector of original carrier phase measurements; λ is the wavelength vector of the original carrier phase; N_{Com} is an unknown ambiguity vector of four Galileo optimal combinations and if we denote ambiguities of original carrier phase measurements as N, C is the transformation matrix from N_{Com} to N, that is $N = CN_{Com}$.

For the improved CAR, original carrier phase measurements are used and all ambiguities of four combinations are included as unknown parameters. In every step, only an ambiguity vector of one combination is fixed and the fixing order is from that with the longest wavelength to that of the shortest one. The mathematical model is updated every step: the fixed ambiguity is included as known parameters and unambiguous measurement is changed to the most precise one currently available.

In Eq. 6-1, the atmospheric effects is not considered and thus it can be considered a short baseline case (most errors are cancelled by the differencing process). For longer baselines (i.e. > 30km), the atmospheric effects cannot be ignored. For long baselines, the double-difference observation equation is:

$$A_i I + B_i X + C_i T + D_i N = L_i \qquad , P_i \quad (6\text{-}6)$$

Where,

I - ionospheric delay parameter vector;

X - coordinate components;

T - zenith tropospheric delay parameter vector;

N - ambiguity vector;

L_i - pseudorange and carrier phase measurements;

B_i - coefficient matrix of X ;

D_i - coefficient matrix of N ;

C_i - mapping function for slant tropospheric delay;

A_i - coefficient matrix of I ;

P_i - weight matrix.

For long baselines, the ionospheric delay is the main problem, due to the fact that the dry component of the tropospheric delay can be accurately modelled. In this study, we will mainly consider how to deal with the ionospheric delays. Combining X, T and N as a vector Y, Eq. 6-6 can be rewritten as:

$$A_i I + B_i Y = L_i \qquad , P_i \tag{6-7}$$

Where, B_i is the coefficient matrix of Y.

The least squares normal equation can be formed:

$$\begin{bmatrix} A_i^T P_i A_i & A_i^T P_i B_i \\ B_i^T P_i A_i & B_i^T P_i B_i \end{bmatrix} \begin{bmatrix} I \\ Y \end{bmatrix} = \begin{bmatrix} N_{11,i} & N_{12,i} \\ N_{21,i} & N_{22,i} \end{bmatrix} \begin{bmatrix} I \\ Y \end{bmatrix} = \begin{bmatrix} A_i^T P_i L_i \\ B_i^T P_i L_i \end{bmatrix} \tag{6-8}$$

To eliminate ionospheric delay parameters, an equivalent elimination process (Xu, 2003) can be applied.

The elimination matrix is formed as $\begin{bmatrix} E & 0 \\ -Z & E \end{bmatrix}$, with $Z = N_{21} N_{11}^{-1}$ and E is the identity matrix. Assuming $J = A_i N_{11,i}^{-1} A_i^T P_i$, then we have:

$$\begin{bmatrix} E & 0 \\ -Z & E \end{bmatrix} \begin{bmatrix} N_{11,i} & N_{12,i} \\ N_{21,i} & N_{22,i} \end{bmatrix} \begin{bmatrix} I \\ Y \end{bmatrix} = \begin{bmatrix} N_{11,i} & N_{12,i} \\ 0 & \overline{N}_{22,i} \end{bmatrix} \begin{bmatrix} I \\ Y \end{bmatrix} = \begin{bmatrix} A_i^T P_i L_i \\ B_i^T P_i (E-J) L_i \end{bmatrix} \tag{6-9}$$

where, $\overline{N}_{22,i} = B_i^T P_i (E-J) B_i$.

Then we have a new normal equation for the i-th epoch with ionospheric delay eliminated:

$$\overline{N}_{22,i} Y = B_i^T P_i (E - J) L_i \tag{6-10}$$

Because matrices J and $E - J$ are idempotent and $(E - J)^T P_i$ is symmetric, we have:

$$\overline{N}_{22,i} = B_i^T P_i (E - J) B_i = B_i^T (E - J)^T P_i (E - J) B_i \tag{6-10}$$

and

$$B_i^T P_i (E - J) L_i = B_i^T (E - J)^T P_i L_i . \tag{6-11}$$

Denoting $F_i = (E - J) B_i$, the new equivalent observation equation of the i-th epoch is:

$$F_i Y = L_i \qquad , P_i \tag{6-12}$$

With multiple epoch data, the observation equation can be rewritten as:

$$AX + BN = L \qquad , P \tag{6-13}$$

where, X is the vector of coordinates and tropospheric delay; N is the ambiguity vector; A and B are corresponding coefficient matrixes. We can see that ionospheric delay parameters are eliminated.

Comparing Eqs (6-13) and (6-1), both equations have a similar form. Therefore, after the ionospheric delay is eliminated using this method, we can apply the same method for the short baseline approach to estimate ambiguity and position parameters for long baselines.

As discussed in Chapter 5, the success rate is a powerful indicator of the geometric strength of ambiguity solution. In the following study, the following criteria for ambiguity resolution validation are applied:

- Partial-solution success rate is larger than $0.999^{\frac{1}{4}}$;
- Ratio critical value is larger than 2.

Assuming that the total ambiguity number is n and the first m ambiguities are fixed, the success rate of partial solution can be calculated according to the following formula (Teunissen et al., 2000):

$$Ps \geq P_{s,B} = \prod_{i=1}^{m} (2\Phi(\frac{1}{2\sigma_{i|I}}) - 1) \tag{6-14}$$

6.2 Performance analysis of the improved CAR method based on simulation

6.2.1 Short baseline

In this section, ambiguity resolution performance with the improved CAR method is investigated based on simulated data described in Section 5.3.2.1. Similar to Section 5.3, the Ambiguity-Fix Rate (AFR) is used again to quantify the quality of ambiguity fixing.

Table 6-1 shows the AFR with carrier phase noise of 3mm (1σ). For comparison, the results obtained in Section 5.3 for the ILS method is also listed in the table. It can be seen that both improved CAR and ILS methods can achieve 100% single epoch AFR with 24-hour simulated data.

Table 6-1 AFR for the improved CAR and ILS methods (phase noise: 3mm)

Time to fix (second)	AFR (%)							
	Code Noise (m)							
	0.5		1.0		1.5		2.0	
	Imp. CAR	ILS	Imp. CAR	ILS	Imp. CAR	ILS	Imp. CAR	ILS
1	100	100	100	100	100	100	100	100

When the carrier phase noise level increases to 6mm, for the improved CAR method, it can still achieve 100% single epoch AFR with 24-hour simulated data (as shown in Table 6-2). Compared with the results of the ILS method, we can see that the performance of the improved CAR method is slightly better than the ILS method.

Table 6-2 AFR of the improved CAR and ILS methods (phase noise: 6mm)

Time to fix (second)	AFR (%)							
	Code Noise (m)							
	0.5		1.0		1.5		2.0	
	Imp. CAR	ILS	Imp. CAR	ILS	Imp. CAR	ILS	Imp. CAR	ILS
1	100	99.68	100	99.63	100	99.72	100	99.58
2	-	100	-	100	-	100	-	100

If the carrier phase noise level increases to 12mm, the improved CAR method cannot resolve the ambiguity in a single epoch all the time (only around 70% of epochs). However, compared with the results of the ILS method with the same noise levels, the improved CAR obviously performs better.

Table 6-3 AFR of improved CAR and ILS (phase noise: 12mm)

Time to fix (second)	AFR (%)							
	Code Noise (m)							
	0.5		1.0		1.5		2.0	
	Imp. CAR	ILS	Imp. CAR	ILS	Imp. CAR	ILS	Imp. CAR	ILS
1	78.6	50.2	72.2	47.8	70.2	47.2	67.2	44.1
2	98.6	92.4	99.1	92.1	98.5	90.9	98.5	91.8
3	99.9	99.0	99.9	99.1	99.9	98.8	99.9	99.1
4	100	99.9	100	99.9	100	99.8	100	99.8
5	-	100	-	100	-	100	-	100

Similar to the study in Chapter 5, single epoch ambiguity resolution performance with the improved CAR method has been investigated. Figure 6-1 shows the percentage of the single epoch $V^T PV$ corresponding to correct ambiguities.

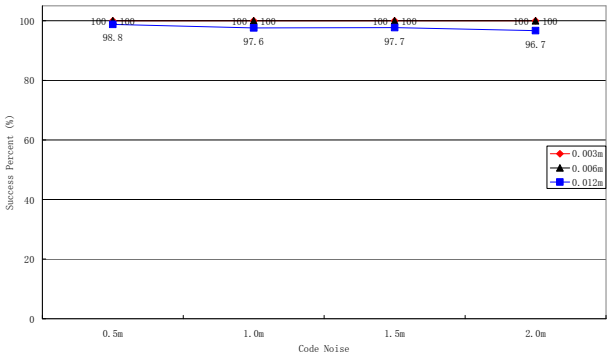

Figure 6-1 Single-epoch performance of the improved CAR method

When the carrier phase noise is less than 6mm (1 sigma), 100% single-epoch ambiguity resolution can be achieved. More than 96% of a total of 86,400 epochs provide correct ambiguity resolutions even when 1 sigma of carrier phase noise is 0.012m, while with the CAR method it is only about 80% and with the ILS method only about 90%.

6.2.2 Long baselines

6.2.2.1 Data simulation

The pseudorange and carrier phase measurements are simulated on frequency bands as listed in Table 6-4. Pseudorange measurement over E6 is not simulated due to its restricted access to public users.

Table 6-4 Simulated pseudorange and carrier phase measurements

Measurement type	Frequency bands
Carrier phase	E1, E6, E5b, E5a
Pseudorange	E1, E5b, E5a

To investigate ambiguity resolution performance of different lengths of baselines, 10 stations are simulated and 9 baselines are formed as listed in Table 6-5 and 6-6.

Table 6-5 Simulated stations

Station Name	X	Y	Z	Longitude	Latitude	Altitude
A	-2420466.778	5388173.100	2398086.812	114.19°	22.23°	1.19m
C	-2443402.300	5363914.722	2428805.036	114.491°	22.531°	1.19m
D	-2466082.725	5339417.907	2459457.750	114.791°	22.831°	1.19m
E	-2488505.564	5314685.322	2490044.121	115.091°	23.131°	1.19m
F	-2506692.778	5294237.100	2515066.812	115.336°	23.377°	2.01m
G	-2548379.778	5245997.100	2573187.812	115.909°	23.950°	1.03m
H	-2589094.778	5196934.100	2631055.812	116.482°	24.523°	1.00m
I	-2628821.778	5147068.100	2688664.812	117.055°	25.096°	1.58m
J	-2667542.778	5096418.100	2746009.812	117.628°	25.669°	1.56m
K	-2812077.778	4886390.100	2972625.812	119.920°	27.960°	1.24m

Table 6-6 Baselines formed

Baselines	Distance (KM)
AC	45
AD	90
AE	135
AF	173
AG	259
AH	345
AI	431
AJ	516
AK	857

Main simulated error sources are listed in Table 6-7.

Table 6-7 Main error sources simulated

Error sources	Size or model
Carrier phase observation noise (sigma)	3mm
pseudorange observation noise (sigma)	1.5m
Tropospheric effect	Hopfield model
Ionospheric effect	Klobuchar model

6.2.2.2 Ambiguity resolution performance analysis

For long baselines, it is difficult to achieve one epoch ambiguity resolution as for the short baselines. However, we still need to know how long is required to resolve for ambiguities. In this study, we start from every epoch in 24-hour simulated data and then examine how long we can achieve a reliable ambiguity resolution. It can be seen from Table 6-8 that the average time for ambiguity resolution over long baselines is in the range of 34 to 64 seconds, depending on the baseline lengths, while the maximum time required for ambiguity resolution is in the range of 3 min to 10 min. For comparison, the corresponding values are also provided for the ILS method (Table 6-9). The mean time for ambiguity resolution with the improved CAR method reduced to about 50%, compared with the ILS method. There are mis-fixed cases (fixed to wrong ambiguities) for both methods. But the mis-fixed percentages are less than 0.1% for both methods.

Table 6-8 Time required for ambiguity resolution for the Improved CAR method

	Baseline								
	AC	AD	AE	AF	AG	AH	AI	AJ	AK
Average time (seconds)	33.8	34.2	35.1	35.8	39.4	40.5	43.2	44.8	63.9
Maximum time (seconds)	180	168	312	167	503	335	549	343	566

Table 6-9 Time required for ambiguity resolution for the ILS method

	Baseline								
	AC	AD	AE	AF	AG	AH	AI	AJ	AK
Average time (seconds)	76.0	77.1	79.7	81.3	87.3	89.7	92.4	98.8	131.9
Maximum time (seconds)	279	241	352	336	511	409	566	350	600

6.2.2.3 Positioning accuracy with ambiguity-fix solution

To assess the positioning performance after the ambiguities are fixed, the positioning results are summarized in Table 6-10 for various baseline lengths: their average, maximum and RMS positioning errors in both horizontal and vertical directions. Two cases are investigated: the first - with just one epoch data and the second – with 30 epochs (30 seconds) data.

From Table 6-10, we can see that:

- The positioning accuracy can reach cm level with single epoch data and mm level with 30 epoch data in both horizontal & vertical components;
- The maximum positioning error will not exceed half a metre with single epoch data and 1 decimeter with 30 epoch data in both horizontal & vertical components;
- With an increase of baseline length, the positioning error increases slightly.

Table 6-10 Positioning errors

			Baselines								
			AC	AD	AE	AF	AG	AH	AI	AJ	AK
Average error (m)	Single epoch	Horizontal (mm)	22	23	25	24	25	26	27	30	38
		Vertical (mm)	22	22	23	24	24	25	27	26	33
	30 epochs	Horizontal (mm)	4.2	4.5	4.8	5.3	5.8	6.3	6.9	8.3	11.3
		Vertical (mm)	4.1	4.2	4.3	5.2	6.3	6.2	6.6	7.7	10.3
RMS (m)	Single epoch	Horizontal (mm)	18	19	24	22	22	23	26	28	52
		Vertical (mm)	18	18	22	21	24	24	28	23	49
	30 epochs	Horizontal (mm)	3.6	4.3	4.3	5.8	5.2	4.8	5.0	7.7	8.7
		Vertical (mm)	3.6	3.8	3.8	5.8	4.7	4.9	5.7	9.5	9.0
Maximum error (m)	Single epoch	Horizontal (mm)	125	132	181	171	162	194	205	212	373
		Vertical (mm)	160	113	191	165	265	248	314	170	429
	30 epochs	Horizontal (mm)	38	55	31	50	77	48	39	98	97
		Vertical (mm)	38	38	30	32	30	30	54	98	99

6.2.2.4 Partial ambiguity resolution

As discussed in Chapter 5, with four Galileo frequency bands, we can form combinations with much longer wavelengths (i.e. Com0, Com2 and Com4 in table 5-10). Therefore, we may resolve the ambiguities with those longer wavelengths much faster. Tables (6-11) and (6-12) give the time required for resolving the first two ambiguities (Com0 and Com2) and three ambiguities (Com0, Com2 and Com4). As the wavelengths of these combinations are larger than 1m, they can be easily fixed to their integers within a few seconds.

Table 6-11 Time required for resolving ambiguities for Com0 ad Com2

	Baseline								
	AC	AD	AE	AF	AG	AH	AI	AJ	AK
Average time (seconds)	2.3	2.3	2.3	2.3	2.3	2.3	2.3	2.3	2.3
Maximum time (seconds)	6	5	5	6	5	5	5	6	5

Table 6-12 Time required for resolving Com0, Com2 and Com4

	Baseline								
	AC	AD	AE	AF	AG	AH	AI	AJ	AK
Average time (seconds)	4.2	4.0	4.2	4.1	4.2	4.3	4.1	4.1	4.4
Maximum time (seconds)	20	18	18	52	22	33	41	45	24

6.2.2.5 Positioning accuracy with fixed ambiguities of the first three combinations

Though the ambiguities of Com0 and Com2 can be resolved for in two or three seconds (Table 6-11), unfortunately since their ionospheric delay coefficients are close (Com0: 1.74 vs. Com4: 1.6 in Table 5-10 of Section 5.2.2), the ionospheric delay can not be estimated precisely. The positioning accuracy with the fixed ambiguity solution of Com0 and Com2 can only reach the metre level.

To assess the positioning performance after the ambiguities of Com0, Com2 and Com4 are fixed, the positioning results are summarized in Table 6-13 for various baseline lengths: their average, maximum, RMS positioning errors and also the percentages with positioning errors less than 0.5m in both horizontal and vertical directions. Two cases are investigated: the first - with just 5 epoch data and the second – with 30 epoch (30 seconds) data.

From Table 6-13, we can see that:

- The positioning accuracy can reach a decimeter level with 5 epoch data and almost cm level with 30 epoch data in both horizontal and vertical directions;
- The maximum positioning error will not exceed 2 metres with 5 epoch data and is generally within 1m with 30 epoch data in both directions;
- With the increase of baseline distance, the positioning error increases slightly ;
- The percentages of positioning errors less than 0.5m in both horizontal and vertical directions are above 80% with 5 epoch data and more than 97% with 30 epoch data.

Table 6-13 Positioning accuracy with first three combinations fixed

			Baseline								
			AC	AD	AE	AF	AG	AH	AI	AJ	AK
Average error (m)	5 epochs	Horizontal	0.28	0.30	0.28	0.28	0.30	0.32	0.32	0.31	0.36
		Vertical	0.27	0.26	0.28	0.28	0.28	0.28	0.28	0.30	0.31
	30 epochs	Horizontal	0.11	0.12	0.11	0.11	0.12	0.12	0.13	0.12	0.14
		Vertical	0.11	0.11	0.12	0.12	0.12	0.11	0.12	0.12	0.11
RMS (m)	5 epochs	Horizontal	0.24	0.28	0.27	0.30	0.31	0.29	0.27	0.29	0.33
		Vertical	0.23	0.23	0. 26	0.25	0.25	0.25	0.23	0.26	0.28
	30 epochs	Horizontal	0.10	0.10	0.10	0.09	0.11	0.11	0.12	0.13	0.13
		Vertical	0.10	0.10	0.10	0.10	0.10	0.14	0.11	0.10	0.10
Maximum error (m)	5 epochs	Horizontal	1.57	1.77	1.69	1.72	1.80	1.74	1.87	1.80	1.87
		Vertical	1.41	1.34	1.61	1.41	1.77	1.58	1.12	1.87	1.93
	30 epochs	Horizontal	0.64	0.82	0.73	0.79	0.95	0.99	0.96	1.04	0.92
		Vertical	0.94	0.90	0.70	0.63	1.00	0.69	0.62	0.82	1.15
Percent with error < 0.5m (%)	5 epochs	Horizontal	88.1	85.3	87.5	87.9	85.2	83.8	84.6	83.3	79.7
		Vertical	87.5	87.8	85.8	84.7	85.2	85.0	84.1	81.6	82.7
	30 epochs	Horizontal	98.7	98.5	99.0	99.6	99.2	98.8	99.2	98.5	97.8
		Vertical	99.3	98.9	99.2	99.2	99.2	99.4	99.2	99.4	99.6

6.3 Summary

In this section, an improved CAR method has been proposed for Galileo multiple frequency ambiguity resolution. Instead of directly using combination measurements in the mathematical model like the CAR method, the original carrier phase measurements are used. Also, a uniform model has been established for both short and long baseline ambiguity resolutions.

Based on the simulated data and optimal combinations, ambiguity resolution performance with the improved CAR is investigated and compared with the ILS method. It has shown that the performance of the new method is better than the ILS method in terms of time required for ambiguity resolution and mis-fixed rate.

For short baselines, with four Galileo frequency bands, it is possible to resolve ambiguity to their integers within a single epoch, with a reasonable carrier phase noise assumption (<6mm).

For longer baselines, it requires on average less than 1 min to fix ambiguities, with the maximum time less than 10 minutes. However, the ambiguities of Com0, Com2 and Com4 are easily fixed and generally only about 4 or 5 seconds are required. The positioning accuracy can almost reach cm level in 30 seconds with the partial ambiguity solution.

Chapter 7 Investigation of ambiguity resolution validation methods

To ensure reliable ambiguity resolution, ambiguity validation is an indispensable step. It has been a challenge for many years and is far from being resolved. In Chapters 5 and 6, it is demonstrated that there are some mis-fixed cases in ambiguity resolution using the ratio test method in the simulation studies.

Various ambiguity validation methods have been proposed since 1990s, such as the R-ratio test (Frei and Beutler, 1990; Landau and Euler, 1992; Euler and Schaffrin, 1991; Leick, 2003), difference test (Tiberius and de Jonge, 1995), projector test (Wang et al., 1998a; Han, 1997) and Ellipsoidal Integer Aperture (EIA) estimator (Teunissen, 2005). It has been shown (Teunissen and Verhagen, 2004; Verhagen, 2005) that all of them belong to a class of Integer Aperture (IA) estimator (Teunissen, 2003).

Compared with other IA estimators, Ellipsoidal Integer Aperture (EIA) estimator is the outstanding one, as the fail-rate of ambiguity fixing is easy to evaluate (Teunissen, 2005). In this chapter, firstly the problems associated with the EIA are analyzed.

Some modifications are suggested to improve EIA performance:

- The overlap of aperture regions is allowed to make EIA more applicable and meet the fail-rate requirement at the same time;
- Ratio test is combined with EIA to maintain the statistical advantage of ambiguity resolution.

Based on this modification, a new procedure is proposed for the ambiguity validation process. Tests are carried out based on kinematic GPS observation and simulated Galileo data. Compared with the R-ratio test or EIA alone, the test results

show that the new method proposed in this chapter, which combines the use of both the EIA and R-ratio test, can improve ambiguity resolution reliability.

7.1 Ellipsoidal Integer Aperture estimator and R-ratio test

7.1.1 Integer Aperture (IA) estimators

The class of integer aperture (IA) estimators was introduced by Teunissen (2003) and it is defined as follows.

Definition 1 (Integer aperture estimators)

Let $\Omega \subset R^n$ be the integer translational invariant, i.e. $\Omega = \Omega + z$, $\forall z \in Z^n$ and let $\Omega_z = \Omega \bigcap S_z$ with S_z the pull-in region of an admissible integer estimation. Then integer aperture estimators are defined as:

$$\hat{a}_{IA} = \hat{a} + \sum_{z \in Z^n} (z - \hat{a}) \omega_z(\hat{a}) \tag{7-1}$$

with $\omega_z(x)$ the indicator function of Ω_z .

The IA estimator is a hybrid estimator having as an outcome either the real-valued float solution $\hat{a}$ if $\hat{a} \notin \Omega$ or equal to z when $\hat{a} \in \Omega_z$. Note, since Ω is the collection of all $\Omega_z = \Omega_0 + z$, that the IA estimator is completely determined once Ω_0 is known. The subset Ω_0 can therefore be seen as an adjustable pull-in region and it determines the aperture of the pull-in region.

An IA estimator can produce one of the following three outcomes: $a \in Z^n$ (correct integer), $z \in Z^n \setminus \{a\}$ (incorrect integer), or $\hat{a} \in R^n \setminus Z^n$ (no integer). The probabilities of success (correct integer), failure (incorrect integer) and undecided (no integer) are given as:

$$\begin{cases} P_S = \int_{\Omega_a} f_{\hat{a}}(x) dx \quad \text{(success)} \\ P_F = \sum_{z \neq a} \int_{\Omega_z} f_{\hat{a}}(x) dx \quad \text{(failure)} \\ P_U = 1 - P_S - P_F \quad \text{(undecided)} \end{cases} \tag{7-2}$$

7.1.2 The definition of Ellipsoidal Integer Aperture estimator (EIA)

The aperture pull-in regions of EIA are defined as:

$$E_z = E_0 + z\,,\ E_0 = S_0 \bigcap C_{\varepsilon,0}\,,\ \forall z \in Z^n \tag{7-3}$$

with S_0 being the least-squares pull-in region and $C_{\varepsilon,0} = \{x \in R^n \mid \|x\|^2_{Q_{\hat{a}}} \le \varepsilon^2\}$, an origin-centred ellipsoidal region of which the size is controlled by the aperture parameter ε.

Assuming the float ambiguity solution is distributed as $\hat{a} \sim N(a, Q_{\hat{a}})$ and let the aperture parameter satisfy $\varepsilon \le \frac{1}{2}\min_{z \in Z^n \setminus \{0\}} \|z\|_{Q_{\hat{a}}}$, the EIA-probabilities of failure, success and undecided are given as:

$$\begin{cases} P_F = \sum_{z \in Z^n \setminus \{0\}} P(\chi^2(n, \lambda_z) \le \varepsilon^2) \\ P_S = P(\chi^2(n,0) \le \varepsilon^2) \\ P_U = 1 - P_F - P_S \end{cases} \tag{7-4}$$

in which $\chi^2(n, \lambda_z)$ denotes a random variable having as pdf the non-central Chi-square distribution with n degrees of freedom and non-centrality parameter $\lambda_z = z^T Q_{\hat{a}}^{-1} z$.

To make it more clear, Figure 7-1 is a two-dimensional de-correlated example of EIA. The original ellipsoidal regions become circular after de-correlation.

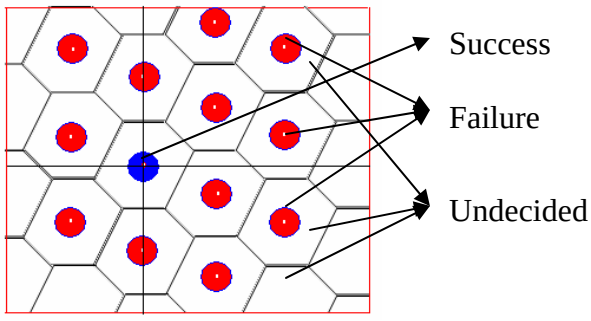

Figure 7-1 Two-dimensional de-correlated example of EIA

The circular region in blue is the aperture region for success; the circular regions in red are the aperture regions for failure; the other parts except the blue and red ones

are regions for undecided. The aperture region sizes are controlled by the aperture parameter ε.

7.1.3 The weaknesses of EIA

- **First weakness**

In the above definition of EIA, to avoid overlap of the aperture regions, the aperture parameter is required to satisfy $\varepsilon \le \frac{1}{2}\min_{z\in Z^n\setminus\{0\}}\|z\|_{Q_{\hat{a}}}$. This requirement is applicable for cases of geometry-free ambiguity resolution with pull-in-region not too narrow like Figure 7-1.

With a narrow pull-in-region as shown in Figure 7-2, the corresponding success and failure probabilities with $\varepsilon = \frac{1}{2}\min_{z\in Z^n\setminus\{0\}}\|z\|_{Q_{\hat{a}}}$ are P_{S0} and P_{F0}. If P_{F0} is too conservative compared with the required fail-rate, generally P_{S0} will be small and the efficiency of ambiguity resolution performance can be very low.

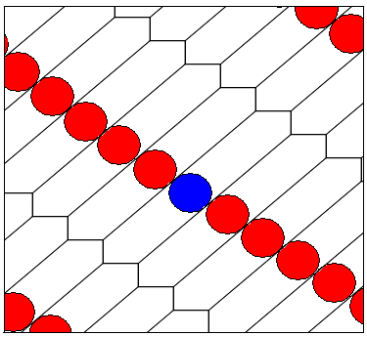

Figure 7-2 Two-dimensional example of EIA with narrow pull-in-region

Such is the case with geometry-based ambiguity resolution: due to the high correlation between ambiguities, the distances $\|z\|_{Q_{\hat{a}}}$ vary greatly and the pull-in-region is generally narrow.

Based on the simulated data in Chapter 5 (code noise: 2m; carrier phase noise: 12mm), the ambiguity resolution performance is investigated with the ILS method and EIA estimator with the required fail rate of 0.001. Figure 7-3 is the time to fix ambiguity with the required fail-rate less than 0.001, Figure 7-4 is the actual fail-rate when fixing ambiguity, and Figure 7-5 is the actual ratio values (Eq. 5-21).

From Figures 7-3 and 7-4, we can see that the actual fail-rate (~10^{-9}) when ambiguities are fixed is much less than the required (~10^{-3}). Hence this requirement on $\varepsilon \le \frac{1}{2}\min_{z\in Z^n\setminus\{0\}}\|z\|_{Q_{\hat{a}}}$ leads to lower performance (long time for ambiguity resolution). In the previous study in Chapters 5 and 6, it has been shown that the time for ambiguity resolution for this data set is only a few seconds with the ratio test method. With the EIA method, there are cases that the required time for ambiguity fixing is beyond one minute (Figure 7-3). From Figure 7-5, it can be seen that the actual ratio values are mostly above 5, and can reach as big as more than 25. This example demonstrates that the EIA method is a very conservative method with a long time for ambiguity resolution, although it is very reliable.

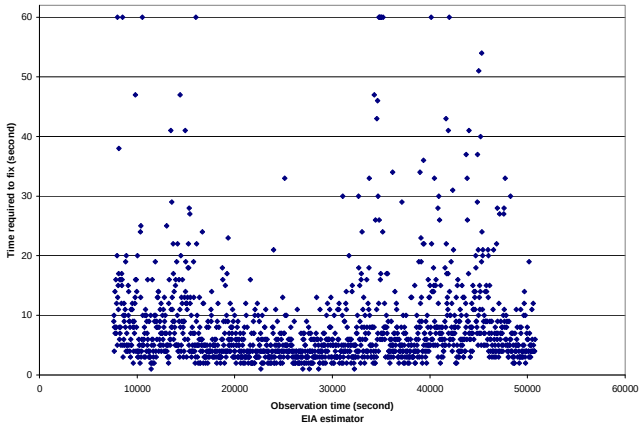

Figure 7-3 Time to fix with the required fail-rate 0.001

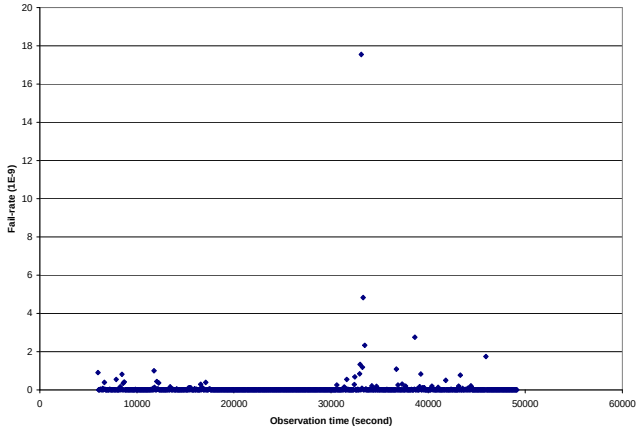

Figure 7-4 Real fail-rate when fixed

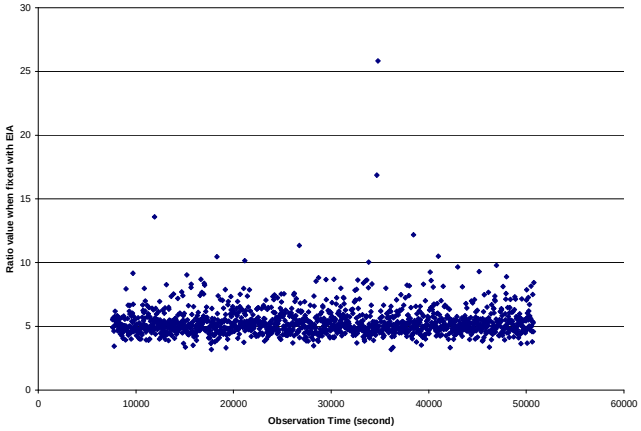

Figure 7-5 Ratio values when fixed

- **Second weakness**

EIA is an estimator with design stage meaning (only use a priori information). It only considers the quality of the best ambiguity resolution candidate and it takes no consideration of the other candidates. In fact, the starting point of EIA is that it first assumes that the best ambiguity resolution candidate is correct, and then calculates its corresponding fail-rate. If the fail-rate meets the requirement, the best ambiguity resolution will be fixed as correct. However, other ambiguity resolution candidates have the possibility to be correct. Especially when the ratio value of the second best to the best is close to 1, they almost have the same possibility of being correct. In this case, even if the fail-rate of EIA very small, the real fail-rate is near to 50%.

As shown in Figure 7-6, when the float ambiguity solution reaches the boundary part (the red part) between two pull-in-regions, the ratio value of the two distances $\|z\|_{Q_{\hat{a}}}$ D1 and D2 (yellow arrows in Figure 7-6) is near to 1, that is, no one is statistically better than the other and the two ambiguity candidates (the central points of the blue parts) have almost equal probability of being correct. Even if the current fail-rate is very small, obviously it is risky to fix ambiguity resolution to this one.

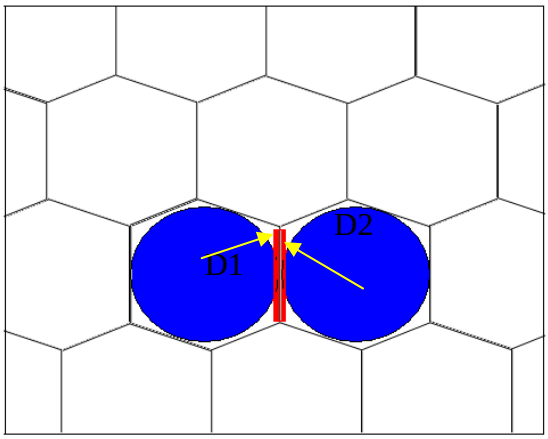

Figure 7-6 Second weakness of EIA

7.1.4 R-ratio validation test

R-ratio test is a popular one used for ambiguity validation (Euler and Schaffrin, 1991; Leick, 2003). If the ratio value between the squared distances (e.g. D1 and D2 in Figure 7-6) of the float ambiguity solution to the best and second best candidates is greater than the predefined critical value (general values: 1.5, 2 or 3), the best candidate will be regarded as statistically better than the others and fixed as correct.

The observation equation strength and observation data quality can affect the reliability of the R-ratio test. For example, when satellite geometry has little change over a short time, the observation equations are always singular and the R-ratio test may become unreliable even with a large predefined critical value. With high level

observation noise or multipath, ambiguities can be mistakenly fixed to wrong ones with the R-ratio test.

7.1.5 Improving EIA

To overcome the first weakness of EIA, the overlap of aperture region is allowed, without the constraint of $\varepsilon \le \frac{1}{2}\min_{z\in Z^n\setminus\{0\}}\|z\|_{Q_{\hat{a}}}$ (see Figure 7-7 as an example).

In Figure 7-8, we can see that the calculated fail-rate $P_F = \sum_{z\in Z^n\setminus\{0\}} P(\chi^2(n,\lambda_z) \le \varepsilon^2)$ (including the overlap parts) is greater than the true fail-rate (excluding the overlap parts) and can be regarded as the upper boundary of the true fail-rate. If $P_F = \sum_{z\in Z^n\setminus\{0\}} P(\chi^2(n,\lambda_z) \le \varepsilon^2)$ is less than the required fail-rate, undoubtedly the true fail-rate also meets the fail-rate requirement. Also, the success aperture region is also expanded by half of the green overlap parts (see Figure 7-7). Therefore, by allowing the overlap of aperture region, the success probability is also increased.

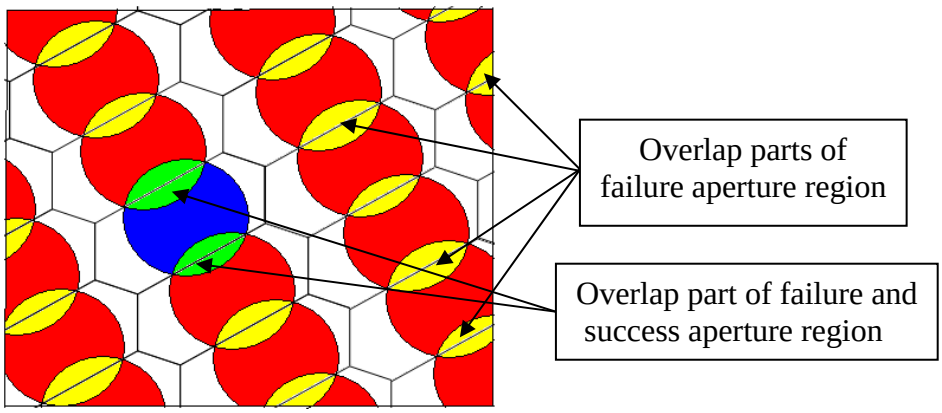

Figure 7-7 Overlapped EIA

7.1.6 EIA and R-ratio test

Both the R-ratio test and EIA belong to a class of IA estimators (Teunissen and Verhagen, 2004; Verhagen, 2005). The R-ratio test can be used to overcome the

second weakness of EIA. That is, the R-ratio test can be used to ensure that the best ambiguity candidate is statistically better than the others, which avoids wrong ambiguity fixing when float ambiguity solution reaches the boundary of the pull-in-region. As shown in Figure 7-9, with the help of the R-ratio test, the aperture region 1 is turned into the undecided aperture region from original failure aperture region of EIA.

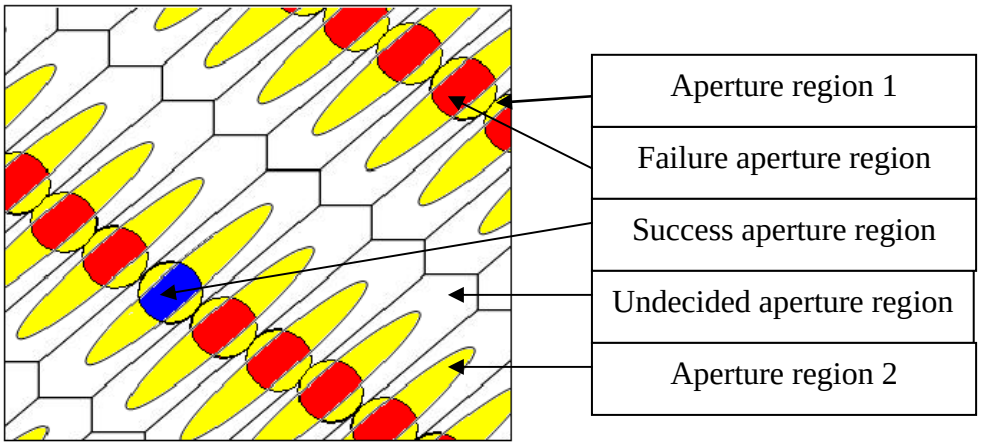

Figure 7-8 EIA + R-ratio test

On the other hand, EIA can help to improve the reliability of the R-ratio test. The fail-rate of EIA is in fact an indicator of both observation equation strength and data quality. With the strict fail-rate requirement of EIA, wrongly fixing cases with the R-ratio test due to big observation errors or poor equation strength can be avoided. As shown in Figure 7-9, the aperture region 2 turned into the undecided aperture region from the original failure aperture region of the R-ratio test.

Based on the above analysis, using the combination of EIA and the R-ratio test for GNSS ambiguity validation is suggested. With this approach, the fail-rate decreases as the failure aperture region becomes smaller. Unfortunately, with the combination the success rate also decreases as the success aperture region becomes the overlapped part of the original regions of EIA and the R-ratio test.

7.2 Estimation of variances of GNSS measurement

The stochastic model represents the quality indicator of observations and is very important for ambiguity resolution. Improper stochastic models on measurement can cause a problem in the calculation of various probabilities (i.e. Eqs 7-2 and 7-4) and therefore can result in wrong decisions in ambiguity validation tests.

Several stochastic models have been proposed in the past years, such as: elevation angle (Euler and Goad, 1991; Gerdan, 1995; Jin, 1996; Han, 1997) or signal-to-noise ratio dependent (Talbot, 1988; Gianniou and Groten, 1996; Langley, 1997), or SIGMA- Δ (Brunner et al., 1999) or ε (Hartinger and Brunner, 1999) and the MINQUE method (Rao, 1971; Wang et al., 1998a) etc. Most of them rely on the priori statistical information. With more frequency band available (i.e. Galileo), it is possible to estimate GNSS measurement error variance directly from the observations. In this section, new models are proposed to estimate both carrier phase and pseudorange measurements errors directly from GNSS observations.

7.2.1 Carrier phase error variance estimation

For each satellite, the carrier phase observation equation can be written as for four frequency bands as:

$$\begin{bmatrix} 1 & \frac{1}{f_1^2} & \lambda_1 & 0 & 0 & 0 \\ 1 & \frac{1}{f_2^2} & 0 & \lambda_2 & 0 & 0 \\ 1 & \frac{1}{f_3^2} & 0 & 0 & \lambda_3 & 0 \\ 1 & \frac{1}{f_4^2} & 0 & 0 & 0 & \lambda_4 \end{bmatrix} \begin{bmatrix} D \\ I \\ N_1 \\ N_2 \\ N_3 \\ N_4 \end{bmatrix} = \begin{bmatrix} L_1 \\ L_2 \\ L_3 \\ L_4 \end{bmatrix} \tag{7-5}$$

where subscript i indicates frequency bands of E1, E6, E5b and E5a respectively; D includes geometric distance plus errors the same for all frequency bands; I is the

ionospheric delay parameter; λ_i, f_i and N_i are wavelength, frequency and ambiguity; L_i is the carrier phase measurements with observation noise and multipath.

Let $A=\begin{bmatrix} 1 & 1 & 1 & 1 \\ \frac{1}{f_1^2} & \frac{1}{f_2^2} & \frac{1}{f_3^2} & \frac{1}{f_4^2} \end{bmatrix}^T$, $B=\begin{bmatrix} \lambda_1 & 0 & 0 & 0 \\ 0 & \lambda_2 & 0 & 0 \\ 0 & 0 & \lambda_3 & 0 \\ 0 & 0 & 0 & \lambda_4 \end{bmatrix}$, $X_1=\begin{bmatrix} D \\ I \end{bmatrix}$, $X_2=\begin{bmatrix} N_1 \\ N_2 \\ N_3 \\ N_4 \end{bmatrix}$,

$L=\begin{bmatrix} L_1 \\ L_2 \\ L_3 \\ L_4 \end{bmatrix}$, Eq. (7-5) can be rewritten as:

$$\begin{bmatrix} A & B \end{bmatrix}\begin{bmatrix} X_1 \\ X_2 \end{bmatrix}=L \tag{7-6}$$

where X_1 includes the time-variant parameters and X_2 includes only the time-invariant ones. Applying the equivalent elimination process (Chapter 6) to delete X_1, we can get:

$$B^T(E-A(A^TA)^{-1}A^T)BX_2=B^T(E-A(A^TA)^{-1}A^T)L \tag{7-7}$$

And

$$B^T(E-A(A^TA)^{-1}A^T)=\begin{bmatrix} 0.0149 & -0.044 & 0.003 & 0.026 \\ -0.054 & 0.176 & -0.060 & -0.061 \\ 0.004 & -0.064 & 0.160 & -0.100 \\ 0.035 & -0.066 & -0.103 & 0.134 \end{bmatrix} \tag{7-8}$$

Denote $V=B^T(E-A(A^TA)^{-1}A^T)L=\begin{bmatrix} v_1 & v_2 & v_3 & v_4 \end{bmatrix}^T$. If there is no cycle slip, the change of V is only affected by observation errors. Thus, the observation data quality of L can be examined from the time series of V.

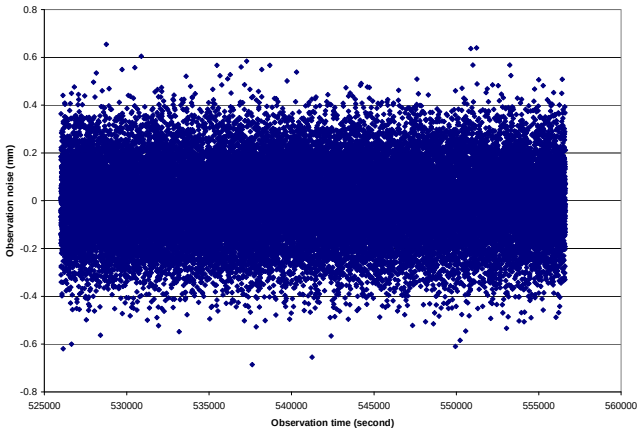

Figure 7-9 time-series of v_1 (simulated with a noise level of 3mm)

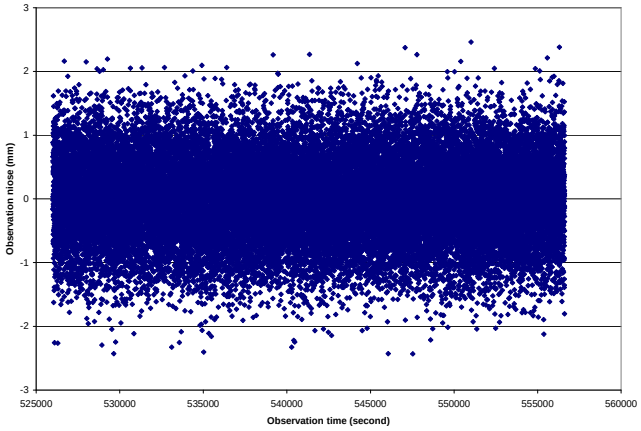

Figure 7-10 time-series of v_1 (simulated with a noise level of 12mm)

Figures 7-9 and 7-10 are two samples of time-series v_1 (with a moving average), simulated with measurement noise of 3mm and 12mm (1σ) respectively.

The RMS values of v1 in Figures 7-9 and 7-10 are 0.064mm and 0.159mm respectively. Based on the error propagation law, we can calculate the standard deviation of the original carrier phase measurement errors, and the results are 3mm and 12mm respectively, which is the same as simulated.

7.2.2 Pseudorange error variance estimation

Pseudorange observation equation can be expressed as:

$$\begin{bmatrix} 1 & \frac{1}{f_i^2} \end{bmatrix} \begin{bmatrix} D \\ I \end{bmatrix} = L_{C_i} \tag{7-9}$$

where, subscript i indicates the frequency bands E1, E6, E5b or E5a.

Combining Eqs (7-9) and (7-5), and applying the equivalent elimination process, we can form an equation that has the same form as Eq. (7-7), and

$$B^T(E - A(A^TA)^{-1}A^T) = \begin{bmatrix} 0.152 & -0.038 & -0.038 & -0.038 & -0.038 \\ -0.047 & 0.176 & -0.063 & -0.065 & -0.002 \\ -0.050 & -0.066 & 0.176 & -0.075 & 0.015 \\ -0.051 & -0.070 & -0.077 & 0.174 & 0.024 \\ 0 & 0 & 0 & 0 & 0 \end{bmatrix} \quad (7\text{-}10)$$

$V = B^T(E - A(A^TA)^{-1}A^T)L = [v_1 \quad v_2 \quad v_3 \quad v_4 \quad v_5]^T$. Because carrier phase observation noise is much smaller than that of pseudorange, V is mainly affected by pseudorange errors. Therefore the time-series V can be used to examine the data quality of pseudorange measurements.

From Equation (7-10), we can see that v_1 is more sensitive to pseudorange measurements due to the bigger coefficient corresponding to the pseudorange.

Figures 7-11 and 7-12 are two samples of time-series v_1, simulated with pseudorange errors of 0.5m and 2m (1σ) respectively.

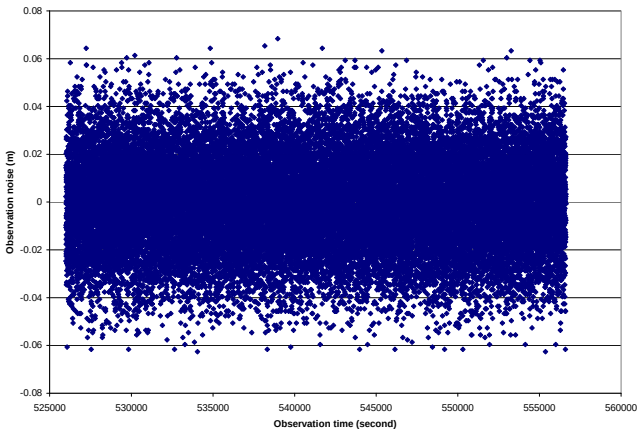

Figure 7-11 Time-series of v_1 (simulated with a noise level of 0.5m)

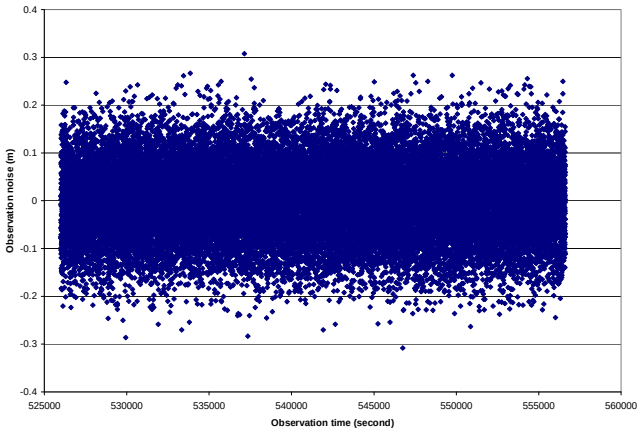

Figure 7-12 Time-series of v_1 (simulated with a noise level of 2m)

The RMS values of the two time series are 0.019m and 0.076m respectively. Based on the error propagation law, the original pseudorange error variances are calculated and the values of 0.501m and 2.007m respectively, almost the same as the values used for the simulation.

7.3 Evaluation of different ambiguity validation methods

The quality of an ambiguity validation method is mainly described by two factors: time required for ambiguity resolution and ambiguity mis-fixed rate. In this section, the performance of three validation methods (R-ratio, EIA and EIA/R-ratio) will be compared, using real GPS kinematic observations and simulated Galileo data (the same as simulated data used in Chapter 5).

7.3.1 Kinematic GPS Experiment

A GPS buoy with Leica dual frequency GPS receivers equipped was set up (Figure 7-14) near the shore of Repulse Bay, Hong Kong and another Leica dual frequency GPS receiver was set up on the shore as a base station. The distance between them was about 200m. The observation time was from 8:13:59 to 19:59:59 on December 8, 2004 and the sampling interval was 1 second.

To examine GPS data quality, the following time series are formed:

$$L_{12} = L_1 - L_2 \tag{7-11}$$

$$P = P_1 - L_1 \tag{7-12}$$

where L_1 and L_2 are double-differenced carrier phase measurements on two frequency bands; P_1 is the double-differenced $C1$ measurements.

As the distance between the two stations was so close (200m), we can assume most GPS errors are cancelled out through double differencing and the remaining are mainly measurement errors. Figures 7-15 and 7-16 show the time series of Eqs. (7-11) and (7-12) for satellite No. 5 respectively. Based on the time series, the error variances of carrier phase and pseudorange measurements can be calculated and they are 5mm and 120mm respectively. Figures 7-17 shows the number of satellites observed during the experiment period, which are between 5 and 9 satellites.

Figure 7-14 GPS buoy at the Repulse Bay, Hong Kong

In the data processing, the ILS method is used to estimate carrier phase ambiguities and three methods are used to validate ambiguity resolution: R-ratio test

(critical value: 2), EIA (with an overlap of aperture region) estimator (critical fail-rate: 0.001), and combined R-ratio test and EIA estimator.

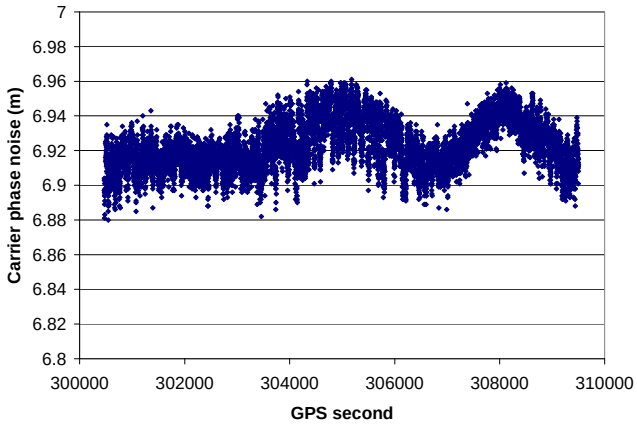

Figure 7-15 Carrier phase error

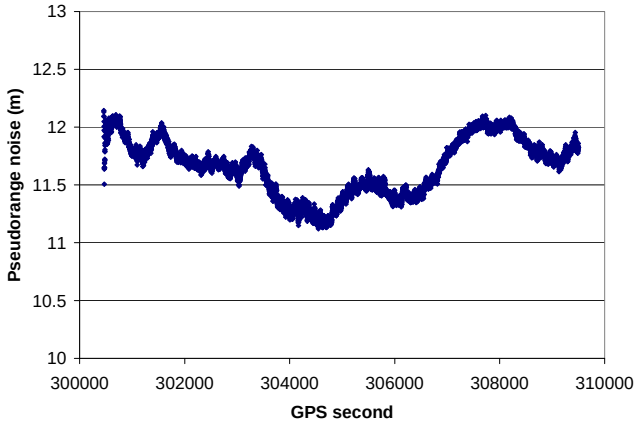

Figure 7-16 Pseudorange measurement Error

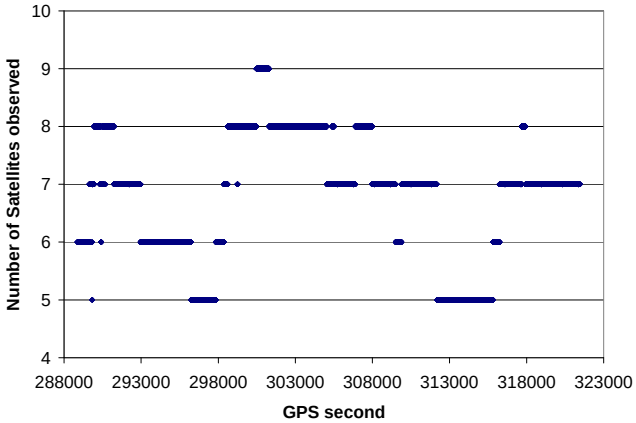

Figure 7-17 Number of satellites observed

In data processing, we start from every epoch until all ambiguities are fixed to their integers. Also the Ambiguity-Fix Rate (AFR) is used to quantify the efficiency performance of ambiguity resolution with the following definition:

$$AFR = \frac{Number\ \ of\ \ eopchs\ \ with\ ambiguity\ \ fixed\ \ to\ integers}{Total\ \ number\ of\ \ epochs\ observed}$$

Table 7-1 shows the AFR values with three validation methods. From the table, it can be seen that the time required for ambiguity resolution with these three validation methods are quite similar, with a few percentage point differences. The best one is the R-ratio test, with 98% of epochs in which the ambiguity can be fixed within a single epoch.

Table 7-1 AFR with ratio test (critical value = 2)

	R-ratio	EIA	EIA/R-ratio
time to fix (second)	AFR (%)	AFR (%)	AFR (%)
1	98.36	91.32	91.26
2	99.19	94.85	94.76
3	99.38	96.60	96.49
4	99.45	97.70	97.57
5	99.50	98.47	98.32
>5 and < 60	99.86	99.97	99.86
> 60	100	100	100

Table 7-2 shows their corresponding mis-fixed rates. We can see that with R-ratio test alone, the mis-fixed rate is 0.01%; with EIA estimator alone, the mis-fixed rate is 0.02%; and with combined EIA and R-ratio test, the performance is obviously better, as there is no mis-fixed case.

Table 7-2 Missed-fix performance

validation method	Mis-fixed rate (%)
R-ratio test	0.01
EIA	0.02
EIA and Ratio test	0

7.3.2 Multiple frequency case with simulated Galileo data

The simulated Galileo data is the same as used in Chapter 5 (i.e. 24 hours, one second

sample data). As demonstrated in Chapters 5 and 6, with lower carrier phase noise levels the ratio test can achieve good results. It is also tested with the EIA and EIA/R-ratio methods, and the results are quite similar. In this case study, it is mainly concentrated on the case when the carrier phase noise level is high (12mm).

Tables 7-3, 7-4 and 7-5 show the AFR values with different validation methods. Again, this example demonstrates that the time required for ambiguity fix is similar among these three validation methods.

Table 7-3 AFR with Ratio test (critical value = 2)

time to fix (second)	AFR (%)			
	code noise			
	0.5m	1.0m	1.5m	2.0m
1	50.87	47.93	46.33	43.40
2	92.33	92.16	91.88	91.79
3	98.84	98.88	98.84	98.89
4	99.80	99.81	99.80	99.82
5	99.95	99.97	99.97	99.96
6	99.99	99.99	99.99	99.99
7	100	100	100	100

The mis-fixed rates for the three methods are given in Table 7-6. There are up to 0.05% of epochs in which ambiguities are fixed to wrong values. For the EIA/R-ratio method proposed in this study, the mis-fixed rate is only 0.00002, which is much smaller than the previous methods.

Table 7-4 AFR with EIA (critical value = 0.001)

time to fix (second)	AFR (%)			
	code noise			
	0.5m	1.0m	1.5m	2.0m
1	53.42	50.67	48.77	46.09
2	91.61	91.41	91.05	90.92
3	99.13	98.96	98.97	99.00
4	99.94	99.94	99.94	99.96
5	99.99	99.99	99.99	99.99
6	99.99	99.99	99.99	99.99
7	100	100	100	100

Table 7-5 AFR with EIA and ratio test

time to fix (second)	AFR (%)			
	code noise			
	0.5m	1.0m	1.5m	2.0m
1	45.07	42.33	40.75	38.34
2	88.89	88.59	88.13	87.86
3	98.31	98.24	98.18	98.22
4	99.75	99.76	99.75	99.79
5	99.95	99.97	99.96	99.95
6	99.99	99.99	99.99	99.99
7	100	100	100	100

Table 7-6 Mis-fixed performance

validation method	Mis-fixed rate (%)			
	code noise			
	0.5m	1.0m	1.5m	2.0m
Ratio test	0.018	0.028	0.046	0.001
EIA	0.035	0.039	0.049	0.028
EIA and Ratio test	0.002	0.002	0	0

7.4 Summary

In this chapter, through analysis, it has been shown that to make the EIA estimator more applicable for practical applications, overlap of aperture regions is necessary. Also, EIA and the R-ratio test are two complementary ambiguity validation methods: EIA can ensure strong observation equation strength and good enough data quality, while the R-ratio test can ensure the statistical advantage of ambiguity resolution.

Tests are carrier out based on simulated Galileo data and real GPS observations. The results show that the combined use of EIA & R-ratio tests can improve ambiguity resolution reliability especially under high observation noise levels, while the efficiency is almost the same as the R-ratio and EIA methods.

Chapter 8 Conclusions and Recommendations

8.1 Conclusions

In this study, the positioning performance of the multiple frequency Galileo system has been systematically analyzed. To achieve this goal, a GNSS data simulator and data processing software are developed, which are able to simulate and process pseudorange and multiple frequency carrier phase data from different GNSS systems, including GPS (and its modernization), GLONASS and Galileo. The navigation performance of integrated GNSS systems has been analyzed, particularly for urban applications. With multiple frequency band data from Galileo and GPS modernization, it is possible to resolve ambiguity much faster and more reliably than current GPS. A new ambiguity resolution method (the improved CAR method) has been developed and the ambiguity resolution performance has been analyzed with different algorithms. The ambiguity validation process is crucial for the success of ambiguity resolution. A new ambiguity validation method is proposed which combines the R-ratio test and EIA for reliable ambiguity resolutions. Based on the study, we can conclude:

1. Integration of multiple GNSS constellations does not significantly improve positioning accuracy. However, the RAIM performance is significantly improved. The simulation study shows that the RAIM position protection levels can be reduced dramatically from 30m and 70m with GPS only for horizontal and vertical components to 15m and 25m with GPS/Galileo constellations respectively.
2. For urban applications, combined constellations can improve the positioning availability in streets. However, it cannot satisfy the requirement for vehicle navigation in urban areas. On the other hand, the discontinuity distances are

significantly reduced with the combined constellations. Therefore, it is possible to use cheap DR systems to bridge the gaps of GNSS positioning, with high accuracy.

3. The ambiguity resolution performances of three different algorithms have been compared, including CAR, ILS and improved CAR methods. From the simulation study, it has been demonstrated that the improved CAR method is better than the other two methods on ambiguity resolution, especially when the carrier phase measurement noise is big (i.e. 12mm). It is recommended that the success rate should be used as the criterion for the selection of different observation combinations.
4. For short baselines, with four frequency Galileo data, it is highly possible to achieve a reliable single epoch ambiguity resolution, when the carrier phase noise level is reasonably low (i.e. less than 6mm). This has been confirmed by both the success rate analysis and simulation study. The carrier phase noise level is an important factor for successful single epoch ambiguity resolution. If the carrier phase noise level increases to 12mm, the performance of single epoch ambiguity resolution degrades significantly. The pseudorange noise levels do not affect ambiguity resolution performance of the ILS method very much, but have strong effects on the CAR method.
5. For long baselines where the ionospheric delays cannot be ignored, an equivalent elimination process is proposed to be applied to eliminate ionopsheric delays and then to use the improved CAR method to resolve the ambiguities. The simulation study has demonstrated that the ambiguity can be determined within 1 minute (average), with a maximum time of 10 min, for baselines up to 800km.

6. When fixing full ambiguities becomes impossible, partial ambiguity-fix solutions can be useful to improve single-epoch positioning accuracy. With the Galileo constellation only, the positioning accuracy does not improve significantly with partial ambiguity resolution. By increasing the number of satellites (GPS/Galileo), positioning error can be significantly reduced. Over 90% of epochs (out of 86,400), the positioning errors are less than 10cm and the maximum error is less than 0.6m.
7. The success rate analysis method is a very powerful tool to study the performance of ambiguity resolution. The ambiguity resolution performance obtained from the success rate analysis is very close to the simulation results.
8. Both EIA and the R-ratio test are recommended for the validation of ambiguity resolution. Using real GPS data and simulated Galileo data, it has been demonstrated that the new method with the combination of EIA/R-ratio performs better then the use of EIA or the R-ratio test alone. With the combination of EIA/R-ratio, the time required for ambiguity resolution is almost the same as using an individual method (slightly worse). On the other hand, the ambiguity mis-fixed rate with the combined method decreases significantly. Applying to real GPS observations with the carrier phase errors of 5mm, the ambiguity mis-fixed rate is 0.01~0.02% for the R-ratio and EIA methods, but there is no mis-fixed case for the EIA/R-ratio method. Using simulated Galileo data (carrier phase error 12mm), the mis-fixed rates for R-ratio or EIA methods reach 0.05%. The mis-fixed rate for the combined method is only 0.00002%.
9. With multiple frequency data (i.e. Galileo), it is possible to estimate the measurement noise level based on observation only. The numerical tests show

that the estimation accuracy is very high.

10. For PPP data processing, the combined constellation with GPS/Galileo can significantly reduce the ambiguity convergence time, from an average time of around 1 hour (3,400s) with GPS alone to less than 15 min (880s) with GPS/Galileo.

8.2 Recommendations for future studies

As Galileo was not fully operational at the time of writing this thesis, for our research purpose, the tests used in this study are based on simulated data. The simulation is based on the error characteristics and models from the study of GPS, which is applicable to both Galileo and GLONASS since they are also transmitting data in the L band. However, simulated data are not real observations after all. For example, because only first-order ionospheric delay effect is simulated, the results with ambiguity resolution performance over long baselines may be a little too optimistic. To validate the conclusions from this study, we need to use real Galileo data in future when they are available.

In this thesis, a new validation method is proposed and the test results show that it can improve ambiguity reliability. In the study, mainly random measurement noises are considered. In fact, the problem of ambiguity validation is far more complicated, and it involves many factors, such as cycle slip, large outliers, suitability of stochastic models and the geometrical strength of satellite distributions. More research and tests should be carried out in this research area.

Satellite navigation in a metropolis like Hong Kong is still a challenge. GNSS alone cannot fulfill the full requirements even with a constellation of three systems

(i.e. GPS + Galileo + GLONASS). It is therefore to integrate with other sensors such as INS or digital maps, etc.

References

1. Agreement on the promotion, provision and use of Galileo and GPS satellite-based navigation systems and related applications (2004). http://ec.europa.eu/dgs/energy_transport/galileo/documents/doc/2004_06_21_summit_2004_en.pdf
2. Alves P (2001) The effect of Galileo on carrier phase ambiguity resolution, Proceedings of ION-GPS 2001.
3. Angel J, Stefano S, Kevin S, Ignacio J (2004) Polaris: a software tool to support GNSS-based application design. The European Navigation Conference, GNSS 2004.
4. Baarda W (1968) A testing procedure for use in geodetic networks. Netherlands Geodetic Commission, New Series, 2, No.4
5. Berefelt F., Boberg B., Nygards J., Stromback P., and Wirkander S.L. (2004) "Collaborative GPS/INS Navigation in Urban Environment". *Proceeding of National Technical Meeting 2004*, San Diego, California, January 26-28, 1114-1125
6. Bisnath S, Langley R (2001a) Precise Orbit Determination of Low Earth Orbiters with GPS Point Positioning. Proceedings of the Institute of Navigation National Technical Meeting, The Institute of Navigation, Long Beach, California, U.S.A., 22-24 January, pp. 725-733
7. Bisnath S, Langley R (2001b) High-Precision Platform Positioning with a Single GPS Receiver. ION GPS 2001, 11-14 September 2001, Salt Lake City, UT,2585-1539
8. Blair P (2005) Potential interference to Galileo from 23cm band operations. Online at: http://www.microwavers.org/papers/ral2005/G3LTF-Galileo.pdf

9. Blomenhofer H, Ehret W and Blomenhofer E (2004) Consideration of operational ourages in Galileo and GPS integrity analysis. The European Navigation Conference GNSS 2004, Rotterdam, Netherlands, 81: 1-12
10. Brunner F, Hartinger H, Troyer L (1999) GPS signal diffraction modeling: the stochastic SIGMA-Δ model. Journal of Geodesy 73: 259-267
11. Civil Aviation Authority (2004) GPS integrity and potential impact on aviation safety. http://www.caa.co.uk/docs/33/CAPAP2003_09.pdf
12. Chen D, Lachapelle G (1995) A comparison of the FASF and least-squares search algorithms for on-the-fly ambiguity resolution. Journal of The Institute of Navigation, Vol. 42, No. 2: 371-390
13. Chen W (1992) Fast Ambiguity Resolution with GPS carrier phase measurement. In: The collected papers on GPS surveying research and applications, Surveying and Mapping Publishing House, Ed G. Wang, pp 165-174 (in Chinese)
14. Chen W, Hu C, Li Z, Chen Y, Ding X, Gao S, Ji S (2004) Kinematic GPS precise point positioning for sea level monitoring with GPS buoy. The 2004 International Symposium on GNSS/GPS Sydney, Australia,6–8 December 2004
15. Cocard M, Geiger A (1992) Systematic search for all possible widelanes. Proceedings of the Sixth International Geodetic Symposium on Satellite Positioning, Columbus, Ohio, 17-20 March, pp 312-318
16. Collins J, Langley R (1999) Possible weighting schemes for GPS carrier phase observations in the presence of multipath. Final contract report for the U.S. Army Corps of Engineers Topographic Engineering Center, No. DAAH04-96-C-0086 / TCN 98151, March. Online available at: http:// gauss.gge.unb.ca/papers.pdf

17. Colombo O, Sutter A, Evans A (2004) Evaluation of Precise, Kinematic GPS Point Positioning. ION GNSS 2004, Sept. 21-24, 2004, Long Beach , CA. pp1423-1430
18. Cross P, Hawksbee D, Nicolai R (1994) Quality measures for differential GPS positioning. The Hydrographic Journal, Hydrographic Society, 72, 17-22
19. Daghay S, Moins M, Bruyninx C, Rolain Y, Roosbeek F (2005) Impact of the combined GPS + Galileo satellite geometry on positioning precision. Proceedings of EUREF 2005, 1-3 June 2005, Vienna, Austria.
20. Dennis M, Alexandru E, Jonas T (2003) A prototyping platform for multi-frequency GNSS receivers. In: Proceedings of ION GPS/GNSS 2003, Portland, Oregon.
21. Dick N, Hans Z, Marjan V (2004) Evaluation of NAUPLIOS initiative, April 27th, 2004. Online available at: http://nauplios.cnes.fr/
22. Elliott D, Christopher J (2006) Understanding GPS Principles and Applications, second edition, Artech House Inc.
23. Enge P (2003) GPS modernization: capabilities of the new civil signals. Invited paper for the Australian International Aerospace Congress, Brisbane, 29 July – 1 August 2003
24. Euler H, Goad C (1991) On optimal filtering of GPS dual-frequency observations without using orbit information. Bull Geod 65: 130-143
25. Euler H, Landau H (1992) Fast GPS ambiguity resolution on-the-fly for real-time application. Proceedings of Six International Geodetic Symposium on Satellite Positioning, Columbus, Ohio, 17-20 March: 650-659
26. Euler H, Schaffrin B (1991) On a measure for the discernibility between different ambiguity solutions in the static-kinematic GPS-mode. IAG Symposia No. 107,

Kinematic Systems in Geodesy, Surveying, and Remote Sensing, Springer-Verlag, New York, pp 285-295

27. European Commission (2002) Galileo Mission High Level Definition Document. Online available at: http://europa.eu.int/comm/dgs/energy_transport
28. Federal Radionavigation Plan 2005, published by Department of Defense, Department of Homeland Security, and Department of Transportation.
29. Forsell B, Martin-Neira M, Harris R (1997) Carrier phase ambiguity resolution in GNSS-2. Proceedings of ION GPS-97, The Institute of Navigation, Sept. 16-19
30. Frei E, Beutler G (1990) Rapid static positioning based on the fast ambiguity resolution approach FARA: theory and first results. Manuscripta Geodaetica, Vol. 15, No. 4: 325-356
31. GADEROS – interface control document, December 28th, 2001. Online available at:

    http://galileo.uic.asso.fr/docs
32. GADEROS – project overview, April 1st, 2002. Online available at:

    http://galileo.uic.asso.fr/docs
33. GALLANT – Galileo safety-of-life applications for driver assistance in road transport, 2002. Online available at:

    http://ec.europa.eu/dgs/energy_transport/galileo/doc/galileo_pp_gallant.pdf
34. GAL OS SIS ICD/D.0, Galileo open service signal in space interface control document, ref GAL OS SIS ICD/D.0, Issue: Draft, Revision: 0, Date: 23/05/2006
35. Galileo System Simulation Facility – Algorithms and Models (2005) Website at: http://www.esa.int/gssf/default.htm
36. Gao Y (1993) Reliability assurance for GPS integrity test, ION GPS-93, Salt Lake City, Utah, September 22-24: 567-574

37. Gao Y, Shen X (2001) Improving Ambiguity Convergence in Carrier Phase-Based Precise Point Positioning, ION GPS 2001, 11-14 September 2001, Salt Lake City, UT,1532-1539
38. Gauthier L, Michel P, Ventura-Traveset J, and Benedicto J (2001) EGNOS: the first step in Europe's contribution to the global navigation satellite system. http://www.esa.int/esapub/bulletin/bullet105/bul105_3.pdf
39. Gerdan G (1995) A comparison of four methods of weighting double-difference pseudorange measurements. Trans Tasman Surv 1: 60-66
40. Gianniou M, Groten E (1996) An advanced real-time algorithm for code and phase DGPS. Paper present at DSNS'96 Conference, St. Petersburg, 20-24 May
41. Global Positioning SPS Performance Standard, 2001. Online available at: http://www.navcen.uscg.gov/gps/geninfo/2001SPSPerformanceStandardFINAL.pdf
42. GLONASS ICD 2002, version 5.0. Online available at: http://gauss.gge.unb.ca/GLONASS.ICD.pdf
43. Goad C and Goodman L (1974) A modified Hopfield tropospheric refraction correction model. The American Geophysical Union, San Francisco: 12-17
44. Grejner-Brzezinska, Toth CK and Yi Y. (2001). "Bridging GPS Gaps in Urban Canyons: The Benefits of ZUPT'S". *Journal of Navigation*, Vol. 48, No. 4
45. Han S (1997) Quality control issues relating to instantaneous ambiguity resolution for real-time GPS kinematic positioning. Journal of Geodesy, 71: 351-361
46. Han S, Rizos C (1996a) Improving the computational efficiency of the ambiguity function algorithm. Journal of Geodesy, Vol. 71, No. 6: 351-361
47. Han S, Rizos C (1996b) Integrated methods for instantaneous ambiguity resolution using new generation GPS receivers. In: Proceedings of IEEE

PLANS'96, Atlanta GA, pp 254-261

48. Hartinger H, Brunner F (1999) Variances of GPS phase observations: the SIGMA-ε model. GPS Solutions, Vol.2, No.4: 35-43
49. Hatch R (1990) Instantaneous ambiguity resolution. Proceedings of KIS'90, Banff, Canada, 10-13 September, pp 299-308
50. Hatch R, Jung J, Enge P, Pervan B (2000) Civilian GPS: The benefits of three frequencies. GPS Solutions 3(4): 1-9
51. Hein G, Pielmeier J, Zink T and Eissfeller B (1997) GPS and GLONASS RAIM availability analysis over Europe. ION GPS-97, Kansas City, Missouri, September 16-19: 465-474
52. Hewitson S, Wang J (2004) GPS/GLONASS/Galileo integration: separation of outliers. 4th Trans-Tasman Surveyors Conference, Auckland, New Zealand, 13-16 October, CD-ROM proc., paper 39.
53. Hewitson S, Lee H, Wang J (2004). Localizability analysis for GPS/Galileo receiver autonomous integrity monitoring, The Journal of Navigation, 57: 245 – 259
54. Hideto T (2004) Japanese regional navigation satellite system "the JRANS concept". Journal of Global Positioning Systems, Vol. 3, No. 1-2: 259-264
55. Hopfield H (1969) Two-quadratic tropospheric refractivity profile for correction satellite data. Journal of Geophysical Research, 74(18): 4487-4499
56. Igor V, Francois C (2003) Integrity equations for safe train positioning using GNSS. Online available at: http://www.its-europe.org/download/locoprol%20documents/gnss_03.pdf
57. Inside GNSS News (2007) http://www.insidegnss.com/node/229

58. Jean M (2003) NAUPLIOS- improving the monitoring of maritime traffic and search & rescue using Galileo, February 2003. Online available at: http://nauplios.cnes.fr/
59. Jean M (2004) Nauplios final report, July 2004. Online available at: http://nauplios.cnes.fr
60. Jeremie G (2003) Galileo spectrum and interoperability issues, 2003. Online available at: http://europa.eu.int/comm/dgs/energy_transport/galileo
61. Jin X (1996) Theory of carrier adjusted DGPS positioning approach and some experimental results. PH.D. thesis. Delft University Press, Delft
62. Joachim F (2003) The activities of the Ionosphere Working Group of the International GPS Service (IGS). GPS Solutions, Volume 7, Number 1: 41-46
63. Jonge P, Tiberius C (1996) The LAMBDA method for integer ambiguity estimation: implementation aspects. Publications of the Delft Geodetic Computing Centre, No. 12, August 1996, pp. 1- 49.
64. Jung J, Enge P, Pervan B (2000) Optimization of cascade integer resolution with three carrier GPS frequencies. In proc. ION-GPS 2000 Conf.
65. Hirahara K (2000) Local GPS tropospheric tomography. Earth Planets Space, 52: 935-939
66. Kim D, Langley R (1999) An optimized least-squares technique for improving ambiguity resolution performance and computational efficiency. Proceedings of ION GPS'99, Nashville, Tennessee, 14-17 September: 1579-1588
67. Kim D, Langley R (2000) GPS ambiguity resolution and validation: methodologies, trends and issues. The 7th GNSS Workshop – International Symposium on GPS/GNSS, Seoul, Korea, Nov. 30-Dec. 2, 2000

68. Klobuchar J (1987) Ionospheric time-delay algorithm for single-frequency GPS users. IEEE Transactions on Aerospace and Electronics Systems, Vo. 23, No.3, 1987: 325-331
69. Klukas R, Lachapelle G, Ma C and Jee G (2003) GPS signal fading model for urban centers. IEE Proc.-Microw. Antennas Propag, Vol. 150, No. 4, August 2003
70. Kouba J, Heroux P (2001) Precise Point Positioning Using IGS Orbit and Clock Products. GPS Solutions, 5(2):12～28
71. Kozlov, D. and M. Tkachenko (1998) "Centimeter-Level Real Time Kinematics Positioning with GPS + GLONASS C/A Receivers". Journal of Navigation Vol. 45 No. 2, 1998
72. Kyle O (2001) Availability and reliability advantages of GPS/Galileo integration. Proceedings of ION GPS 2001, Session C4, Salk Lake City, UT, September 11-14: 1-10
73. Lachapelle G and Mezentsev O (2005) Pedestrian dead reckoning – a solution to navigation in GPS signal degraded areas? Geomatica, Vol. 59, No. 2, 2005: 175-182
74. Landau H, Euler HJ (1992) On-the-fly ambiguity resolution for precise differential positioning. Proceedings of the Institute of Navigation's ION GPS-1992, Albuquerque, NM, pp 607-613
75. Langley R (1997) GPS receiver system noise. GPS World 8: 40-45
76. Lee Y (2004) Investigation of extending Receiver Autonomous Integrity Monitoring (RAIM) to combined use of Galileo and Modernized GPS. ION GNSS 2004, Long Beach, California, September 21-24: 1691-1698
77. Leica A (2004) GPS satellite surveying (Third Edition). John Wiley & Sons, Inc. 2004.

78. Leick A (2004) GPS Satellite Surveying, 3rd edition. John Wiley and Sons, New York

79. Liu J, Wang Z (2003) Model of inter-frequency combinations of Galileo GNSS. Wuhan University Journal (Natural Science), 8(6): 723-727

80. LOCOPROL- project presentation, February 22nd, 2002. Online available at: http://www.ertico.com/en/activities/activities/locoprol_website.htm

81. Luigi M (2004) INSTANT: a dynamic push model for mobile architectures, 2004. Online available at: http://www.instant-olympic.com/INStANT-index.htm

82. Luigi M (2004) A distributed and mobile system to support emergency situations management, 2004. Online available at: http://www.instant-olympic.com/INStANT-index.htm

83. Martin-Neira M, Toledo M, Pelaez A (1995) The null space method for GPS integer ambiguity resolution. Proceedings of DSNS'95, Bergen, Norway, April 24-28, Paper No. 31

84. McDonald K (2001) A future GNSS concern on the modernization of GPS and the evolution of Galileo, Proceedings of ION GPS-01, 11-14 September, Salt Lake City, UT, pp. 2804-2809

85. Miller L, Bartlett S, Peterson B and McKaughan M (1995) Evaluation of Radionavigation Systems in an Urban Environment. *NTM 1995*. 293-302

86. Mohamed A, Sergei L, Oleg T and Javier D (2000) Performance analysis of GPS positioning using WAAS and EGNOS. GNSS 2000 Conference, Edinburgh, Scotland, UK, May 1-4, 2000, pp:1-10

87. Niell A (1996) Global mapping functions for the atmosphere delay at radio wavelengths. J. geophys. Res. 101(B2): 3227-3246

88. O'Keefe K (2001) Availability and reliability advantages of GPS/Galileo integration. ION GPS 2001, Salt Lake City, Utah, September 11-14: 1-10
89. Ober P (2003) Integrity prediction and monitoring of navigation systems. Integricom Publishers, Leiden, Netherlands
90. Ochieng W, Sauer K (2001) Potential performance levels of a combined Galileo/GPS navigation system, Journal of Navigation, Vol. 54, No. 2, pp 185-197.
91. Ochieng W, Sheridan K, Sauer K, Han X, Cross P, Lannelongue S, Ammour N, Petit K (2002) An assessment of the RAIM performance of a combined Galileo/GPS navigation system suing the marginally detectable errors (MDE) algorithm, GPS SOLUTIONS, Vol. 5, No. 3, pp. 42-51 (2002).
92. Oliver M, Christoph G, Sebastian G, Miquel G, Johann F, Hanspeter K (2002) GIOVE-A initial signal analysis. GPS Solution (2006) 10: 146-153
93. Píriz P, Fernández V, Auz A, Tavella P, Sesia I, Cerretto G, Falcone M, Navarro D, Hahn J, González F, Tossaint M and Gandara M (2006) The Galileo system test bed V2 for orbit and clock modeling. ION GNSS conference, Fort Worth, Texas, September 2006
94. Rao CR (1971) Estimation of variance and covariance components – MINQUE. J Multivar Anal 1: 257-275
95. Rizos C (2007) The future of global navigation satellite systems. http://www.gmat.unsw.edu.au/snap/publications/rizos_2007a.pdf
96. Romay M, Alarcon A, Villares I and Monseco E (2001) An integrated GNSS concept, Galileo & GPS, benefits in terms of accuracy, integrity, availability and continuity. ION GPS 2001, Salt Lake City, UT, 11-14 September: 2114-2124

97. Rossbach U (2000) Positioning and Navigation Using the Russian Satellite System GLONASS, PH.D. Thesis, University FAF Munich, Faculty of Civil and Surveying Engineering, Neubiberg, Germany

98. Ryan S and Lachapelle G (2000) Impact of GPS/Galileo integration on marine navigation. IAIN World Congress / ION Annual Meeting: 721-731

99. Saastamoinen J (1973) Contribution to the theory of atmospheric refraction. Bulletin Geodesique, 107: 13-34

100. Sang J and Kubik K (1997) A probabilistic approach to derivation of geometrical criteria for evaluating GPS RAIM detection availability. ION GPS-97, Kansas City, Missouri, September 16-19: 511-517

101. Schlotzer S, Martin S (2005) Performance study of multi carrier ambiguity resolution techniques for Galileo and modernized GPS. In: Proceedings of the Institute of Navigation's ION 2005, Long Beach, CA., pp 142-151

102. Scott P, Gerald F, Irving L, David F, Donna F, Donald K and Monica P (1995) The Global Positioning System: Assessing National Policies. Rand Critical Technologies Institute, http://www.rand.org/publications/MR/MR614

103. Stephen M and Willy I (1989) Demonstration of sub-meter GPS orbit determination and 1.5 parts in 10^8 three-dimensional baseline accuracy. Journal of Geodesy, 63(2): 167-189

104. Svehla D and Rothacher M (2006) Combined processing and orbit determination of Galileo and GPS satellites using phase clocks. http:// www.cosis.net/abstracts/COSPAR2006/03004/COSPAR2006-A-03004-4.pdf

105. Talbot N (1988) Optimal weighting of GPS carrier phase observations based on the signal-to-noise ratio. Proc Int Symp Global Positioning Systems, Brisbane, October, pp 4.1-4.17

106. Teunissen P (1993) Least-squares estimation of the Integer GPS ambiguities. Invited lecture, Section IV: Theory and Methodology, IAG General Meeting, Beijing, China, August

107. Teunissen P (1994) A new method for fast carrier phase ambiguity estimation. Proceedings of IEEE PLANS'94, Las Vegas, NV, April 11-15: 562-573

108. Teunissen P (1995) The least-squares ambiguity decorrelation adjustment: a method for fast GPS integer ambiguity estimation. Journal of Geodesy, 70(1-2): 65-82

109. Teunissen P, Odijk D (1997) Ambiguity Dilution of Precision: definition, properties and application. In: Proceedings of The Institute of Navigation's ION GPS-1997, Kansas City, pp 891-899

110. Teunissen P (1998a) Success probability of integer GPS ambiguity rounding and bootstrapping. Journal of Geodesy, 72(10): 606-612

111. Teunissen P (1998b) Quality control and GPS, Chapter 7 in GPS for Geodesy, Eds Teunissen P and Kleusberg A Springer Verlag, 2nd Edition

112. Teunissen P, Joosten P, Tiberius C (1999) Geometry-free ambiguity success rates in case of partial fixing. Proc. NTM-99, pp 201-210

113. Teunissen P, Jonkman N, Joosten P, Tiberius C (2000) Long baseline 3 frequency differential GNSS. IEEE 2000: 7-14

114. Teunissen P (2003) An invariant upper bound for the GNSS bootstrapped ambiguity success rate. Journal of Global Positioning Systems, 2(1): 13-17

115. Teunissen P (2003) Integer aperture GNSS ambiguity resolution. Artificial Satellites, 38(3): 79-88

116. Teunissen P, Verhagen S (2004) On the foundation of the popular ratio test for GNSS ambiguity resolution. In: Proceedings of ION GNSS-2004, Fairfax, VA. pp 79-88

117. Teunissen P (2005) GNSS ambiguity resolution with optimally controlled failure-rate. Artificial Satellites, 40(4): 219-227

118. Tiberius C, Jonge P (1995) Fast positioning using the LAMBDA method. Proceedings of DSNS-95, Bergen, Norway, Paper No.30

119. Tiberius C, Pany T, Eissfeller B, Joosten P, Verhagen S (2002) 0.99999999 confidence ambiguity resolution with GPS and Galileo. GPS Solutions, 6(2): 96-99

120. Urech A, Perez D, Gonzalez O (2002) GADEROS, a Galileo demonstrator for railway operation system, 2002. Online available at: http://galileo.uic.asso.fr/docs

121. USA and CE (2004) Agreement on the promotion, provision and use of Galileo and GPS satellite-based navigation systems and related allocations, 28/06/2004. Online available at: http://pnt.gov/public/docs/2004-US-EC-agreement.pdf

122. Veit O, Francesco L, Juan-Pablo B, Roland S, Hans L (2004) The Galileo integrity concept. ION GNSS 17th international technical meeting of the satellite division, 21-24 Sept. 2004, Long Beach, CA: 604-615

123. Verhagen S (2002) Performance analysis of GPS, Galileo and integrated GPS-Galileo, ION GPS 2002, Portland, Oregon, September 24-27: 2208-2215

124. Verhagen S (2005) The GNSS integer ambiguities: estimation and validation. PH.D. thesis, Publications on Geodesy, 58, Netherlands Geodetic Commmission, Delft

125. Vlcek C (1993) GPS/Dead Reckoning for vehicle tracking in the urban canyon environment. IEEE – IEE Vehicle Navigation & Information Systems Conference, Ottawa – VNIS'93

126. Vollath U, Birnbach S, Landau H (1998) Analysis of three-carrier ambiguity resolution (TCAR) technique for precise relative positioning in GNSS-2. In: Proceedings of ION GPS-98, Nashville, USA, pp 417-426

127. Walter T and Enge P (1995) A weighted RAIM for precision approach. ION GPS-95, Palm Springs, California, September, 12-15

128. Wang J, Stewart M, Tsakiri M (1998) A discrimination test procedure for ambiguity resolution on-the-fly. Journal of Geodesy, 72: 644-653

129. Wang J, Stewart M, Tsakiri M (1998a) Stochastic modelling for static GPS baseline data processing. J Surv Engn 121: 171-181

130. Wang Z, Liu J, Zhang K (2004) Multiple carrier ambiguity resolution method for Galileo. The 2004 international symposium on GNSS/GPS, Sydney, Australia, 6-8 December, pp 1-8

131. Werner W, Winkel J (2003) TCAR and MCAR options with Galileo and GPS. In: Proceedings of ION GPS/GNSS 2003, Portland, Oregon, pp 790-800

132. Wei M, Schwarz K (1995) Fast ambiguity resolution using an integer nonlinear programming method. In: Proceedings of ION GPS-1995, Palm Springs CA, pp 1101-1110

133. Xu G (2003) GPS theory, algorithms and applications. Springer, Berlin.

134. Yu M, Li Z, Chen Y and Chen W (2006) Improving integrity and reliability of map matching techniques. Journal of Global Positioning Systems (2006) Vol. 5, No. 1-2: 40-46

135. Zhang W, Cannon M, Julien O, Alves P (2003) Investigation of combined GPS/Galileo cascading ambiguity resolution schemes. In: Proceedings of ION GPS/GNSS 2003, Portland, USA, pp 2599-2610

136. Zhang W (2005) Triple frequency cascading ambiguity resolution for modernized GPS and Galileo. UCGE Reports Number 20228, 2005

137. Zumberge J, Heflin M, Jefferson D, Watkins M, and Webb F (1997) Precise Point Processing for the Efficient and Robust Analysis of GPS Data from Large Networks. J Geophys. Res., 102 (B3), 5005-5017

Bibliography

1. Abdel-Hafez M, Speyer J, Lee Y and Williamson W (2003) A multiple hypothesis Wald sequential probability ratio test for integer ambiguity resolution. AIAA Guidance, Navigation, and Control Conference and Exhibit, August 2003
2. Aragón A, Orús R, Amarillo F, Hernández-Pajares M, Juan M and Sanz J (2005) Preliminary NeQuick assessment for future single frequency users of GALILEO. 6th Geomatic Week, 8th-11th February 2005, Barcelona
3. Bazlov Y, Galazin V, Kaplan B, Maksimov V and Rogozin V (1999) Propagating PZ 90 to WGS 84 transformation parameters. GPS Solutions, Vol. 3, No. 1, pp: 13-16
4. Beran T, Kim D and Langley R (2003) High-precision single-frequency GPS point positioning. Proceedings of ION GPS 2003, 16th International Technical Meeting of the Satellite Division of The Institute of Navigation, Portland, Oregon, 9-12 September, in press
5. Bisnath S (2000) Efficient, automated cycle-slip correction of dual-frequency kinematic GPS data. In proceedings of ION GPS 2000, pp: 145-154
6. Bisnath S, Kim D and Langley R (2001) A new approach to an old problem: carrier-phase cycle slips. GPS World, Vol. 12, No. 5, May, pp: 46-51
7. Blanchard W (2003) Achieving GPS-Galileo interoperability: the challenges ahead. Space Policy 19(2), pp: 95-99
8. Blomenhofer H, Ehret W, Blomenhofer E (2003) Performance analysis of GNSS global and regional integrity concepts. In the Proceedings of ION GPS/GNSS 2003, Portland, Oregon, pp: 991-1001
9. Bond J, Kim D, Langley R and Chrzanowski A (2003) An investigation on the use of GPS for deformation monitoring in open pit mines. Proceedings of the CAMI

(Computer Applications in the Minerals Industries) 2003 meeting, Calgary, British Colombia, Canada, in press

10. Bossche M, Bourga C, and Lobert B (2004) GPS Galileo time offset: How it affects positioning accuracy and how to cope with it. In the Proceedings of ION GNSS-04, 21-24 September, Long Beach, CA, pp: 654-659
11. Brown A and Stolk K (2002) Rapid ambiguity resolution using multipath spatial processing for high accuracy carrier phase. Proceedings of ION GPS 2002, Porland OR
12. BROWN C, ROBERTS G, ATKIN C, MENG X and COLFORD B (2007) Deflections and frequency responses of the Forth Road Bridge Measure by GPS. In: DR R LARK, ed. Fifth international Conference on Current and Future Trends in Bridge Design, Construction and Maintenance, pp: 479-486
13. Cederholm P (2005) PDOP values for simulated GPS/Galileo positioning. Surv. Rev. 38(297): 218-228
14. Chao C and Gick R (2004) Long-term evolution of navigation satellite orbits: GPS/GLONASS/GALILEO. Adv. Space Res. 34(5): 1221-1226
15. Enderle W (2003) Galileo: Impact on spacecraft navigation systems. Journal of GPS 2(2), pp: 135-138
16. Enge P, Jung J and Pervan B (1999) High integrity carrier phase navigation for future LAAS using multiple civilian GPS signals. Proceedings of the American Control Conference, San Diego, California, pp: 3650-3654
17. Feng Y (2003) Combined Galileo and GPS: a technical perspective. Journal of Global Positioning Systems, Vol. 2, No. 1, pp: 67-72
18. Feng Y (2005) Future GNSS performance: predictions using GPS with a virtual Galileo constellation. GPS World 16(3): 46-52

19. Feng Y, and Rizos C (2005) Three carrier approaches for future global, regional and local GNSS positioning services: concepts and performance perspectives. In the proceedings of ION GNSS 2005, pp: 2277-2287
20. Feng Y, Rizos C, and Moody M (2006) Exploring performance benefits from multiple satellite systems and multiple carrier signals using GPS and virtual Galileo measurements. IGNSS Symposium 2006, Holiday Inn Surfers Paradise, Australia
21. Forden G (2004) The military capabilities and implications of China's indigenous satellite-based navigation system. Science and Global Security, 12, pp: 219-250
22. Fraenz M and Harper D (2002) Heliospheric coordinate systems. Plan. Space Sci., 50, pp: 217-233
23. Furthner J, Moudrak A, Konovaltsev A, Hammesfahr J, and Denks H (2004) Time dissemination and common view time transfer with Galileo: how accurate will it be? 35th Annual Precise Time and Time Interval (PTTI) Meeting.
24. Gibbons G (2004) GPS & Galileo: Prospects for building the next generation of global navigation satellite systems. Journal of GPS 3(1-2): 12-15
25. Grejner-Brzezinska D, Da R and Toth C (1998) GPS error modeling and OTF ambiguity resolution for high-accuracy GPS/INS integrated system. Journal of Geodesy, 72: 626-638
26. Han S and Johnson R (2001) Survey quality real-time GPS: solving the time to fix vs. reliability paradox. ION GPS 2001, Salt Lake City, Utah
27. Hein G, Godet J, Issler J, Martin J, Erhard P, Lucas R and Pratt T (2002) Status of Galileo frequency and signal design. In proceedings of ION GPS 2002.
28. Heinrichs G, Löhnert E, Wittmann E and Kaniuth R (2007) Opening the gate. Germany's Galileo test and development environment. Inside GNSS 2(4): 44-52

29. Hernandez-Pajares M, Zomoza J, Subirana J and Colombo O (2003) Feasibility of wide-area subdecimeter navigation with Galileo and modernized GPS. IEEE Transactions on Geoscience and Remote Sensing, Vol. 41, No. 9, pp: 2128-2131
30. Hu G, Abbey D, Castleden N, Featherstone W, Earls C, Ovstedal O and Weihing D (2005) An approach for instantaneous ambiguity resolution for medium- to long-range multiple reference station networks. GPS Solutions, 9: 1-11
31. Jan S (2002) Analysis of a three-frequency GPS/WAAS receiver to land an airplane. In the Proceedings of ION GPS 2002, Portland, OR, September 24-27, 2002
32. Januszewski, J (2001) Visibility and geometry of Galileo constellation, Artificial Satellites, 36(4), pp: 131-142
33. Januszewski J (2006) Combined constellation GPS and Galileo systems. Artificial Satellites 41(2): 67-77
34. Jonathan D, Walton R and Jason L (2001) Hypothesis testing for resolving integer ambiguity in GPS. ION GPS 2001, pp: 1522-1531
35. Jong K (2002) Success rates for integrated GPS and Galileo ambiguity resolution. Journal: Revista Brasileira de Cartografia, Vol. 54, pp: 1-9
36. Joosten P and Teunissen P (2001) On the error sensitivity of the GPS ambiguity success rate. In. Proceeding KIS2001, International Symposium on Kinematic Systems in Geodesy, Geomatics and Navigation, pp: 317-320
37. Julien O, Macabiau C, Issler J and Ries L (2007) Two for one: Tracking Galileo CBOC signal with TMBOC. Inside GNSS 2(3): 50-57
38. Kim D, Shim Y and Kim J (1997) Trajectory and attitude determination system of a high-speed flying vehicle using GPS. Proceedings of the 4th GNSS Workshop -

International Symposium on GPS/GNSS, Seoul, Korea, 17-19 November, pp: 580-590

39. Kim D and Langley R (2000) A Reliable Approach for Ambiguity Resolution in Real-Time Long-Baseline Kinematic GPS Applications. In: Proceedings of ION GPS 2000, pp: 1081-1092
40. Kim D and Langley R (2000) A reliable approach for ambiguity resolution in real-time long-baseline kinematic GPS applications. Proceedings of ION GPS 2000, 13th International Technical Meeting of the Satellite Division of The Institute of Navigation, Salt Lake City, UT, 19-22 September, pp: 1081-1091
41. Kim D and Langley R (2000) GPS ambiguity resolution for long-baseline kinematic applications. Proceedings of the GEOIDE Second Annual Conference, Calgary, 25-26 May
42. Kim D and Langley R (2000) Kalman-filter-based GPS ambiguity resolution for real-time long-baseline kinematic applications. Satellite Navigation in CEI (Central European Initiative) Area, Proceedings of the 2nd International Workshop, University of Warmia and Mazury in Olsztyn, Olsztyn, Poland, 3-5 July
43. Kim D and Langley R (2000) The multipath divergence problem in GPS carrier-smoothed pseudorange. Proceedings of the 47th Annual Conference of the Canadian Aeronautics and Space Institute, Ottawa, 30 April - 3 May, pp: 161-163
44. Kim D and Langley R (2001) Estimation of the stochastic model for long-baseline kinematic GPS applications. Proceedings of The Institute of Navigation 2001 National Technical Meeting, Long Beach, CA, U.S.A., 22-24 January, pp: 586-595

45. Kim D and Langley R (2001) Instantaneous real-time cycle-slip correction of dual-frequency GPS data. Proceedings of The International Symposium on Kinematic Systems in Geodesy, Geomatics and Navigation, Banff, Alberta, Canada, 5-8 June, pp: 255-264
46. Kim D and Langley R (2001) Mitigation of GPS carrier phase multipath effects in real-time kinematic applications. Proceedings of ION GPS 2001, 14th International Technical Meeting of the Satellite Division of The Institute of Navigation, Salt Lake City, UT, 11-14 September, pp: 2144-2152
47. Kim D and Langley R (2001) Quality control techniques and issues in GPS applications: Stochastic modelling and reliability testing. Proceedings of the 8th GNSS Workshop - 2001 International Symposium on GPS/GNSS, Jeju Island, Korea, 7-9 November, Tutorial/Domestic Session, pp: 76-85
48. Kim D, Langley R and Kim S (2002) High-precision crane guidance: Shipyard giants. GPS World, Vol. 13, No. 9, September, pp: 28-34
49. Kim D and Langley R (2002) Instantaneous real-time cycle-slip correction for quality control of GPS carrier-phase measurements. Navigation: Journal of The Institute of Navigation, Vol. 49, NO. 4, pp: 205-222
50. Kim D and Langley R (2002) On ultrahigh-precision positioning and navigation. Proceedings of ION GPS 2002, 15th International Technical Meeting of the Satellite Division of The Institute of Navigation, Portland, Oregon, 24-27 September, pp: 904-913
51. Kim D and Langley R (2003) A dual-mode GPS real-time kinematic system for seamless ultrahigh-precision positioning and navigation. Proceedings of ION GPS 2003, 16th International Technical Meeting of the Satellite Division of The Institute of Navigation, Portland, Oregon, 9-12 September, in press

52. Kim D and Langley R (2003) A gantry crane auto-steering system based on GPS RTK technology. The European Navigation Conference, GNSS 2003, Graz, Austria, 22-25 April
53. Kim D and Langley R (2003) Gantry crane auto-steering: Ultrahigh-precision GPS positioning and navigation. GIM International, in press
54. Kim D, Langley R, Bond J and Chrzanowski A (2003) Local deformation monitoring using GPS in an open pit mine: Initial study. GPS Solutions, in press. Presented at IUGG 2003, Sapporo, Japan, July
55. Kim D and Langley R (2003) On ultrahigh-precision positioning and navigation. Navigation: Journal of the Institute of Navigation, Vol. 50, No. 2, Summer, pp: 103-116
56. Kim D and Langley R (2003) Ultrahigh-precision GPS applications using real-time kinematic technology. EGS-AGU-EUG Joint Assembly: Real Time Geodesy (G16), Nice, France, 7-11 April. Poster presentation
57. Kim D and Langley R (2005) Nullification of differential ionospheric delay for long-baseline real-time kinematic applications. ION 61st Annual Meeting, Cambridge, Massachusetts\
58. Kovar P, Vejrazka F, Seidl L and Kacmaric P (2005) Galileo receiver core technologies. J. GPS 4(1-2): 176-183
59. Kreye C, Niedermeier H, Heyen R, Stelkens-Kobsch T and Boedecker G (2006) Galileo and the Earth's gravity field. Using GNSS for airborne gravimetry - an overview. Inside GNSS 1(8): 53-65
60. Kreher J (2004) Galileo Signal Baseline. ICAO NSP WGW – IP/17, June 2004
61. Lachapelle G, Cannon M, O'Keefe K and Alves P (2002) How will Galileo improve positioning performance? GPS World, 13(9)

62. Landau H, Vollath U, Chen X and Allison T (2004) Benefits of modernized GPS/Galileo to RTK positioning. The 2004 International Symposium on GNSS/GPS, Sydney, Australia
63. Landry R, Boutin P and Constantinescu A (2006) New anti-jamming technique for GPS and GALILEO receivers using adaptive FADP filter. Digital Signal Processing 16(3): 255-274
64. Lee E, Chun S, Lee Y, Kang T, Jee G and Abdel-Hafez M (2006) Performance improvement of Wald test for resolving GPS integer ambiguity using a baseline-length constraint. International Journal of Control, Automation, and Systems, Vol. 4, No. 3, pp: 333-343
65. Lee S, Shim Y, Kang C, Yoo C, Kim D, Tunik A and Kim J (1998) RGPS-based automatic landing system for light and commuter aircraft. Proceedings of the 14th International Federation of Automatic Control (IFAC) Symposium on Automatic Control in Aerospace, Seoul, Korea, 24-28 August
66. Lightsey E, Crassidis J and Markley F (1999) Fast integer ambiguity resolution for GPS attitude determination. Proceedings of the AIAA Guidance, Navigation and Control Conference, Portland, OR
67. Lohan E, Lakhzouri A and Renfors M (2006) Complex double-binary-offset-carrier modulation for a unitary characterization of Galileo and GPS signals. IEE Proc. Radar, Sonar Navig. 153(5): 403-408
68. McDonald K and Hegarty C (2000) Post-modernized GPS performance capabilities. In Proceedings of ION 56th Annual Meeting
69. McDonald K (2002) The modernization of GPS: plans, new capabilities and the future relationship to Galileo. Journal of GPS, 1(1), pp: 1-17

70. Meng X, Dodson A and Roberts G (2007) Global Navigation Satellite System (GNSS) for bridge deflection monitoring: recent activities by the University of Nottingham. In: Collected Works of Famous Educators in Highway Engineering of China: Celebration Proc. of Professor Zhuzhao Hong 80th Birthday. China Communications Press, pp: 425-434
71. Meng X, Dodson A, Moore T and Robeerts G (2007) Towards ubiquitous positioning (UbiPos): a GNSS perspective. In: ION 2007 National Technical Meeting
72. Meng X, Dodson A, Moore T and Roberts G (2007) Ubiquitous positioning: anyone, anything, anytime, anywhere. GPS World, 18(6), pp: 60-65
73. Milbert D (2005) Influence of pseudorange accuracy on phase ambiguity resolution in various GPS modernization scenarios. Navigation 52(1): 29-38
74. Miller J (2004) GPS & Galileo : Evolution towards GNSS, Presentation at ION NTM-04, 26-28 January, San Diego, CA, pp: 73-91
75. Misra P and Bednarz S (2004) Navigation for precision approaches: robust integrity monitoring using GPS+Galileo. GPS World 15(4): 42-49
76. Montillet J, Meng X and Roberts G (2007) Precise positioning in urban canyons using GPS and GSM. In: Proc of the Second European Conference on Mobile Government
77. Moudrak A, Konovaltsev A, Furthner J and Hammesfahr J (2004) Timing aspects of GPS-Galileo interoperability: challenges and solutions. 36th Annual Precise Time and Time Interval (PTTI) Meeting.
78. Mowlam A (2004) Fast ambiguity resolution performance using partially-fixed multi-GNSS phase observations. In: the 2004 International Symposium on GNSS/GPS, Sydney, Australia, 6-8 December 2004

79. O'Donnell M, Watson T, Fisher J, Simpson S, Brodin G, Bryant E and Walsh D (2003) Galileo performance: GPS interoperability and discriminators for urban and indoor environments, GPS World, 14(6), pp: 38-45
80. Pagni R, Dardelet J and Chenebault J(2005) From EGNOS to Galileo: A European vision of satellite-based navigation. Ann. Telecomm. 60(3-4): 357-375
81. Petovello M, O'Keefe K, Lachapelle G and Cannon M (2005) Quantifying ambiguity resolution performance in the presence of time-correlated measurement errors using geometric-based techniques. Proceedings of ION AM 2005, The Institute of Navigation, Fairfax, VA, pp: 1073-1085
82. Petovello M (2006) Narrowlane: is it worth it? GPS Solution (2006) 10: 187-195
83. Pozzobon O, Wullens C and Kubik K (2004) Secure tracking using trusted GNSS receivers and Galileo authentication services. Journal of GPS 3(1-2), pp: 200-207
84. Pratt M, Burke B and Misra P (1998) Single-epoch integer ambiguity resolution with GPS-GLONASS L1-L2 Data. In: Proceedings of ION-98, pp: 389-398
85. Qi H, Xia S, Chen Y and Dai J (2006) Passive positioning algorithm based on Beidou Double-Star. Proceedings of the 6th World Congress on Intelligent Control and Automation, June 21-23, 2006, Dalian, China, pp: 1791-1794
86. Radovanovic R, Fotopoulos G, and El-Sheimy N (2001) On optimizing GNSS multi-frequency carrier phase combinations for precise positioning. Presentation at IAG 2001 Scientific Assembly, Budapest, Hungary
87. Rizos C and Han S (1998) Precise kinematic applications of GPS: prospects and challenge. Boletim Ci. Geodesicas, Curitibo, 3, pp: 3-33
88. Roberts G, Meng X and Dodson A (2002) Using adaptive filtering to detect multipath and cycle slip in GPS/Accelerometer bridge deflection monitoring data. In: XXII International Congress of the FIG, TS6.2 Engineering Survey for

Construction Works and Structural Engineering II, 19-26 April, 2002m Washington DC, USA

89. Roberts G and Badley M (2007) Deformation monitoring trials using a Leica HDS3000. In: FIG Working Week 2007.
90. Roberts G, Brown C, Atkins C and Meng X (2007) Further results from using GPS to monitor the deflections of the Forth Road Bridge. In: FIG, ed. FIG Working Week 2007.
91. Roberts G, Meng X, Taha A and Montillet J (2007) The location and positioning of buried pipes and cables in built up areas. In: Proceedings of the FIG XXIII Congress.
92. Roberts G, Brown C, Meng X and Dallard P (2007) Using GPS to measure the deflections and frequency responses of the London Millennium Bridge. In: DR R LARK, ed. Fifth international Conference on Current and Future Trends in Bridge Design, Construction and Maintenance. pp: 486 – 496
93. Rodriguez A, Irsigler M, Hein G and Pany T (2004) Combined galileo/gps frequency and signal performance analysis. In the Proceedings of ION GNSS 2004
94. Ron C (2002) The tables of the difference between the nutation series IAU2000, IERS1996 and IAU1980. In: Proceedings of the IERS Workshop on the Implementation of the New IAU Resolutions, Observatoire de Paris, Paris, France, 18-19 April 2002, pp: 111-113
95. Rossi A, Valsecchi G and Perozzi E (2005) Risk of collision for the navigation constellations: The case of the forthcoming Galileo. J. Astronaut. Sci.52(4): 455-474

96. Santerre R, Langley R, Ueno M, Biron A, Kim D, Parrot D, St-Pierre C, Tetreault P, Marceau G and Langelier D (2000) Improvement of kinematic OTF-GPS positioning over long distances: Applications to bathymetric surveys. Proceedings of the Canadian Hydrographic Conference 2000, Montreal, Quebec, May 15-19

97. Schüler E and Schüler T (2007) Active GNSS networks and the benefits of combined GPS+Galileo positioning. Inside GNSS 2(8): 46-55

98. Seynat C, Kealy A and Zhang K (2004) A performance analysis of future global navigation satellite systems. Journal of Global Positioning Systems, Vol. 3, No. 1-2, pp: 232-241

99. Shah M and Lai Y (2004) Performance of integer parameter estimation algorithm for GPS signals in noisy environment. ION GNSS 17th International Technical Meeting of the Satellite Division, pp: 166-174

100. Swann J, Chatre E and Ludwig D (2003) Galileo: benefits for location based services. Journal of GPS 2(1), pp: 57-66

101. Teunissen P (1997) Some remarks on GPS ambiguity resolution. Artificial Satellites, Vol. 32, No. 3, pp: 119–130

102. Teunissen P (1997) A canonical theory for short GPS baselines, Part IV: precision versus reliability. Journal of Geodesy (1997), 71: 513-525

103. Teunissen P (1998) Success Probability of Integer GPS Ambiguity Rounding and Bootstrapping. Journal of Geodesy,1998, 72: 606-612

104. Teunissen P (1998) On the integer normal distribution of the GPS ambiguities. Artificial Satellites, Vol. 33, No. 2, pp: 1-13

105. Teunissen P (1998) The ionosphere-weighted GPS baseline precision in canonical form. Journal of Geodesy, Vol. 72, pp: 107-117

106. Teunissen P, Odijk D, and Joosten P (1998) A Probabilistic Evaluation of Correct GPS Ambiguity Resolution. In Proceedings of ION GPS-98, the 11th International Technical Meeting of the Satellite Division of The Institute of Navigation, Nashville, Tennessee, September 15-18, 1998, pp: 1315-1323

107. Teunissen P (1999) The mean and the variance matrix of the "fixed" GPS baseline. Acta Geod. Geophys. Hung., 34(1-2), pp: 33-40

108. Teunissen P (1999) The probability distribution of the GPS baseline for a class of integer ambiguity estimators. Journal of Geodesy, 73, pp: 275-284

109. Teunissen P (1999) A theorem on maximizing the probability of correct integer estimation. Artificial Satellites, Vol. 34, No. 1, pp: 3-9

110. Teunissen P (1999) The effect on GNSS ambiguity resolution of using an approximate weight matrix. Artificial Satellites, Vol. 34, No. 2, pp: 59-64

111. Teunissen P, Joosten P and Odijk D (1999) The reliability of GPS ambiguity resolution. GPS Solutions, vol. 2, pp: 63-69

112. Teunissen P (2000) ADOP based upperbounds for the bootstrapped and the least-squares ambiguity success rates. Artificial Satellites, Vol. 35, No. 4: 171 - 179

113. Teunissen P, Odijk D and Jong C (2000) Ambiguity dilution of precision: an additional tool for GPS quality control. LGR-Series: Publ. Delft Geod. Computing Centre, No. 21, pp: 261-270

114. Teunissen P (2000) The success rate and precision of GPS ambiguities. Journal of Geodesy, 74: 321-326

115. Teunissen P (2001) Statistical GNSS Carrier Phase Ambiguity Resolution: a Review. IEEE Symposium Statistical Signal Processing, Singapore, 2001, pp: 4-12

116. Teunissen P (2001) GNSS ambiguity bootstrapping: Theory and application. In: International Symposium on Kinematic Systems in Geodesy, Geomatics and Navigation, Banff, Canada, 5-8 June 2001, pp: 246-254

117. Teunissen P (2002) The parameter distributions of the integer GPS model. Journal of Geodesy, 76: 41-48

118. Teunissen P (2003) A carrier phase ambiguity estimator with easy-to-evaluate fail-rate. Artificial Satellites Vol. 38, No. 3: 89–96

119. Teunissen P (2003) Rank-defect integer estimation and phase-only modernized GPS ambiguity resolution. Journal of Geodesy, 76: 523-535

120. Teunissen P (2003) Towards a unified theory of GNSS ambiguity resolution. Journal of Global Positioning Systems, Vol. 2, No. 1, pp: 1-12

121. Teunissen P (2004) Penalized GNSS ambiguity resolution. Journal of Geodesy, Vol. 78, No. 4-5, pp: 235-244

122. Teunissen P (2005) GNSS best integer equivariant estimation. International Association of Geodesy Symposia: 128, Berlin: Springer, pp: 422-427

123. Teunissen P (2005) Integer aperture bootstrapping: a new GNSS ambiguity estimator with controllable fail-rate. Journal of Geodesy, 79 (2005), pp: 389-397

124. Teunissen P (2005) Integer aperture least-squares estimation. Artificial Satellites, Vol. 40, No. 3, pp: 149-160

125. Teunissen P (2005) On the computation of the best integer equivariant estimator. Artificial Satellites, Vol. 40, No. 3, pp: 161-171

126. Teunissen P (2006) Least-squares collocation with integer parameters. Artificial Satellites, Vol. 41, No. 2, pp: 59-66

127. Tiberius, C and Jong K (2002) Developments in global navigation satellite systems: GPS modernized, Galileo launched. Hydrographic Journal, 104, pp: 3-7

128. Vaschoenbeek I, Bonhoure B, Boschetti M and Legenne J (2007) GNSS time offset: effects on GPS-Galileo interoperability performance. Inside GNSS 2(6): 60-70

129. Verhagen S (2004) Integer ambiguity validation: an open problem? GPS Solutions, Vol. 8, pp: 36-43

130. Verhagen S (2005) On the reliability of integer ambiguity resolution. Journal of The Institute of Navigation, Vol. 52, No. 2, pp: 99-110

131. Verhagen S and Teunissen P (2006) On the probability density function of the GNSS ambiguity residuals. GPS Solutions 10(1): 21-28

132. Vollath U (2004) The Factorized Multi-Carrier Ambiguity Resolution (FAMCAR) approach for efficient carrier-phase ambiguity estimation. In Proc. ION GNSS-04, Long Beach, CA, pp: 2499-2508

133. Wang J, Stewart M and Tsakiri (2000) A comparative study of the integer ambiguity validation procedures. Earth Planets Space, Vol. 52, No. 10, pp: 813-817

134. Wang J, Lee H, Hewitson S, Rizos C, and Barnes J (2003) Sensitivity analysis for GNSS integer carrier phase ambiguity validation test. The University of New South Wales, Australia

135. Wang J, Keller W and Sharifi M (2006) Comparison of availability of Galileo, GPS, and a combined Galileo/GPS navigation system. Artificial Satellites 41(1): 3-15

136. Wu F, Kubo N and Yasuda A (2003) A study of hybrid modernized GPS and Galileo positioning in Japan. The Journal of Japan Institute of Navigation, September, Vol. 109.

137. Zhao C, Ou J, Yuan Y (2005) Positioning accuracy and reliability of GALILEO, integrated GPS-GALILEO system based on single positioning model. Chinese Sci. Bull. 50(12): 1252-1260

138. Zhodzishsky M, Vorobiev M, Khvalkov A and Ashjaee J (1998) Real-time kinematic (RTK) processing for dual-frequency GPS/GLONASS. In proceedings of ION GPS'1998, Nashville, TN, pp: 1325-1331